2011

The Role of 53BP1 in DNA Double-Strand Break Repair

Anne Helen Bothmer

The Role of 53BP1 in DNA Double-Strand Break Repair

A Thesis Presented to the Faculty of
The Rockefeller University
in Partial Fulfillment of the Requirements for
the Degree of Doctor of Philosophy

by

Anne Helen Bothmer

June 2011

The Role of 53BP1 in DNA Double-Strand Break Repair

Anne Helen Bothmer, Ph.D.
The Rockefeller University 2011

DNA double-strand breaks (DSBs) are dangerous insults to DNA integrity and can lead to genome instability if left unrepaired. However, the immune cell diversification reactions V(D)J recombination and Class Switch Recombination (CSR) require the formation of DSB intermediates, a process that is tightly controlled and strictly limited to developing B and T cells. CSR in B cells diversifies antibodies by joining DSBs between highly repetitive DNA elements, which are separated by 60-200 kb. Switch region DSBs are joined by a mechanism that requires an intact DNA damage response and classical or alternative non-homologous end-joining (C-NHEJ and A-NHEJ). Among DNA damage response factors, absence of 53BP1 leads to the most severe defect in CSR. Similarly, the loss of 53BP1 leads to impaired joining of distal DSBs during V(D)J recombination and results in abrogated trans-chromosomal fusions of dysfunctional telomeres. Interestingly, joining of proximal switch region internal DSBs is not affected by the absence of 53BP1, leading to the hypothesis that 53BP1 affects the joining of only a subset of DSBs. Here I use the I-SceI meganuclease system to introduce site-directed DSBs in order to establish the effect of 53BP1 on the joining of trans-chromosomal and intra-chromosomal DSBs separated by various distances. I provide evidence that 53BP1 facilitates joining of intra-chromosomal DSBs, but that this effect is limited to a range that coincides with the spread of DNA damage response factors. I then explore the role of 53BP1 in DNA repair, and find that the absence of 53BP1 results in a distance-independent

increase in DNA end resection and that resected DNA is preferentially repaired by microhomology mediated A-NHEJ. Furthermore, analysis of 53BP1 mutants shows that chromatin association, oligomerization, and N-terminal ATM phosphorylation sites are all required for preventing DNA end resection and joining as measured by immunoglobulin CSR.

In summary, these data provide new insights the molecular mechanisms by which 53BP1 facilitates DSB joining during CSR and its contribution towards the maintenance of genomic stability.

Diese Arbeit ist meinen geliebten Großeltern

Helga und Wolfgang Bothmer gewidmet.

ACKNOWLEDGEMENTS

First and foremost, I would like to thank my advisor Michel Nussenzweig for his guidance and support over the last five years. I am grateful to have been part of his laboratory, in which I had the freedom and means to pursue my own interests and find my own path, without ever feeling lost. You have shown enthusiasm for my research, provided encouragement when necessary and well directed criticism when appropriate. I greatly appreciate that the door to your office was always open and that you took the time address questions or problems promptly.

I would also like to thank the members of my thesis committee, Titia de Lange and David Allis, who have taken time out of their busy schedules to listen to my progress, provide ideas and different perspectives and point to problems - I have learned a lot from our annual meetings. I would also like to thank Fred Alt for serving as the external examiner on my thesis committee.

A very special thank you is directed to Davide Robbiani, whom I closely worked with during my time in Michel's lab. You have taught me not only how to address a scientific problem, but also how to choose which problem is addressable and worth addressing, how to design experiments, how to analyze and interpret data, how to present data and how to write about it. You have taught me, a German, how to work with Swiss precision. I have enjoyed and will miss our conversations about science, which frequently led to new ideas and experiments and occasionally ended in tangential discussions about politics.

I would like to thank all members of the Nussenzweig lab for making our lab such an enjoyable place on a day-to-day basis. I would especially like to thank the members of the "B cells/DNA repair group": Anna Gazumyan and Mila Jankovic for many scientific insights and their almost parental support and wisdom concerning non-science related issues; Isaac Klein for stimulating scientific discussions and many non-scientific humorous moments; Michela Di Virgilio, Rushad Pavri and Kevin McBride for providing their scientific expertise, advice and many entertaining lunch table discussions. Moreover, I would like to thank David Bosque, Kai-Hui Yao and Tom Eisenreich for helping me take care of my mouse colonies.

In addition, many thanks to the Dean's Office, our lab assistant Virginia Menendez and our lab manager Zoran Jankovic, who have made my time at Rockefeller administratively hassle-free.

I would like to thank my friends far away in Europe and here at Rockefeller, particularly my fellow graduate students and apartment mates and Moritz Armbruster and Manuel Leonetti, whose companionship and culinary skills I have greatly enjoyed. To Diana Otalvaro, my very best friend: I can't possibly list all the things I am thankful for.

Most importantly, I would like to thank my parents, Ramona and Dietmar Bothmer, without whose loving encouragement I would have never succeeded in a place so far away and so different from home. You have instilled in me the values of

hard work and perseverance and have taught me to never choose something only because it is easy or convenient. I am deeply grateful for having such a loving home.

I dedicate this thesis to my grandparents, Helga and Wolfgang Bothmer. Thinking of you makes me feel at home anytime and anywhere. Thank you for your unconditional love and support. Your life stories are an inspiration and if I only were to acquire a fraction of your knowledge and wisdom I would consider it a success.

TABLE OF CONTENTS

LIST OF FIGURES

CHAPTER 1:

Introduction

A DNA double-strand break (DSB) is one of the most serious insults to the integrity of our genome and can pose a threat to the survival of the entire organism: unrepaired DSBs can induce genomic rearrangements such as chromosomal deletions, amplifications and translocations – all of which are hallmarks of cancer. The origins of DSBs are diverse and can be generally classified as arising from either exogenous or endogenous sources. Exogenous sources of DSBs include exposure to ionizing radiation (IR), ultraviolet light (UV), chemicals or genotoxic agents, for example during chemotherapy treatment. Endogenous DSBs can form as accidental by-products of normal cellular metabolism: replication fork collapse, reactive oxygen species, collision of transcription and replication or the presence of critically short telomeres. Lastly, DSBs arise as intermediates in physiological reactions, most prominently in the developing immune system during V(D)J recombination and Class Switch Recombination (CSR), and in germ cells during cross-over reactions in meiosis. Regardless of their origin, DSBs are toxic and unrepaired damage may lead to genomic instability with detrimental consequences for possibly the entire organism. To ensure the faithful repair of DSBs the cell has evolved a complex system of DNA damage sensors, signal transducers and effector proteins. Together this system arrests the cell cycle and invokes DNA repair or initiates apoptosis if the damage is too severe to be repaired. The importance of a functional DNA damage response is exemplified by the clinical manifestations of mutations in DNA damage response pathways. Individuals inflicted with

inherited defects display to various degrees immune deficiencies, sterility, developmental disorders, neurodegenerative diseases and a marked predisposition to cancer.

In my thesis work, I will explore the role of the DNA damage response and of DNA repair in CSR, one of two immune diversification reactions that require DSB intermediates. The first part of the introduction focuses on the DNA damage signaling pathways involved in the recognition of DSBs and the repair pathways that are employed by cells to fix the damage. In the second part of the introduction I will focus on programmed DSBs in the context of immune system diversification reactions. I will describe the molecular mechanisms by which DSBs are introduced, the role of DNA damage signaling and the role of repair pathway choices during those reactions. This will lay the groundwork for the experimental design in which we use immune cells to study aspects of DNA repair as they pertain to the outcome of immune cell diversification reactions.

The DNA damage response

The DNA damage sensor: MRN

MRN is a large multiprotein complex comprising of two MRE11, two RAD50 and a yet undetermined number of NBS1 molecules (1). MRN is one of the first complexes to recognize a DSB and initiate repair (2, 3). MRE11 forms a homodimer and when associated with RAD50 possesses DNA binding activity as well as single-stranded DNA (ssDNA) endonuclease activity and 3'-5' exonuclease activity (4-7). This endows the MRN complex with the ability to initiate processing of broken ends for further DNA repair steps.

RAD50 contains an N-terminal Walker A and a C-terminal Walker B domain, which interact with each other forming a globular ATPase domain, while the intervening part extends as a coiled-coil. The globular part of RAD50 is also the site at which it binds to MRE11, leading to formation of the $MRE11_2RAD50_2$ complex (1, 8, 9).

NBS1, the third component of the MRN complex, binds to MRE11 (10). In contrast to MRE11 and RAD50, NBS1 has no known catalytic activity, but instead is essential for nuclear localization of MRE11 and RAD50 and for activation of downstream DNA damage signaling (11, 12). NBS1 contains a Fork-Head Associated (FHA) domain at its N-terminus followed by tandem BRCA1-Related C-Terminal (BRCT) domains; both are phosphopeptide-binding motifs commonly found in DNA damage response proteins (10, 12). Moreover, NBS1 contains several S/T-Q motifs, which are targets of ATM kinase phosphorylation (13). Importantly, NBS1 is responsible for recruiting and concentrating ATM at the site of the break (11, 12).

Besides NBS1 mediated activation of downstream signaling, the MRE11 component of the MRN complex can juxtapose two broken ends to facilitate DNA repair (9), while RAD50 may be involved in promoting long-range interactions between two sister chromatids through dimerization of the coiled-coil domains (4).

The importance of the MRN complex is reflected by the embryonic lethality of null mutations of any of its components (14-16). Human patients bearing a hypomorphic mutation of the NBS1 gene display Nijmegen breakage syndrome, which is characterized by cancer predisposition, immunodeficiency and developmental defects (17). Similarly, hypomorphic mutations in MRE11 lead A-T like disorder, a disease that is similar to the defect displayed in the absence of its downstream signaling partner ATM (18).

Central player in the DNA damage response: ATM

Ataxia-telangiectasia mutated (ATM) was identified as the gene that is mutated in patients with the rare autosomal recessive disorder ataxia-telangiectasia, leading to the name A-T mutated (ATM; (19). Mutations in the *atm* gene lead to a wide array of symptoms, the most pronounced of which are cancer predisposition, radiation sensitivity, cerebellar ataxia and progressive neurodegeneration. The severe phenotypes observed in A-T patients underscore the importance of ATM as one of the central players for the maintenance of genome integrity.

ATM is a member of the phosphoinositide 3-kinase-related protein kinase (PIKK)-family and like other members of this kinase family preferentially phosphorylates serine or threonine residues followed by glutamine (consensus

phosphorylation site: S/T-Q; (20, 21). ATM phosphorylates more than 700 downstream targets, which are involved in cell-cycle regulation and DNA repair (22, 23). The first identified target of ATM phosphorylation after DNA damage was p53, which in turn induces p21, resulting in the inhibition of the CyclinE/CDK2 complex leading to cell-cycle arrest at the G1-S transition (24, 25). Furthermore, ATM signaling can activate the intra-S phase checkpoint by phosphorylating the effector kinase CHK2, which then phosphorylates and thereby marks for degradation the phosphatase CDC25A, resulting in the inhibition of DNA replication (26, 27). Moreover, ATM signaling can arrest cells at the G2/M checkpoint by activating the CHK2 kinase, which then phosphorylates the phosphatase CDC25C, leading to the inactivation of CyclinB/CDC2, whereby transition into mitosis is prevented (28).

ATM is a predominantly nuclear protein, which in the absence of DNA damage forms an inactive dimer (29). The C-terminal portion of NBS1 recruits ATM to the site of the break, followed by ATM autophosphorylation at serine 1981 leading to its dissociation into active monomers.

The functional significance of ATM autophosphorylation of serine 1981 remains controversial. An $ATM^{-/-}$ mouse expressing ATM with a phosphorylation site mutation (serine 1987 mutated to alanine) using a BAC transgene did not show radiation sensitivity, cell-cycle defects or deficiencies in phosphorylation of downstream targets such as CHK2 or p53 (30). Since the hallmarks of ATM activation are intact in those mice, serine 1987 autophosphorylation in mice does not seem to be exclusively responsible for ATM activation.

At the site of the DSB, ATM phosphorylates a plethora of targets, including NBS1 of the MRN complex, establishing a positive feedback loop, which leads to the

recruitment of more ATM and MRN, amplifying the damage signal (3, 11). This amplification step is thought to be an essential component of the DNA damage response, ultimately leading to the formation of cytologically visible DNA damage foci.

DNA damage factor recruitment hub: γH2AX

DNA damage leads to modifications of the chromatin surrounding the DSB. The hallmark of an active DNA damage response is the ATM dependent phosphorylation of the C-terminal serine 139 residue of the chromatin component histone H2AX (γH2AX, (31, 32)). This modification is very rapidly induced and nuclear γH2AX foci at the site of the DSB can be observed as soon as one minute after damage induction (33). However, the absence of ATM still leads to detectable γH2AX focus formation, indicating significant redundancy in the phosphorylation pathways: two other PIKKs, ATR and DNA-PKcs, have been implicated in H2AX phosphorylation in the absence of ATM during replication stress (34). The phosphorylation of H2AX is thought to spread to hundreds of kilobases surrounding the break (33). H2AX serves as an anchor and promotes the recruitment and accumulation of many downstream targets, initiated by its direct interaction with the tandem BRCT domains of the mediator protein MDC1 (35, 36).

H2AX deficient mice are viable, but harbor an increased frequency of chromosome and chromatid breaks after IR, indicating a defect in DNA repair (37, 38). In contrast to ATM deficient mice, H2AX deficiency leads to increased tumor incidence only in the absence of p53, which is required for the induction of

apoptosis in cells with unrepaired DSBs (39, 40). Furthermore, H2AX$^{-/-}$ mice display increased sensitivity to radiation and males are infertile due to a defect in DSB break repair during meiotic recombination in germ cells (41).

Mediator of DNA damage factor recruitment: MDC1

MDC1 is a large nuclear protein that similarly to many other members of the DNA damage response contains an N-terminal FHA domain and C-terminal tandem BRCT domains (36, 42-44). MDC1 interacts constitutively with the MRN complex mediated by binding of the FHA domain in NBS1 to a DNA damage independent phosphorylation site in MDC1 (45-48). Importantly, the BRCT domains of MDC1 bind to DNA damage inducible γH2AX, which is consistent with kinetic studies of DNA damage focus formation that have shown γH2AX foci to precede MDC1 foci (36, 49).

Recently, ubiquitylation of DSB flanking chromatin has been discovered as an entire new arm of the DNA damage response (50-52). The recruitment of factors mediating ubiquitylation crucially depends on MDC1 and will be described in more detail in the next paragraph. MDC1$^{-/-}$ mice are viable and closely resemble the phenotype of H2AX$^{-/-}$ mice: male infertility, radiosensitivity and checkpoint defects (35).

Chromatin modifications: RNF8 and RNF168

RNF8 is a DNA damage response protein that contains an N-terminal FHA domain and a C-terminal RING-finger domain and thereby is functionally classified as a member of the E3 ubiquitin ligase family (50-52). RNF8 rapidly

forms foci at sites of DSBs and this accumulation is dependent on the previous recruitment of MDC1 and by extension on H2AX. Specifically, the FHA domain of RNF8 binds a phosphorylated S/T-Q motif in the N-terminus of MDC1 (50-52). In contrast, the RING-domain mediated ubiquitin ligase activity of RNF8 is dispensable for its accumulation at sites of DNA damage, but is required for ubiquitylation of H2AX or H2A (50-52). Interestingly, the recruitment of downstream factors such as 53BP1 and BRCA1 is severely compromised in the absence of RNF8 catalytic activity, indicating that ubiquitylation plays in important role in regulating DNA repair. $RNF8^{-/-}$ mice display increased chromosome instability and predisposition to cancer. In addition, RNF8 deficiency leads to male infertility as a result of meiotic defects (53, 54).

Although required, RNF8 is not sufficient to maintain ubiquitylation of damaged chromatin. Another layer of regulation has been uncovered with the identification of RNF168, which similarly to RNF8 is a member of the RING-finger ubiquitin ligase family (55, 56). RNF168 contains two MIU (Motif interacting with Ubiquitin) motifs, which allow for its direct association with ubiquitin moieties, a process that is dependent on previous ubiquitylation of H2A-type histones by RNF8. The association of RNF168 with the ubiquitin conjugating enzyme UBC13 is required for sustained ubiquitylation of damaged chromatin and the catalytic activity of RNF168 is essential for efficient accumulation of 53BP1 and BRCA1 at sites of DSBs (55, 56). Interestingly, mutations in the *rnf168* gene were identified in patients with a rare disorder called RIDDLE syndrome, which is characterized by radiosensitivity, immunodeficiency, dysmorphic features and learning disabilities (56).

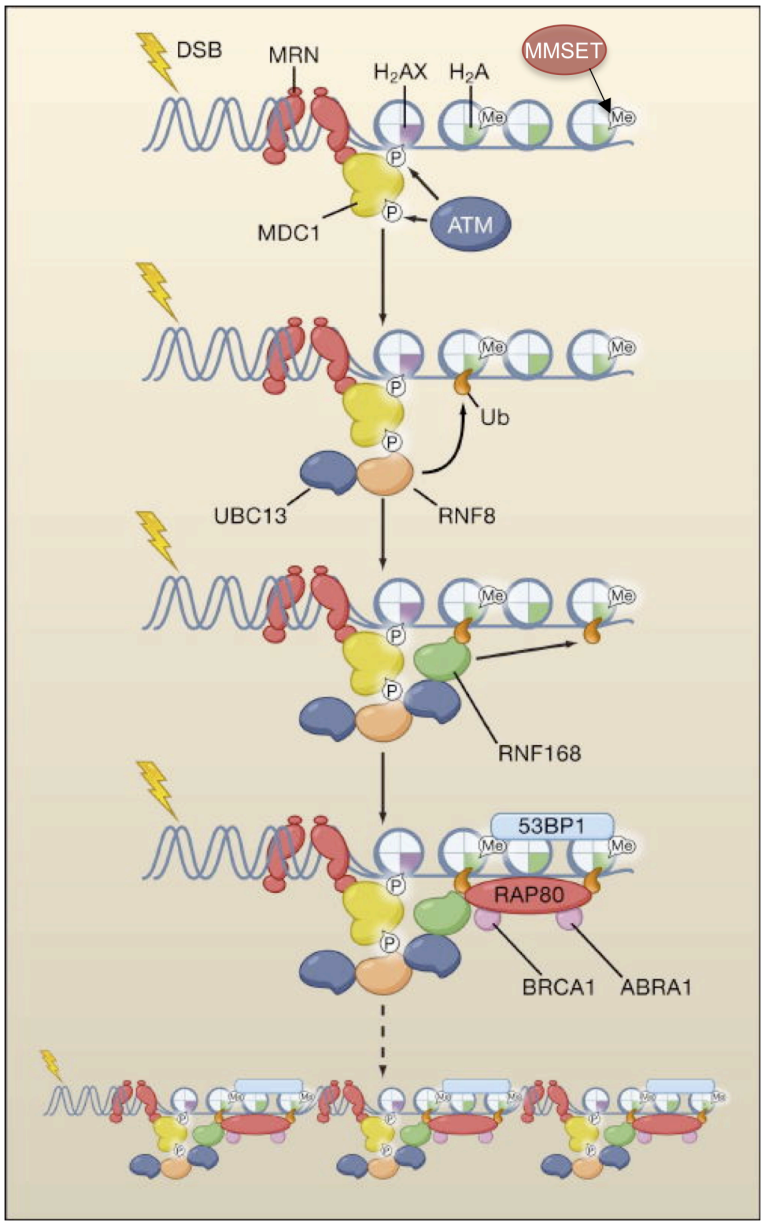

Figure 1.1. Accumulation of DNA damage response factors at DSBs

DSBs are sensed by the MRN complex, which recruits and activates ATM at the site of the break. ATM activation leads to the phosphorylation of many downstream proteins, such as the histone variant H2AX. Phosphorylated H2AX recruits MDC1, which in turn recruits RNF8, RNF168 and UBC13 to induce ubiquitylation of damaged chromatin. This then leads to the recruitment of downstream components such as 53BP1 and BRCA1. Phosphorylation of H2AX spreads to areas surrounding the DSB, leading to the accumulation of DNA damage response factors several hundred kilobases away from the DSB. *(image adapted from Nussenzweig et al., Cell 2010)*

DNA damage effector: 53BP1

The protein 53BP1 was discovered in a yeast two-hybrid screen tailored to identify new interaction partners of p53 (57). A wild type fragment of murine p53 was fused to the Gal4 DNA binding domain, while a cDNA library was fused to the activation domain, leading to transcription of a target gene only if the p53 fragment interacts with a partner fused to the transactivation domain. 53BP1 (p53 binding protein 1) emerged from this screen as a novel p53 interacting protein.

In those early years 53BP1 was mainly studied to gain mechanistic insight into p53 function. In this context, 53BP1 was shown to bind to the central DNA binding domain of p53 (57). Functionally 53BP1 enhances p53 transactivation activity *in vitro*, and is therefore considered a transcriptional coactivator of p53 (58). 53BP1 itself moved into the spotlight when an amino acid homology to the BRCT domain was identified (59). BRCT domains are commonly found in proteins involved in the recognition and repair of DNA damage. Furthermore, the sequence homology to Rad9, a central DNA damage induced checkpoint protein in *S.cerevisiae*, strongly implied a function for 53BP1 in response to DNA damage (60). Indeed, upon treatment with IR 53BP1 rapidly forms distinct nuclear DNA damage foci and colocalizes (among many other factors) with γH2AX (60-62). 53BP1 is also a substrate of the ATM kinase (61), but ATM activity is not essential for 53BP1 focus formation upon IR (60, 62). The functional significance of ATM mediated phosphorylation of 53BP1 is not well understood.

53BP1 is a large nuclear protein of 1972 amino acids (Figure 1.2). Besides the well-defined C-terminal tandem BRCT domains, 53BP1 contains a tandem tudor domain spanning amino acids 1486-1540 (human 53BP1; (63)). This domain displays a high degree of conservation throughout evolution and is present in the 53BP1 orthologues Crb2 and Rad9 of *S.pombe* and *S.cerevisiae*, respectively (64). Importantly, the tandem tudor domain of 53BP1 is strictly required for focus formation after IR induced damage (63, 64). Tudor domains are methylated histone-binding motifs; however, the identity of the histone interaction partner of 53BP1 remains controversial. In an initial study, the structure of the tudor domain was solved by X-ray crystallography and a pocket between the two tudor folds was shown to interact selectively with dimethylated H3K79 (HeK79me2; (64)). Moreover, mutational analysis of residues within the binding pocket, specifically substitution of the aspartic acid residue at position 1521 with arginine (D1521R), completely abrogates 53BP1 focus formation. However, in a subsequent study a genetic depletion of DOT1, which is the enzyme responsible for the dimethylation of H3K79, showed no impaired focus formation of 53BP1, leading to the conclusion that the histone interaction is probably not mediated through H3K79me2 (65). The search for an alternative interaction partner resulted in the identification of dimethylated H4K20 (H4K20me2) as a preferential binding partner and at lower affinity monomethylated H4K20 (H4K20me1; (65)). H4K20me2 appears to be a constitutive histone mark (65, 66) and is catalyzed by the histone methyltransferases SUV4-20H1 and SUV4-20H2 (67, 68). A double knockout of both enzymes leads to the expected decrease of H4K20me2 species, but again focus formation of 53BP1 was only mildly affected by the combined absence of these two methyltransferases (69). One possible

explanation for this observation is that H4K20me1 (which is increased as a result of the SUV4-20H1/H2 double knockout) is sufficient to mediate 53BP1 chromatin interaction. An alternative explanation is that both H3K79me2 and H4K20me2 can mediate binding of the tudor domain to chromatin, or that a different histone modification altogether is the tudor domain binding partner.

Both H4K20me2 and H3K79me2 are constitutive histone marks and do not appear to change globally after DSB formation. In contrast, phosphorylation of histone H2AX on serine 139 is induced by DNA damage and stable 53BP1 focus formation is dependent on this modification (70-72). Although weak 53BP1 foci form 30-45 min after IR exposure of $H2AX^{-/-}$ MEFs, 53BP1 foci are not maintained at later time points (70, 73). A set of early experiments showed that γH2AX can immunoprecipitate 53BP1 upon IR-mediated DNA damage (62, 72). However, the interaction between γH2AX and 53BP1 is likely not direct but occurs via γH2AX dependent recruitment of the E3 ubiquitin ligases RNF8 and RNF168 (50-52). Consistent with this model is the finding that deficiencies in RNF8 or RNF168 abrogate sustained 53BP1 focus formation. However, the precise mechanism by which ubiquitylation of damaged chromatin regulates 53BP1 recruitment remains to be elucidated, as there is also no evidence for a direct interaction between 53BP1 and ubiquitin moieties.

In summary, these observations imply that 53BP1 binding to dimethylated histones is required, but binding is not sufficient for 53BP1 focus formation. Sustained accumulation of 53BP1 in a focus requires ongoing DNA damage signaling. Interestingly, a recent report showed that the histone methyltransferase MMSET dimethylates H4K20 locally at the site of the DSB

whereby it recruits 53BP1 (74). However, recruitment of MMSET is dependent on damage-induced γH2AX, indicating the presence of only one, damage-inducible 53BP1 recruitment pathway.

An additional requirement for focus formation is the ability of 53BP1 to form homo-oligomers and the domain responsible for this activity mapped to residues 1231-1277 (75, 76).

The fragment of 53BP1 spanning aa 1220-1711 is the minimal region required for focus formation and includes the oligomerization domain, the tandem tudor domains and the nuclear localization sequence (NLS) (63, 72). Interestingly, overexpression of the focus-forming fragment was shown to suppresses homologous recombination in a human cell line, indicating a role for 53BP1 in DNA reapir (77).

The C-terminal BRCT domains and the N-terminal portion of 53BP1 comprising of multiple S/T-Q motifs (phosphorylation targets of ATM) are dispensable for the accumulation of 53BP1 at sites of DNA damage (78). However, although loss of ATM mediated phosphorylation of the N-terminus does not affect 53BP1 focus formation, repair of DSBs is negatively affected, as evidenced by sustained H2AX phosphorylation (75).

$53BP1^{-/-}$ mice are viable and do not display cell proliferation defects, have only minor checkpoint defects and are mildly susceptible to thymic lymphomas (79). Tumors develop more rapidly in the combined absence of p53, indicating that p53 acts cooperatively with 53BP1 in tumor suppression (80).

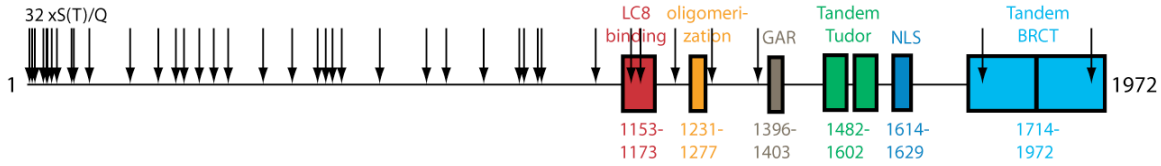

Figure 1.2. Schematic of human 53BP1 functional domains and phosphorylation sites.

Human 53BP1 is a 1972 amino acid protein. The predominantly N-terminal ATM phosphorylation consensus sites (S/T-Q motifs) are indicated by black arrows. The LC8 domain which interacts with the dynein light chain is shown in red. The oligomerization domain is shown in orange, the Glycine Arginine Rich (GAR) domain that becomes substrate for PRMT1 mediated methylation is shown in grey. The chromatin interacting tudor domain is shown in green, followed by the NLS in light blue. The C-terminal BRCT portion of the molecule is shown in dark blue. Amino acid positions are induicated below the respective functional domain.

DNA repair pathways

DSBs can be repaired by one of two evolutionarily conserved pathways: Homology directed repair (HR) or non-homologous end joining (NHEJ).

During HR, the undamaged sister chromatid is used as a template for repair. This ensures a high degree of fidelity but also limits the utility of this pathway, as templates for repair are only present in late S phase and during the G2 phase of the cell cycle. In contrast to HR, NHEJ functions independently of the cell cycle. NHEJ comprises of two pathways: classical-NHEJ (C-NHEJ) and alternative-NHEJ (A-NHEJ). While the C-NHEJ pathway is very well characterized, the molecular constituents of A-NHEJ are only beginning to be understood. For both pathways small deletions and insertions are frequent, which make C-NHEJ and A-NHEJ less conservative form of DSB repair than HR.

Homologous recombination

Templates for accurate repair of DSBs by HR are only proximal once the respective chromosomes have been replicated in late S phase and during G2. HR is initiated by resection of the 5′ strand at the site of the DSB, leaving a 3′ ssDNA overhang. The enzymatic machinery required for efficient end resection has recently been described in *S.cerevisiae*, where end resection occurs in two phases.

In the first phase resection is initiated by the recruitment of the Mrx complex, followed by Sae2 accumulation. Whereas initial Mrx recruitment to the site of the DSB is ATM independent, Sae2 recruitment requires ATM activity (81-83). The initial actions of Mrx and Sae2 (at the site of the DSB expose ~ 50 - 100 nt of ssDNA (84-86). DNA repair pathway choice is made at the step of end resection

and it is therefore not surprising that end-resection is regulated in a cell-cycle specific manner. Specifically, Sae2 is phosphorylated on serine 267 by the S-phase specific kinase Cdk2, activating Sae2 catalytic activity. Accordingly, mutation of serine 267 leads to severely impaired resection activity in areas proximal to a DSB (87, 88).

Subsequently, more extensive end resection is initiated by the combined activities of Sgs1 (DNA helicase), the 5'-3' exonuclease Exo1 and the helicase and nuclease Dna2. Dna2 and Exo1 are redundant with respect to end processing. The combined absence of Exo1 and Sgs1 leads to a more severe resection defect than the combined absence of Sgs1 and Dna2, leading to the conclusion that Sgs1 and Dna2 operate in the same pathway and Exo1 is responsible for DNA end resection in the absence of Dna2 (84-86). However, even the most drastic long distance resection defect observed in the combined absence of Dna2, Sgs1 and Exo1 leads to severely, but not completely, compromised homologous recombination (a functional readout of end resection proficiency). Likely, the initial end trimming of 50 - 100 nt by the Mrx complex and Sae2 is sufficient for the repair of a DSB by homologous recombination, albeit at reduced frequency.

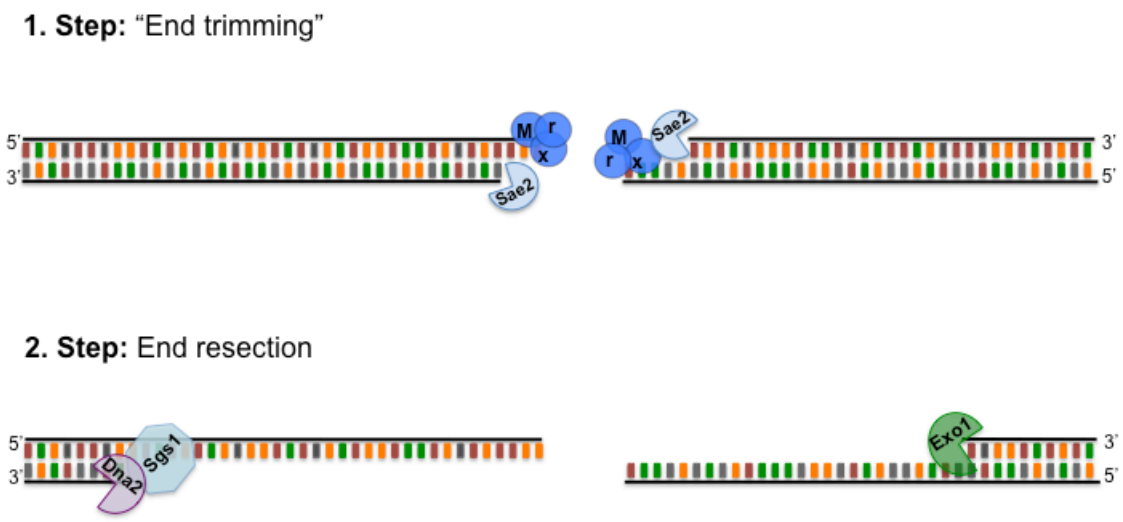

Figure 1.3. DNA end processing after DSB formation.
In the initial "end trimming" step the Mrx complex with Sae2 process the broken DNA ends endo– and exonucleolytically, revealing 50-100 nts of 3′ ssDNA overhang. The then following end resection step is mediated by the enzymes Sgs1/Dna2 or Exo1. Extensive end resection is required for efficient repair by homologous recombination.

The 3′ ssDNA overhang generated by resection of the 5′ strand is rapidly bound by the abundant ssDNA binding protein Replication Protein A (RPA), which recruits the ATRIP/ATR complex along with the RAD9-RAD1-HUS1 complex leading to the activation of the checkpoint protein CHK1. This in turn halts the cell cycle by activation of the G2/M checkpoint (89, 90).

The ssDNA-RPA complex recruits another protein, RAD51, which forms a nucleoprotein filament (91, 92). This intermediate is essential for HR because it mediates homology search by strand invasion of the sister chromatid or the homologous chromosome, leading to the formation of a displacement loop. DNA synthesis is initiated and leads to the extension of the 3′ invading strand to copy

the sequence information of the sister chromatid or homologous chromosome (reviewed in (93). Subsequently, repair can progress through several pathways with different outcomes: during synthesis-dependent strand annealing (SDSA) the extended strand dissociates and re-anneals to the complementary DNA end that was exposed during resection, in which case the repair reaction is completed in the most conservative form, without a crossover reaction. Alternatively, the second broken DNA end can be "caught" by the displacement loop, forming a double Holliday junction. Depending on which enzymes resolve the Holliday junction, these repair reactions can result in non-crossover or crossover repair products.

Classical non-homologous end-joining (C-NHEJ)

During NHEJ DSBs are repaired without the "help" of homologous sequence. This pathway is inherently error prone and can entail loss of sequence or mutations at the junctions. The core NHEJ machinery consists of the KU70/KU80 complex, XRCC4 and DNA Ligase IV (LIG4) (reviewed in (94). All of the core NHEJ factors are evolutionarily conserved. The non-conserved accessory factors DNA-PKcs and Artemis facilitate end-joining of certain complex end structures, but are not absolutely required for DNA repair.

C-NHEJ is initiated by the rapid binding of the KU70/80 complex to the DSB (95, 96). The KU complex specifically interacts with DNA ends and is unable to associate with or dissociate from circular DNA (97). Binding of the Ku complex leads to the recruitment of DNA-PKcs, which upon binding to the DSB acquires serine/threonine kinase activity (98, 99). The KU/DNA-PKcs complex acts as a protein hub for the recruitment of many downstream DNA repair factors such as

Artemis, Polymerase μ (Polμ), XRCC4 and LIG4 (100-102). Pathologic DSBs leave behind greatly varying substrates and NHEJ must therefore possess great flexibility to efficiently join such vastly differing end structures. Trimming of the ends in preparation for ligation is stimulated by DNA-PKcs induced phosphorylation of Artemis, an exo- and endonuclease, which cleaves off both 5′ and 3′ overhangs (101, 103, 104). After initial nucleolytic end processing, the error-prone polymerase Polμ can add nucleotides to the end in a template-independent fashion (105). Polμ is one of the most flexible polymerases in its family and therefore ideally suited to process ends during NHEJ. Subsequently, the ligation components XRCC4 and LIG4 ligate the processed ends together. LIG4 is a flexible ligase: it can ligate blunt ends and ends with small microhomologies (106, 107). In summary, the C-NHEJ pathway is characterized by small end modifications (nucleotide losses or additions) and limited microhomology at the junction ranging from 0-4 nt, with the majority of the ends being ligated without the presence of microhomology.

Alternative non-homologous end-joining

A-NHEJ is a still poorly defined pathway, which is characterized by the predominance of microhomology at the joining junction and extensive sequence deletions, making it a less conservative pathway than the already error-prone C-NHEJ pathway. Joining by A-NHEJ was first encountered in cell lines deficient for C-NHEJ components KU80, XRCC4 or LIG4 (108-110). The molecular requirements for A-NHEJ remain to be elucidated. Repair factors that have been shown to contribute to A-NHEJ are MRE11 and CTIP, both of which are also

responsible for the first phase of end-resection during HR (111). End resection is thought to be involved during A-NHEJ, as stretches of homology can be exposed and used for annealing. A-NHEJ may be less efficient and kinetically slower than C-NHEJ and entails sequence deletions (112). Though the physiological function of this pathway has not yet been established, A-NHEJ is thought to mediate the joining of a subset of DSBs during chromosome translocation (113-116).

Model Systems

In the next paragraphs model systems will be described, which are used to study the DNA damage response and DNA repair processes. A brief discussion on using ionizing radiation for DSB formation is followed by the description of endonucleases as tools to induced DSBs. Finally, we will briefly discuss how the ends of chromosomes, telomeres, are perceived as DSBs in the absence of proper protection.

Ionizing radiation induced DSBs

Treatment of cells with IR results in the formation of DSBs, either by direct collision of high frequency electromagnetic waves with DNA, or indirectly, through the ionization of H_2O molecules, leading to the creation of hydroxy radicals (OH^-). Radicals are extremely reactive intermediates with the potential to damage molecules in their vicinity. By far the most frequent insults to DNA after IR are single strand breaks (SSBs). In addition, each Gy of IR leads to the formation of ~ 35 DSBs per cell (32). IR induced DNA damage is a convenient way of introducing high amounts of DNA damage that has been and still is used by many laboratories to assay functional aspects of the DNA damage response. However, a major drawback of using IR is the heterogeneity of the type of lesions introduced and the lack of spatial control. The DNA damage response is context dependent and differs for example for lesions in heterochromatic versus euchromatic regions (117), or depends on the quality of the lesion. Hence, fine mapping of DNA damage signaling networks requires the ability to introduce DSBs in a spatially and temporally controlled manner.

Endonuclease induced DSBs

Homing endonucleases are enzymes, which recognize specific DNA target sites and induce DNA cleavage (reviewed in (118). The first homing endonuclease to be identified was a protein called I-SceI that mediates lateral transfer of genetic information in yeast. The I-SceI recognition site is an 18 nt sequence, that is not present in either the mouse or human genome. If introduced by gene targeting or random integration, I-SceI sites can serve as unique recognition sites for the I-SceI enzyme, leading to the formation of a DSB. The advantage of this system is the exquisite temporal and spatial control over DSB formation. Also, the end structure of the broken DNA is known: cleavage of the I-SceI recognition site by the I-SceI endonuclease results in a 4 nt 3' overhang. Similar to I-SceI, the HO endonuclease in yeast, which initiates mating type switching, is commonly used to address DNA damage and repair kinetics.

Dysfunctional telomeres

Telomeres are specialized structures at the ends of linear chromosomes that protect them against degradation. Linear chromosomes are protected from recognition by the DNA damage response by the presence of telomeric DNA and the protein complex shelterin, which specifically binds to telomeric repeat sequences (reviewed in (119). Shelterin is composed of six individual proteins: TRF2, TRF1, POT1, RAP1, TIN2 and TPP1. The absence of protective factors leads to the activation of the DNA damage response and DNA repair, leading to aberrant chromosome-to-chromosome fusions. Loss of the shelterin component POT1 leads to the activation of ATR kinase signaling, leading to predominantly post-replicative chromatid or sister fusions (120, 121).

In contrast, the absence of TRF2 leads to the rapid activation of the ATM signaling pathway resulting in chromosome-type fusions involving ~30-60% of all chromosomes, detectable in metaphase spreads or in southern blot assays (120, 122, 123). Upon TRF2 deletion, DNA damage response factors such as the MRN complex, ATM, γH2AX, MDC1 and 53BP1 accumulate at the telomeric repeat sequences in specialized structures, called telomere dysfunction-induced foci and promote checkpoint signaling and fusion (124-126). Interestingly, DNA damage response factors are required for fusion of dysfunctional telomeres. For instance, NBS1 deficiency leads to a failure to activate ATM signaling, revealing that the MRN complex is the sole sensor for ATM activation (127). Furthermore, loss of NBS1 leads to abrogated chromosome fusions in G1. Similarly, ATM deficiency leads to ~ 15 fold reduction in chromosome fusion (122). Strikingly, the most severe fusion defect is observed in the absence of 53BP1, where only 1-2% of residual fusions are detectable (124). Telomere fusions in the absence TRF2 are facilitated by telomere mobility, which allows for the sampling and eventually encounter other telomeres to initiate the fusion reaction. The absence of 53BP1 in this context was shown to severely compromise the mobility of dysfunctional telomeres in an ATM dependent manner, indicating that 53BP1 enhances chromatin dynamics and thereby facilitates joining of distal chromosome ends (124).

Facilitated by DNA damage response factors, chromosome fusions in the absence of TRF2 are dependent on LIG4 and KU70 activity and are therefore mediated by the C-NHEJ pathway in the G1 phase of the cell cycle (122, 128).

V(D)J recombination and CSR

The immune system requires DSBs as intermediates during endogenous rearrangement reactions that generate antibody diversity and enhance its ability to recognize and eliminate antigens. Many discoveries, especially related to the end-joining pathways, have been made using developing lymphocytes as model system for DNA repair. The following sections will describe the rearrangement reactions and the ensuing steps of DNA damage recognition and repair in detail.

DSBs in Immune System Diversification Reactions

Adaptive immunity has evolved to effectively protect against a wide array of disease-causing organisms. Receptors on B and T lymphocytes are capable of recognizing the enormous diversity of pathogens by displaying an almost infinite range of antigen binding specificities. This remarkable variety cannot be encoded in the genome, but is created *de novo* by somatic gene alteration mechanisms. Immunogloblins (Igs) are the antigen receptors on B cells, and are either expressed on the cell surface or secreted into the bloodstream as soluble antibody molecules. Though not a focus of this thesis, antigen recognition by T cells is mediated by a membrane bound T cell receptor, of which, however, no soluble version exists.

Antibody diversification mechanisms

An antibody molecule consists of two identical heavy chains and two identical light chains (Figure 1.3 A). The heavy chains are connected to each other and to the light chains through disulfide bonds. The N-terminal portions of the heavy and light chains physically interact with the antigen and are collectively referred to as the antigen-binding site or variable region (Figure 1.3 B). Not surprisingly it is this part of the antibody molecule that needs to display the highest degree of diversity. Early in B cell development, before exposure to antigen, B cells assemble the variable region by a process called V(D)J recombination, which involves the combinatorial shuffling of different gene segments. Assembly of the variable region of the heavy chain involves rearrangement of variable (V), diversity (D) and joining (J) gene segments. The variable region of the light chain

is assembled by a rearrangement reaction of V and J gene segments only, either at the Igλ or Igκ locus. After stimulation with antigen, B cells can undergo two additional Ig diversification reactions: Somatic Hypermutation (SHM) and Class Switch Recombination (CSR).

SHM introduces non-templated point mutations into the previously assembled variable region. Mutations resulting in increased affinity for the antigen are selected for in the germinal center reaction, yielding antibodies of enhanced specificity to the antigen.

CSR modifies the C-terminal portion of the antibody molecule, also called the constant region. The constant region determines the IgH isotype of the antibody and antibodies of different isotypes mediate different effector functions. During CSR one constant region is exchanged for another through a deletional recombination reaction. Thereby CSR alters the effector function of the antibody molecule but maintains the same antigen specificity.

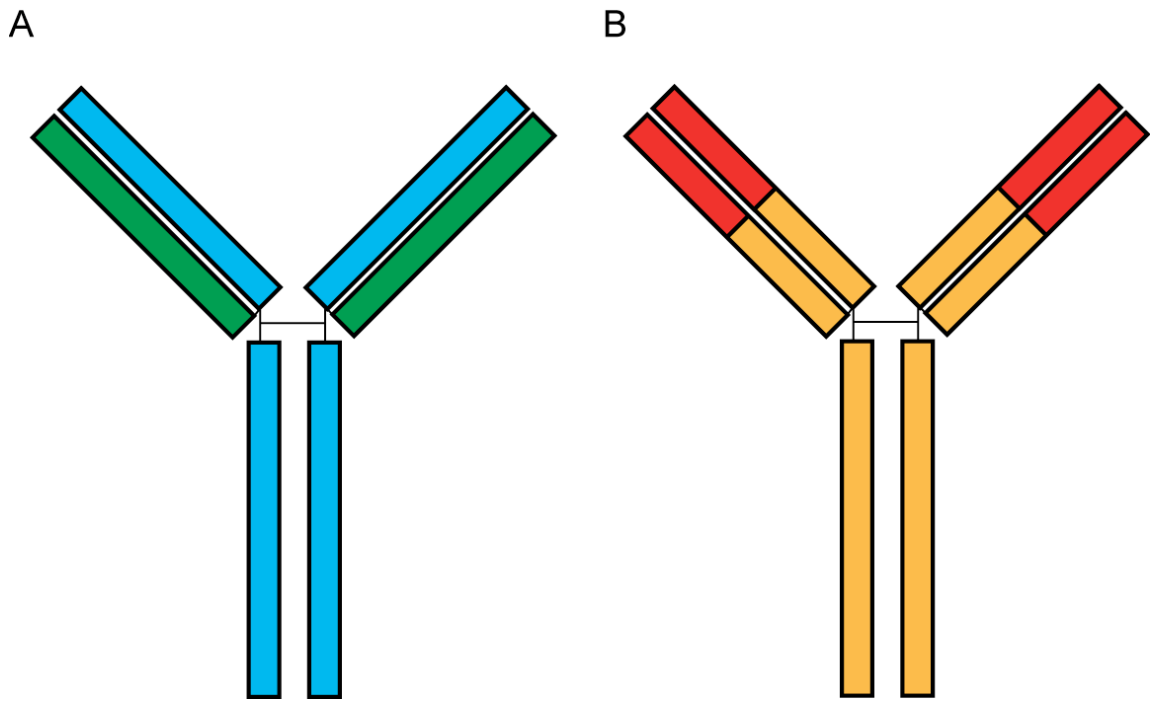

Figure 1.4. Schematic of an Immunoglobulin molecule.
(A) Immunoglobulins are composed of two identical heavy chains (blue) and two identical light chains (green). Disulfide bonds connect heavy chains to each other and light chains to heavy chains.
(B) Shown in red is the variable (V) – region, which recognizes and physically interacts with antigen. Shown in orange is the constant region, which is encoded by the immunoglobulin heavy chain locus and determines the effector function of the antibody.

V(D)J recombination

V(D)J recombination is the reaction through which the variable region is assembled in developing B and T lymphocytes. In this section V(D)J recombination is described using the assembly of the variable region of the heavy chain in B cells as an example. Though different in details, the general mechanism is conserved for light chain assembly and during T cell receptor rearrangement.

The process of V(D)J recombination involves the *de novo* combinatorial assembly of V, D and J gene segments and solves the problem of how antigens of unlimited diversity can be recognized by highly specific antigen receptors with only a limited number of available genes. The mouse Ig heavy chain locus (IgH) contains several hundred V, 13 D and 4 J gene segments spanning a ~ 1 Mb region on chromosome 12. Expression of the Recombinase Activating Genes 1 and 2 (RAG 1 and 2) initiates V(D)J recombination. Both the expression of RAG1 and RAG2 is strictly limited to developing B and T lymphocytes (129, 130) and absolutely required for V(D)J recombination (131, 132).

Recombination signal sequences (RSS), which flank each gene segment, serve as the recognition sites for the RAG recombinase enzymes. RSS consist of a conserved heptamer and nonamer sequence separated by either 12 or 23 nt of non-conserved spacer sequence (133, 134). Spacer sequences guide the assembly of the variable region, as RAGs are only able to join gene segments flanked by an RSS with a 12 nt spacer to segments containing a 23 nt spacer. All V and J gene segments are flanked by a 23 nt RSS while all D gene segments are flanked by a 12 nt RSS. This arrangement prevents nonproductive recombination within gene segment families.

In the precleavage complex, RAG1/2 associate with the respective gene segments by binding to the conserved nonamer and heptamer sequences (135, 136). The RAGs then introduce a single-stranded nick between the gene segments and the non-coding RSS heptamer . This creates a nucleophilic 3'OH group at the 3' end of the gene segment, which attacks the opposite DNA strand leading to the formation of a hairpin (referred to as the coding end; (137, 138). The RSS containing end of the DSB remains blunt (referred to as the signal end).

The RAG complex reamins associated with the broken DNA in a post-cleavage complex in order to protect DNA ends from degradation, recruit repair factors or aid in the positioning of ends for completion of the joining reaction (139, 140).

Ligation of the two gene segments requires the C-NHEJ machinery, comprising of KU70/80, XRCC4 and LIG4 (reviewed in (94). The signal ends are blunt and provide an immediate substrate to the C-NHEJ machinery. In contrast, in order for the coding ends to be joined, the protective hairpins at the respective gene segments must first be opened. This is accomplished by the action of the endonuclease Artemis, which is phosphorylated and activated by DNA-PKcs (101, 103, 104). The opening of the hairpin generates a substrate for additional modifications of the coding ends such as nucleotide additions and deletions by the lymphocyte specific enzyme TdT, leading to yet another layer of diversification beyond the combinatorial gene rearrangement process itself (141). Once the coding ends have been processed, the XRCC4 and LIG4 ligation complex performs the joining reaction. C-NHEJ factors are absolutely required for V(D)J recombination. The absence of any of the evolutionarily conserved C-NHEJ factors (KU70, KU80, XRCC4 or LIG4) leads to a complete absence of rearranged antigen receptor genes, resulting in a severe combined immunodeficiency (SCID) phenotype (142-145). Similarly, mice deficient for DNA-PKcs or Artemis display a SCID phenotype due to the inability of coding joint formation (103, 104, 146).

The sustained presence of RAG proteins in a post-cleavage complex is thought to "shepherd" the repair of the broken ends towards the C-NHEJ pathway (147). RAG mutants that retain their ability to perform the cleavage reaction but lose their ability to remain associated after cleavage show a dramatically increased

incidence of HR using reporter substrates (148). Furthermore, removal of the RAG2 C-terminus allows for repair of DSBs by the microhomology dependent A-NHEJ, indicating that this part of the molecule is crucial for channeling the repair towards C-NHEJ (147). The A-NHEJ activity in cells expressing a RAG2 C-terminal truncation protein was shown to be independent of C-NHEJ factors such as XRCC4 and DNA-PKc. A-NHEJ in the absence of the RAG2 C-terminus was surprisingly robust, suggesting that while the A-NHEJ machinery is expressed in wild type cells, it is actively excluded during V(D)J recombination by the RAG enzymes (147).

V(D)J recombination proceeds via RAG induced DSB intermediates, leading to the activation of the canonical DNA damage response. ATM induced γH2AX focus formation can be detected at the TCRα locus during V(D)J recombination (149). Mice deficient for ATM and H2AX show a reduction in the number of B and T lymphocytes in the bone marrow and thymus, but do not display an overt V(D)J recombination defect by themselves (37, 150, 151). Interestingly the absence of the effector protein 53BP1 does not lead to a joining defect per se, but selectively impairs the joining of distal V to DJ segments during the assembly of the TCRα locus (152). Thus, the absence of DNA damage response factors leads to an at most moderate defect in V(D)J recombination and is not considered an integral component of the V(D)J recombination reaction. However, the absence of functional DNA damage recognition leads to an increased half-life of DSB intermediates, which may become substrates for chromosome translocations (150, 153).

Class Switch Recombination

The IgH isotype of an antibody molecule is determined by the expression of one of eight heavy chain constant region (C_H) genes: Cμ, Cδ, $C\gamma_3$, $C\gamma_1$, $C\gamma_{2b}$, $C\gamma_{2a}$, Cε and Cα (Figure 1.4 A). C_H genes are clustered in this order in a region spanning ~200 kb on the heavy chain locus on mouse chromosome 12, downstream of the V, D and J gene segments. Naïve B cells emerging from the bone marrow having assembled a functional variable region initially express the constant region genes Cμ and Cδ and are therefore IgM and IgD positive. CSR is the mechanism by which upon antigen encounter, B cells exchange the initially expressed constant region genes Cμ/Cδ for a different constant region gene (Figure 1.4 B-D). Different IgH isotypes are responsible for mediating different effector functions: antibodies of IgM isotype typically form pentamers and are predominantly found in the bloodstream where they can efficiently bind to bacterial polysaccharide antigens. In contrast, antibodies of IgA isotype can be secreted across the mucosal epithelium and into milk. The most abundant IgH isotype with its various subtypes, IgG, can neutralize toxins and viruses and opsonize pathogens for phagocytosis. Furthermore, different IgH isotypes bind and activate distinct Fc receptors on immune effector cells (such as macrophages, neutrophils or eosinophils) and can activate different arms of the complement system.

Mechanistically, CSR is a deletional recombination reaction that similarly to V(D)J recombination necessitates DSB intermediates at the regions to be joined together. However, in contrast to V(D)J recombination DSB formation during

CSR does not occur at a precisely defined location such as a RSS, but is targeted to switch regions, the non-coding stretches of repetitive DNA preceding each constant region gene (except for Cδ). Once DSBs are formed, they are recognized by the DNA damage response, which facilitates the successful completion of CSR. Finally, two DSBs in two different S-regions are joined together by the C-NHEJ or A-NHEJ DNA repair machinery. In the next sections, the three steps of CSR (formation of the DSB, activation of DNA damage response, and DNA end joining) will be discussed in more detail.

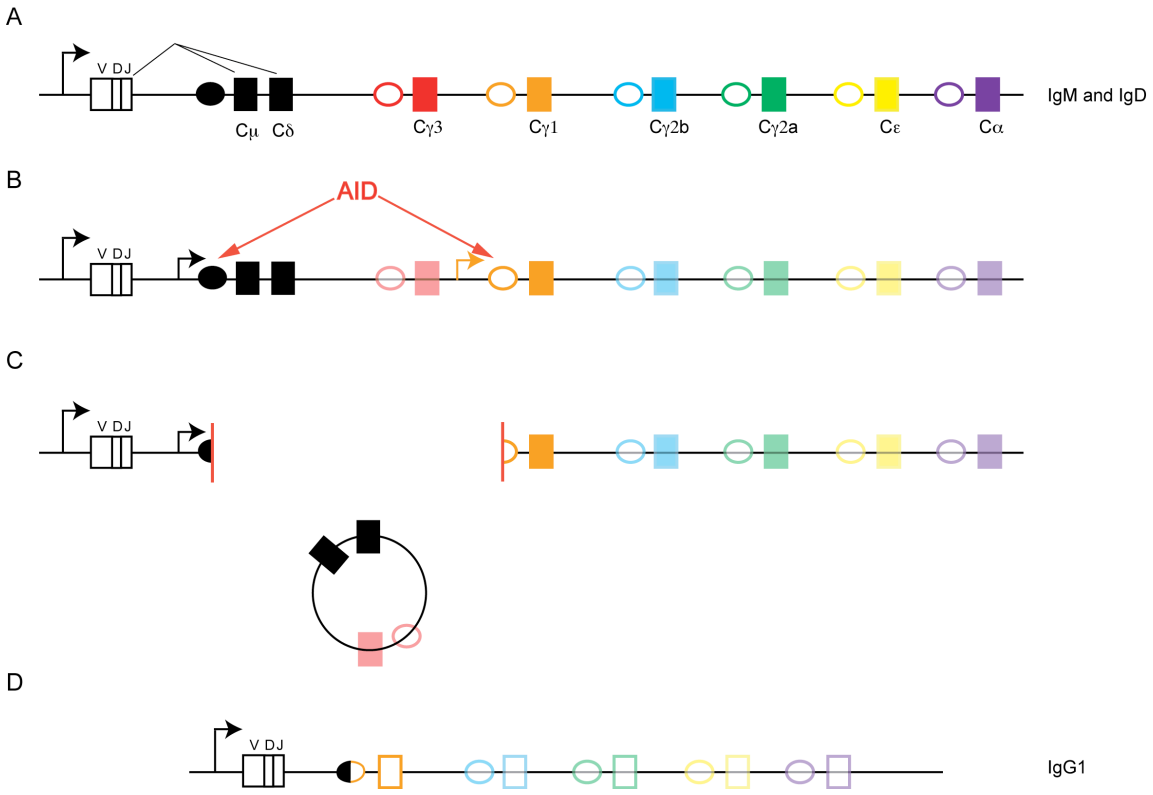

Figure 1.5. CSR is a deletional recombination reaction with DSB intermediates.
(A) Structure of the IgH locus with constant region genes (rectangles) and unique S-regions (circles) preceding the respective constant region genes. Naïve B cells express IgM and IgD by alternative splicing.
(B) Upon antigen encounter *in vivo* or *in vitro* stimulation with cytokines, S-region and constant region transcription is initiated. AID expression is induced and deamination activity is targeted to S-regions.
(C) Deaminated cytosines are processed into DSBs in donor and acceptor S-regions.
(D) The intervening sequence is excised, circularized and lost from the genome. Two DSBs are joined together, resulting in a hybrid S-region and expression of the same variable region with a new constant region.

Formation of DSBs inS-regions by AID

DSB formation in S-regions is initiated by activation-induced cytidine deaminase (AID), an enzyme that deaminates cytosine residues leading to their conversion into uracils. AID was discovered through a subtractive hybridization screen in the murine cell line CH12F3 by Tasuku Honjo's group in 1999 (154) and subsequently shown to be essential for CSR and SHM in both mice (155) and humans (156). Loss of AID in mice leads to the complete absence of CSR and SHM. Similarly, human patients harboring mutations in the *aicda* gene display Hyper-IgM syndrome, indicative of the failure to produce antibodies of different isotypes. The homology to the RNA editing enzyme APOBEC-1 at first suggested that AID acts on RNA (155). However, *in vitro* deamination assays with purified AID and evidence for mutation in bacterial genes upon ectopic AID expression soon revealed that the target of AID deamination activity is not RNA but cytosines in single-stranded DNA during transcription (157-162). In addition, it was shown that γH2AX and NBS1 DNA damage foci form in an AID dependent manner at the IgH locus in B cells stimulated to undergo CSR, suggesting that the deamination of cytosines by AID is required for DSB formation (163). Subsequently, the use of LM-PCR has shown the fragmentation of S-regions is AID dependent (164). These findings showed that AID activity is required for DSB formation, but could not explain the mechanism by which a cytosine deamination event is transformed into a DSB. Neuberger's group and others showed that members of the Base Excision Repair (BER) machinery recognize and process the mismatch into a SSB. After cytosine deamination the resulting uracil forms a mismatch with guanine, which is recognized and the uracil excised

by uracil DNA glycosylase (UNG; (160, 165, 166)). Mice deficient for UNG display greatly reduced CSR levels and strongly reduced DSB formation at S-regions (165). Similarly, patients with mutations in UNG display Hyper-IgM syndrome, indicative of a CSR deficiency (167). After UNG activity the ensuing abasic site is detected by members if the APE endonuclease family, which make incisions in the phosphate backbone at the site of the lesion, leading to the transformation of an abasic site into a SSB (168). The absence of members of the BER machinery severely impairs CSR.

The Mismatch Repair (MMR) pathway contributes to DSB formation after cytosine deamination by AID, but is not absolutely required for CSR (169-174). The MSH2-MSH6 complex recognizes a nucleotide mismatch, which is thought to recruit Exo1, leading to the excision of the mismatched nucleotide by strand resection (175). Long-range strand resection would lead to the formation of a DSB if another AID induced ssDNA lesion were encountered in the opposite strand. However, mice deficient for members of the MMR pathway display a CSR defect less severe than the absence of BER family members, leading to the conclusion that this pathway is required for the formation of some, but not all DSBs (169, 171, 173, 174, 176). How exactly the uracil:guanine mismatch induced by AID is converted into a DSB is still not completely understood and remains an active area of investigation.

AID preferentially deaminates WRCY motifs (W= A or T, R= A or G, Y= C or T) (161). While S-regions are enriched for these motifs, WRCY sequences are not exclusively found in those regions and are also present at other locations in the genome. Aberrant AID activity at non-Ig genes contributes to cancer formation

by introducing point mutations in tumor suppressor genes or through DSB induced chromosome translocations (177-181). Hence, targeting of AID to its physiologic substrates is crucial for the maintenance of genome integrity. AID activity is associated with transcribed genes. Stimulation of B cells with cytokines either in a germinal centre or *in vitro* induces differential transcription of S-regions from their cytokine inducible promoters (182-184). For example, stimulation with LPS and IL-4 stimulates germline transcription at Sμ and Sγ1. Only transcriptionally active S-regions become substrates of AID deamination activity and will undergo CSR. It is therefore plausible that transcription plays a role in AID targeting (185). Consistent with this hypothesis of transcriptional targeting, AID has been shown to interact with RNA Pol II (186, 187). Recently, the interaction of AID with RNA Pol II and its targeting to S-regions was shown to be dependent on the transcriptional elongation factor SPT5 (187). Interestingly, SPT5 normally associates with Pol II during transcriptional stalling and the Ig locus harbors the highest levels of SPT5 and therefore stalled polymerases in the B cell genome. Transcriptional stalling could provide AID with sufficient time and ssDNA substrate for the deamination activity. However, in such a model only the non-template strand is single stranded; the template strand associates in a duplex with the nascent transcript. Recently, the RNA exosome complex has been shown to impart AID deamination activity onto both the non-template and template strands in vitro, possibly involving RNA removal from the template strand by polymerase backtracking during stalling *in vivo* (188).

The DNA damage response during CSR

The formation of DSBs in S-regions leads to the activation of the canonical DNA damage response. As described in the previous Chapter, the sensor that recognizes DSBs is the MRN complex, which recruits the ATM kinase to the site of the break (11, 12). ATM is responsible for cell cycle arrest and recruitment of downstream repair factors. One major target of the ATM kinase is the C-terminal tail of histone variant H2AX, which is phosphorylated on serine 139. The phosphorylation of H2AX spreads on nucleosomes to areas surrounding the DSB, which leads to the amplification of the DNA damage signal (33). γH2AX then recruits a variety of downstream mediator proteins, such as MDC1, RNF8, RNF168 and 53BP1 (49). The accumulation of DNA damage response factors at the *IgH* locus during CSR can be detected in immuno-FISH experiments (163, 189). Interestingly, DNA damage response factors are required for efficient CSR, but the mechanistic basis of how CSR is facilitated is not understood. For instance, loss of the DNA damage-sensing component NBS1 leads to a two- to three-fold decrease in CSR efficiency (190). Similarly ATM deficiency leads to an approximately three-fold reduction of CSR levels (191, 192). A more severe CSR defect is observed in the absence of H2AX, in which B cells undergo CSR at a four-to five-fold reduced frequency (193). Strikingly, the most pronounced CSR defect occurs in the absence of 53BP1 (194, 195). Loss of this molecule leads to an almost complete abrogation of CSR to all isotypes. As described in the previous chapter, 53BP1 focus formation after DNA damage depends on the binding of its tandem tudor domain to H4K20me2. However, the combined conditional deletion of SUV4-20H1 and SUV4-20H2, the enzymes responsible for dimethylation of H4K20, show only two-to three-fold reduction in CSR (69). This

relatively mild defect compared to the complete absence of CSR in 53BP1$^{-/-}$ B cells implies that 53BP1 is recruited to DNA damage foci through either a different histone modification or that the SUV4-20H1/H2 enzymes are not the sole methylatransferases mediating dimethylation of H4K20. Evidence for both alternatives exists: recently the methyltransferase MMSET was shown to dimethylate H4K20 locally after DSB formation. The contribution of MMSET towards CSR is not yet established, as mice deficient for this methyltransferase are not yet available for analysis. Alternative histone modfications to which the tudor domain could bind in the absence of H4K20me2 inculde H4k20me1 and H3K79me2. Furthermore, damage induced γH2AX dependent recruitment of RNF8 and RNF168 to chromatin and their subsequent ubiquitylation of histone H2AX is required for efficient accumulation of 53BP1 at the site of a DSB. Again, neither H2AX nor RNF8 deficient mice display a CSR defect as severe as 53BP1$^{-/-}$ mice (53). The combined absence of RNF8 and H2AX leads to CSR levels that are comparable to the levels displayed by H2AX$^{-/-}$ mice, suggesting that those two proteins act epistatically (53). The contribution of RNF168 to CSR has only been assessed using siRNA in CH12 cells, which yielded reduced CSR to levels less severe than RNF8. Human patients with a mutation in *rnf168* have severely reduced serum Ig levels, indicative of a CSR defect. However, a mouse model for RIDDLE syndrome is not yet available.

While loss of 53BP1 leads to the most severe CSR defect of all DNA damage response proteins assayed to date, switch region internal deletions (joining of two DSBs within the same S-region) occur at elevated levels (196). This is especially interesting considered that loss of ATM or loss of H2AX does not lead

to increased S-region internal deletions (193). This clearly indicates a role for 53BP1 during CSR that is not shared by other DNA damage response factors in the ATM signaling pathway.

End-joining during CSR

AID mediated DSBs are limited to the G1 phase of the cell cycle (164). As described in the previous Chapter, C-NHEJ is the preferred pathway for repairing DSBs in the absence of a proximal sister chromatid or homologue. The classical end-joining pathway, comprising of the KU70/80 complex, XRCC4 and LIG4, is characterized by the predominance of joins with no or little microhomology at the junction and minor (if any) nucleotide loss. Sequencing of switch junctions from B cells having successfully undergone CSR showed that the majority of joins contain little to no microhomology, indicating that C-NHEJ joins DSBs during CSR (197). As C-NHEJ is absolutely required for V(D)J recombination, the effects of C-NHEJ deficiency in the context of CSR can only be addressed using mice with preassembled Ig light and heavy chain (IgH+L) knock-in alleles or in mice with conditional deletions of C-NHEJ factors at a late B cell developmental stage, following V(D)J recombination. Using those systems, it was shown that the C-NHEJ pathway is not absolutely essential for CSR, as the absence of either XRCC4 or LIG4 leads to surprisingly robust CSR at ~ 50% of wilt type levels (112, 113, 197-199). Interestingly, in the absence of these molecules the spectrum of switch junctions changed dramatically towards the usage of junctional homologies, indicative of joining through the A-NHEJ pathway. However, absence of either LIG4 or XRCC4 retained the upstream components of the C-NHEJ pathway, which may have led to residual C-NHEJ by

the KU70/80 complex. Recently, the deletion of both LIG4 and KU70 in mice with preassembled IgH+L variable regions was shown to display relatively robust CSR at the level of $KU70^{-/-}$ B cells, leading to the conclusion that A-NHEJ is a truly independent pathway that can ligate DSBs suring CSR (198). Interestingly, the absence of KU70 alone or the combined absence of KU70 and LIG4 lead to significantly more direct joins than the absence of LIG4 alone. This indicates that the A-NHEJ in the absence of LIG4 proceeds through a KU complex dependent pathway (198). It is possible that there are more types of A-NHEJ: one that is KU dependent and one that functions in the absence of KU.

An alternative resolution of an AID induced DSB in activated B cells is the re-ligation of the break to either another DSB within the same S-region or to itself, leading to the formation of S-region internal deletions (ISDs). Such deletions were readily observed in the absence of C-NHEJ factors (LIG4, XRCC4, KU70, KU80), but rarely in wild type cells. This indicates that A-NHEJ preferentially ligates DSBs within one S-region. A possible mechanistic explanation for this observation is that microhomologies present within one S-region are the preferred substrate for A-NHEJ. Alternatively, A-NHEJ may have a preference for proximal joining while C-NHEJ may be more efficient at catalyzing distal joining events.

Somatic Hypermutation

SHM is the reaction whereby point mutations are introduced into B cell receptor variable region genes after antigen encounter (reviewed in (200). Similarly to CSR, SHM is strictly dependent on AID induced cytosine deamination. The resulting uracil is converted into a mutation by either replicating across the

mismatch, the action of BER pathway or processing by Mismatch Repair pathway. In contrast to CSR, hypermutation does not require DSB intermediates and is entirely unaffected by the absence of DNA damage response proteins and DNA repair proteins such as H2AX, 53BP1, KU80 and LIG4 (200). B cells with mutations that increase affinity to antigen are selected for and clonally expanded *in vivo*, leading to an improved clearance of the antigen.

Chromosome translocations as a byproduct of antigen receptor diversification reactions

DSBs pose a threat to genome integrity and can lead to chromosome rearrangements such as deletions, translocations or amplifications, which can lead to malignant transformation. While deletions occur on one chromosome in cis, chromosome translocations and amplifications involve the joining of one DSB on one chromosome to another DSB on a different chromosome. In a reciprocal translocation the telomeric portion of one chromosome is fused to the centromeric portion of another chromosome, resulting in the formation of two stable chromosomes. While balanced chromosome translocations can be stably propagated during cell division, non-reciprocal translocations can result in the formation of genetically unstable dicentric or acentric chromosomes. Particularly dicentric chromosomes pose a serious threat to genome integrity since their replication leads to additional DSBs, which can become substrates for yet more chromosome abnormalities.

Most hematopoietic malignancies harbor clonal reciprocal translocations (reviewed in (201). Lymphocytes are particularly prone to chromosome translocations as DSBs are obligate intermediates during their development.

Translocations can induce oncogenic transformation through different mechanisms. For example, a highly active promoter or cis-regulatory element can be juxtaposed to a proto-oncogene and now highly transcribed, the proto-oncogene acquires oncogenic potential. An "infamous" example is the juxtaposition of the 3' regulatory elements of the IgH locus to the c-myc proto-oncogene in B cells (202). Furthermore, a chromosome translocation can result in the expression of a chimeric protein by fusing together parts of two different genes. For example, the BCR-ABL fusion protein results in constitutively active abl kinase, leading to chronic myeloid leukemia (201).

Chromosome Translocations as a byproduct of V(D)J recombination

V(D)J- recombination is the first lymphocyte diversification reaction and requires DSB formation at antigen receptor loci in both B and T cells. The RAG1/2 enzymes are highly specific for RSS sequences, but can rarely produce DSBs in "off-target" genes containing cryptic RSS or genes with non-canonical DNA structure. Such aberrant targeting can lead to the joining of two different chromosomes (203-205). However, those events are rarely observed. In contrast, the absence of damage response factors, particularly ATM, results in the persistence of programmed RAG induced DSBs at antigen receptor loci, which more frequently become substrates for chromosome translocations (150). Mice deficient in C-NHEJ components do not display overt tumor susceptibility due to the intact p53 checkpoint, which efficiently eliminates cells with unrepaired DSBs. The combined absence of p53 and a C-NHEJ factor leads to rapid tumor development of predominantly B cell origin (206, 207).

AID induced translocations during CSR and SHM

In contrast to the exquisite specificity for the RSS displayed by the RAG enzymes, AID only has a weak preference for the WRCY motif that is strongly overrepresented in the IgH locus, but still relatively common genome wide. Many proto-oncogenes have been found to harbor AID dependent mutations, including c-myc, Bcl6, Pax5 and Pim1. In fact, almost 25% of the expressed genes in germinal center B cells harbor to some extent AID induced mutations, indicating the oncogenic potential of this mutator enzyme (178). Proof of the direct involvement of AID in the formation of chromosome translocations came from experiments showing that the *c-myc*/*IgH* translocation is dependent on AID and the downstream processing enzyme UNG (Uracil-N-glycosylase)(208). However, AID overexpression in itself is not sufficient for B cell transformation, only if p53 is concomitantly deleted can B cell tumors be detected (209). This indicates that intact checkpoint signaling networks are crucial for the maintenance of genome integrity in AID expressing B cells. Consistently, the checkpoint protein ATM, which is activated after AID induced DSB formation at the IgH locus during CSR, protects against chromosome translocations. $ATM^{-/-}$ B cells stimulated with cytokines in vitro display increased frequencies of *c-myc*/*IgH* translocations (208). In contrast, loss of the DNA damage protein 53BP1 does not increase the frequency of *c-myc*/*IgH* translocations, presumably due to the fact that the upstream checkpoint is intact and can eliminate cells harboring translocation that exhibit oncogenic stress (208). Interestingly, $53BP1^{-/-}$ B cells stimulated to undergo CSR contain many chromosome abnormalities that are limited to the IgH locus (196). Consistent with the hypothesis that translocations

inducing oncgenic stress are efficiently deleted through the activation of checkpoint proteins is the finding that the translocation frequency between IgH and Igβ, which does not lead to oncogenic stress, is not altered in the absence of p53 (210).

Furthermore, loss of C-NHEJ proteins leads to increased chromosome translocation in the absence of p53. Interestingly, sequencing of translocation breakpoints showed extensive microhomology at the junction, indicative of joining by the A-NHEJ pathway (114, 116). Consistent with the idea that A-NHEJ catalyzes chromosome translocations, I-SceI endonuclease induced translocations do not depend on C-NHEJ factors and are mediated in part by A-NHEJ (115, 189). It is possible that C-NHEJ is protective against chromosome translocations by actively excluding the more translocation prone A-NHEJ pathway.

Summary and Outlook

DSBs are necessary intermediates for both V(D)J recombination and CSR. Particularly CSR, and to a lesser extent V(D)J recombination, relies on a functional DNA damage response for successful completion of the rearrangement reaction. Among DNA damage response factors, the most pronounced defect in CSR occurs upon loss of 53BP1, a chromatin binding protein that is also an ATM target. Only distal DSB joining between two S-regions is impaired in the absence of 53BP1, while S-region internal deletions, which occur between proximal DSBs within one S-region, are in fact increased (194-196). Similarly, only distal V-DJ joining is affected by the absence of 53BP1 during V(D)J recombination (152). In addition, the distal joining of de-protected

telomeres resulting in chromosome fusions is strongly impaired in the absence of 53BP1 (124). Several non-mutually exclusive models have been proposed to account for the effects of 53BP1 on CSR, V(D)J recombination, and telomere fusion: 53BP1 may enhance synapsis and long-range interactions between two distal DSBs and thereby promote CSR (194-196) possibly by altering local chromatin structure (152) or increasing chromatin mobility (124). Interestingly, the defects observed in the absence of 53BP1 are more severe than in the upstream regulators such as ATM or H2AX, leading to the conclusion that 53BP1 plays an additional role in those reactions.

While DNA damage factors are required to facilitate CSR, they are also crucial for the maintenance of genomic integrity. Loss of functional DNA repair can lead to chromosome translocations, which are often found in immune cell tumors of mice that lack DNA damage response factors.

In Chapter 2 I will describe experiments in which we use the I-SceI meganuclease system to investigate the etiology of the *c-myc*/*IgH* translocation that arises as a byproduct of CSR. In Chapter 3 I apply the I-SceI system to introduce paired intra-chromsomal DSBs on mouse chromosome 12 in B lymphocytes to systematically examine the role of 53BP1 and chromosomal distance in DSB joining. In Chapter 4 I investigate the role of 53BP1 in DNA repair pathway choice. Lastly in Chapter 5, I focus on the functional domains of 53BP1 and determine their contributions towards CSR and repair pathway choice.

CHAPTER 2:

Role of AID in the Formation of *c-myc/IgH* Chromosome Translocations

Chromosome translocations require paired DSBs on heterologous chromosomes. B cell lymphomas often harbor characteristic chromosome translocations, frequently involving their antigen receptor genes (201). DSBs that arise during antigen receptor diversification reactions such as CSR and SHM can become substrates for chromosome translocations that can initiate oncogenic transformation. Both SHM and CSR are strictly dependent on AID activity. While AID acts predominantly on *IgH* switch regions during CSR and variable region genes during SHM, non-Ig loci can harbor AID dependent mutations, although at a lower frequency than physiologic targets (178). The proto-oncogene *c-myc*, which is the translocation partner of *IgH* in human Burkitt's lymphoma and mouse plasmacytoma (211-222) displays AID dependent mutations that are orders of magnitude lower than at the *IgH* locus, and is also less frequently mutated than many other AID off-target genes (178). The source of the DSB in the antigen receptor loci is clearly dependent on AID; the source of the DSB in *c-myc* however remains enigmatic (208, 223). Besides the possibility that AID activity is responsible for DSB formation at *c-myc*, sources for DSBs in *c-myc* include non-canconical, fragile DNA configurations such as Z-DNA, H-DNA and G-quadruplex DNA (224-226). Such structural variations could enhance susceptibility to spontaneous DSB formation during transcription or replication. In addition, metabolic intermediates such as reactive oxygen species have been

implicated in the generation of DSBs at *c-myc* that lead to its translocation to *IgH* (227).

In the following chapter we will induce artificial DSBs with the yeast endonuclease I-SceI to examine the role of AID in DSB formation at the *c-myc* locus that leads to the *c-myc*/*IgH* translocation.

AID overexpression leads to DSBs and mutations at *c-myc*

AID dependent DSBs during CSR can be detected by the efficient accumulation of the DNA damage response protein 53BP1 at the *IgH* locus (Figure 2.1). In contrast, physiologic levels of AID expression during CSR did not result in 53BP1 accumulation at *c-myc* (Figure 2.1). Only retroviral overexpression of AID leads to detectable 53BP1 focus formation at *c-myc*, indicating that *c-myc* can be a target of AID activity (Figure 2.2 A). Similarly, the AID mutation footprint can be detected at *c-myc* only if AID is retrovirally overexpressed (Figure 2.2 B).

Figure 2.1. Wild type B cells show AID-dependent focus formation at IgH, but not *c-myc*.

(A) Immuno-FISH analysis of 53BP1 DNA damage foci at *IgH* or *c-myc* loci in activated B cells. Representative images showing co-localization of the indicated loci with 53BP1 in LPS and IL-4 stimulated wild type (WT) B cells.

(B) Immuno-FISH analysis of 53BP1 DNA damage foci at *IgH* or *c-myc* loci in activated B cells. Representative images showing co-localization of the indicated loci with 53BP1 in LPS and IL-4 stimulated $AID^{-/-}$ B cells.

(C) Table showing co-localization frequencies as percentage of cells analyzed in LPS and IL-4 stimulated wild type (WT) and $AID^{-/-}$ B cells. The number of cells analyzed is shown in parentheses. Three independent experiments.

A

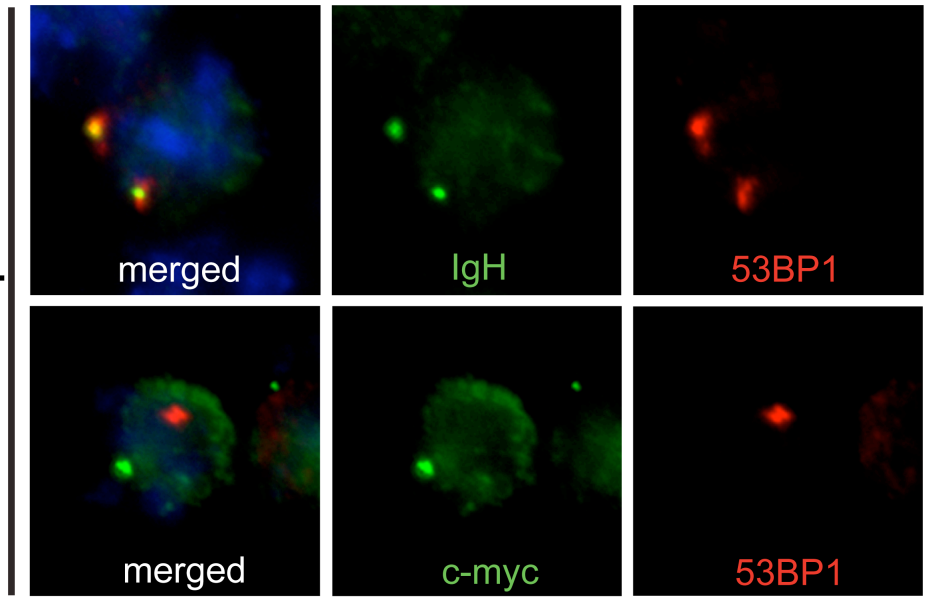

B

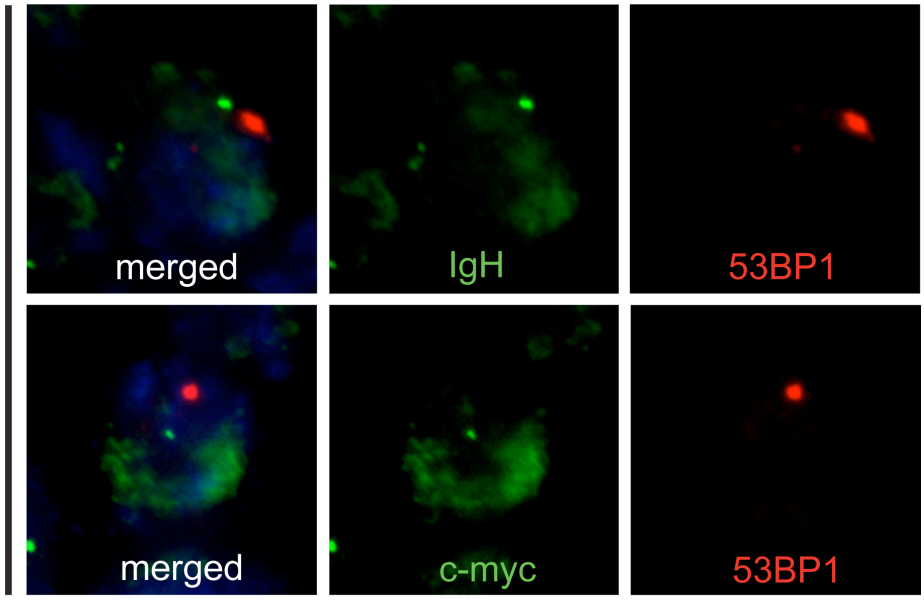

C

	IgH	c-myc
WT	42.5% (219)	6.8% (132)
AID$^{-/-}$	7.6% (211)	5.4% (223)

A

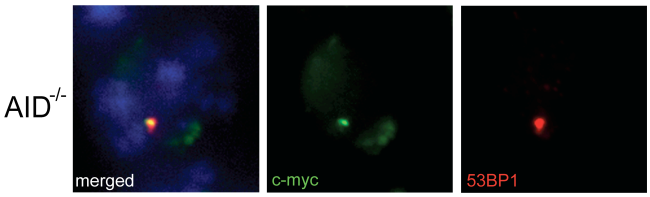

	+ AID	+ empty
AID$^{-/-}$	12.2% (171)	4.3% (186)

B

Genotype	Retrovirus	Frequency of unique mutations	Mutations at C/G (%)	Transitions at C/G (%)
WT	-	0.3 x 10^{-4} (87890)	33.3	100
AID$^{-/-}$	AID	1.2 x 10^{-4} (101541)	66.7	75
AID$^{-/-}$	empty	< 0.07 x 10^{-4} (136800)	-	-

Figure 2.2. Retroviral overexpression of AID leads to DSBs and mutations at *c-myc*.
(A) Immuno-FISH analysis of AID induced 53BP1 DNA damage foci in AID$^{-/-}$ B cells infected with AID or empty virus control. Representative images and table showing co-localization frequencies at *c-myc*. The number of cells analyzed is shown in parentheses. p = 0.007 with student's t-test. Three independent experiments.
(B) Mutation frequency at *c-myc* locus of wild type (WT) or AID$^{-/-}$ B cells infected with the indicated retroviruses. Indicated in parentheses are the total number of nucleotides analyzed.

I-SceI induced DSBs at *c-myc* and *IgH*

To further examine the requirements and consequences of DSB formation at *c-myc* and *IgH* at physiologic AID levels, we introduced I-SceI recognition sites by gene targeting at both *c-myc* and *IgH* (Myc$^{I/+}$ and IgH$^{I/+}$ respectively, for details see Methods section). In the absence of AID, retroviral infection of Myc$^{I/+}$AID$^{-/-}$ or IgH$^{I/+}$AID$^{-/-}$ B cells with the enzyme I-SceI leads to efficient DSB formation at

Myc$^{I/+}$ and IgH$^{I/+}$, respectively (Figure 2.3). In contrast, a retrovirus harboring a catalytically inactive I-SceI* did not induce 53BP1 focus formation in the I-SceI-site bearing lymphocytes. We therefore conclude that I-SceI efficiently and specifically introduces DSBs at loci bearing its recognition sites in primary B cells.

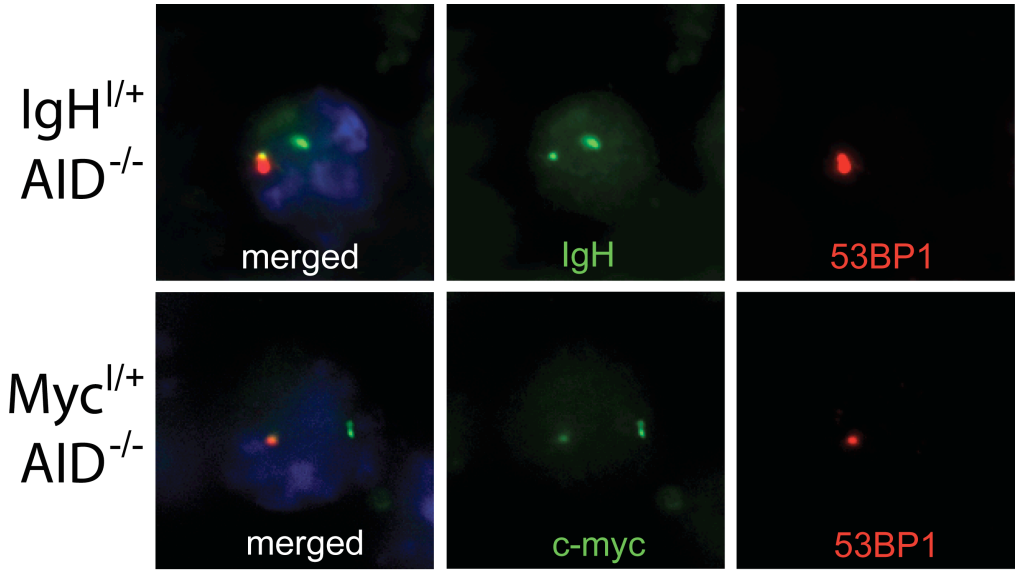

		I-SceI	I-SceI*
IgH$^{I/+}$	AID$^{-/-}$	21.9% (91)	7.5% (80)
Myc$^{I/+}$	AID$^{-/-}$	30.8% (68)	8.3% (72)

Figure 2.3. I-SceI induced DSBs at *c-myc* and *IgH*.
Immuno-FISH analysis of I-SceI induced 53BP1 DNA damage foci in IgH$^{I/+}$AID$^{-/-}$ (top) or Myc$^{I/+}$AID$^{-/-}$ B cells (bottom). Representative images and table showing co-localization frequencies at *IgH* or *c-myc* (as indicated) in I-SceI or I-SceI* expressing B lymphocytes. The number of cells analyzed is shown in parentheses.

I-SceI induced translocations in AID deficient B lymphocytes

To establish whether I-SceI induced DSBs at *c-myc* and *IgH* can serve as substrates for *c-myc*/*IgH* translocations, we generated $Myc^{I/+}IgH^{I/+}AID^{-/-}$ B cells (Figure 2.4 A). Retroviral infection with I-SceI to introduce DSBs at both loci leads to robust *c-myc*/*IgH* translocation, while catalytically inactive I-SceI* does not ($10x10^{-5}$ for I-SceI infection versus 0 for I-SceI*, Figure 2.4 B). To precisely establish where the DSB occurred, we sequenced translocation junctions. The range of translocation breakpoints as determined by sequencing of PCR junctions varied from 0 - 2178 nt away from the I-SceI site (Figure 2.4 C). 19 out of 21 translocation junctions sequenced harbored 1-7 nt microhomology at the junction, and two included insertions (Figure 2.5 D). We conclude that I-SceI can efficiently mediate *c-myc* to *IgH* translocation in $Myc^{I/+}IgH^{I/+}AID^{-/-}$ B cells and that translocations are frequently processed leading to the formation of microhomolgy at the junction.

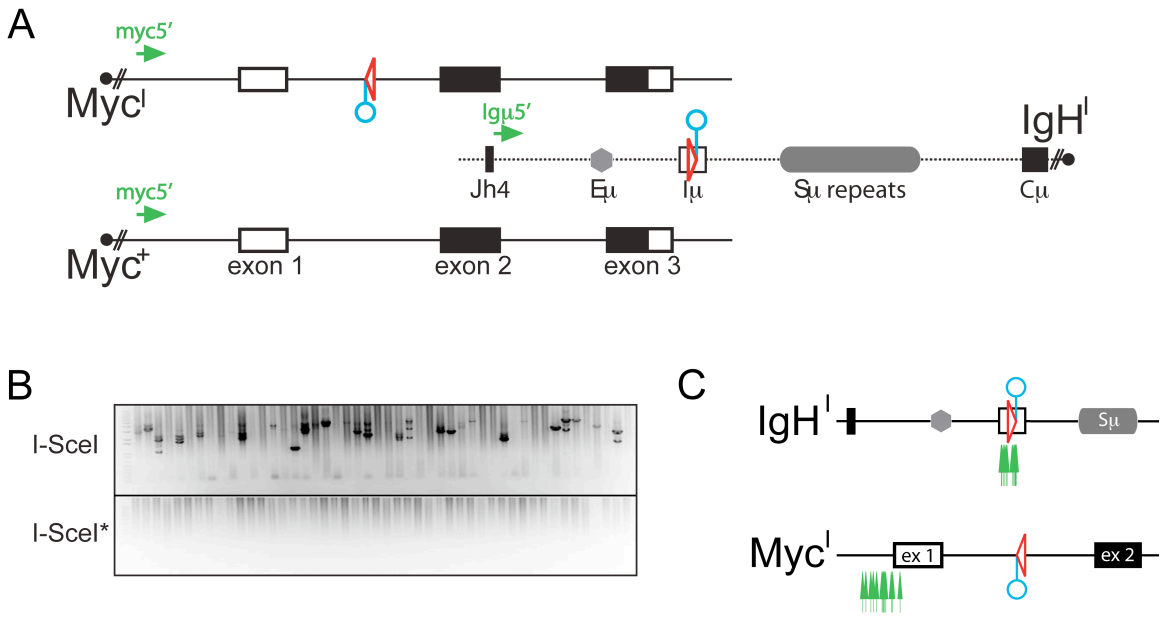

Figure 2.4. I-SceI induced translocations in AID deficient B lymphocytes.

(A) Schematic representation of the Myc^{I}, Myc^{+} and IgH^{I} alleles with the PCR primers for detecting der15 *c-myc/IgH* translocations. Circles point to the position of the I-SceI sites.

(B) I-SceI rescues translocations in the absence of AID. Representative agarose gels with PCR products corresponding to *c-myc/IgH* translocations (as verified by sequencing and/or Southern Blot). The size of PCR amplified translocation products varies significantly depending on DNA repair induced sequence deletions at the junction. $Myc^{I/+}IgH^{I/+}AID^{-/-}$ B cells were stimulated with LPS and IL-4 and infected with I-SceI or I-SceI* control retroviruses. 100,000 cells were assayed in each lane. Three independent experiments.

(C) Map of translocation breakpoints from I-SceI expressing $Myc^{I/+}IgH^{I/+}AID^{-/-}$ B cells. Arrows point to *c-myc/IgH* translocation breakpoints for der15.

DSBs in *c-myc* are limiting for *c-myc*/*IgH* translocations

To determine whether I-SceI induced DSBs can be joined to AID induced DSBs, we infected $Myc^{I/+}$ B cells with I-SceI or I-SceI*. The translocation frequency was significantly increased in the presence of I-SceI induced DSBs versus I-SceI*($0.8x10^{-5}$ and $0.2x10^{-5}$ respectively, Figure 2.5). In agreement with this result, we found by sequencing translocation junctions that 15 out of 17 translocations were directly at or within 74 nt of the I-SceI site. The two remaining translocations involved the wt allele. In contrast, all translocations from wild type B cells spread over several kb around exon 1. The translocation junctions involved predominantly blunt joins, or a small degree of microhomology (1-3 nt, Figure 2.5 D). We conclude that I-SceI induced DSBs at *c-myc* can be joined to AID induced DSBs at *IgH* and that the DSB at *c-myc* is limiting for the translocation reaction. Furthermore, the presence of AID leads to predominantly blunt translocation junctions.

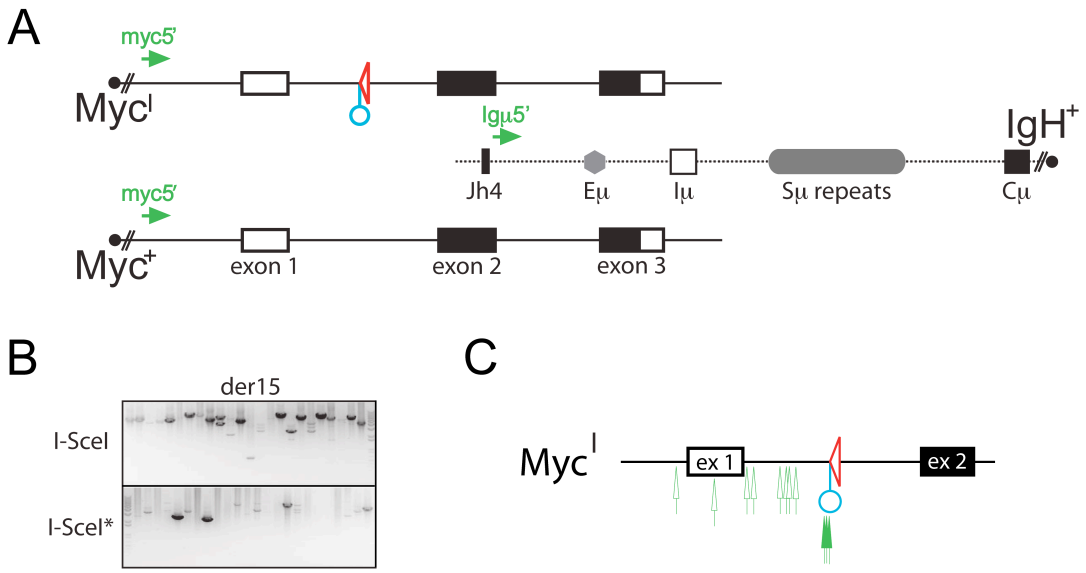

D

	I-SceI	blunt	1-3 nt	>3 nt	insertion
$IgH^{I/+}Myc^{I/+}AID^{-/-}$	+	0	13	6	2
$Myc^{I/+}$	+	7	6	0	2
WT	-	5	5	0	1

Figure 2.5. DSBs in *c-myc* are limiting for *c-myc/IgH* translocations.

(A) Schematic representation of the Myc^{I}, Myc^{+} and IgH^{+} alleles with the PCR primers for detecting der15 *c-myc/IgH* translocations. Circle points to recognition sequence for I-SceI.

(B) I-SceI directed translocations in the presence of AID. Representative agarose gels with PCR products corresponding to *c-myc/IgH* translocations (as verified by sequencing and/or Southern Blot). $Myc^{I/+}$ B cells were stimulated with LPS and IL-4 and infected with I-SceI (three independent experiments) or I-SceI* control. 100,000 cells were assayed in each lane.

(C) Map of translocation breakpoints from stimulated $Myc^{I/+}$ B cells infected with I-SceI. Filled arrows point to *c-myc/IgH* translocation breakpoints from der15. Empty arrows indicate the distribution of breakpoints obtained in the absence of I-SceI.

(D) Table shows summary of the extent of junctional microhomology from *c-myc/IgH* translocations.

DSBs at *IgH* are not limiting for *c-myc*/*IgH* translocation

We next tested whether the DSB in *IgH* is limiting for *c-myc*/*IgH* translocation. To this end we infected $IgH^{I/+}$ B cells with I-SceI or inactive I-SceI* and found no significant difference in translocation frequency ($0.14x10^{-5}$ for I-SceI and $0.2x10^{-5}$ for I-SceI*, Figure 2.6). We conclude that DSBs at *IgH* are not limiting for the translocation reaction.

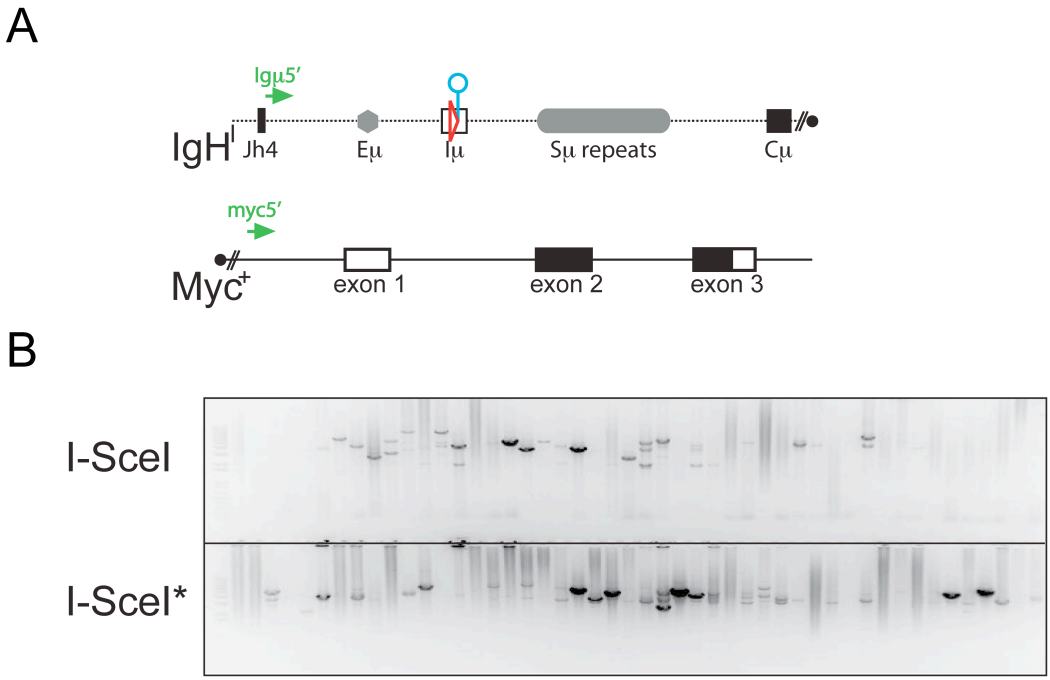

Figure 2.6. I-SceI induced translocations in AID deficient B lymphocytes.
(A) Schematic representation of the Myc^+ and IgH^I alleles with the PCR primers for detecting der15 *c-myc*/*IgH* translocations. Circles point to the position of the I-SceI sites. **(B)** Representative agarose gels with PCR products corresponding to *c-myc*/*IgH* translocations (as verified by sequencing and/or Southern Blot). $IgH^{I/+}AID^{-/-}$ B cells were stimulated with LPS and IL-4 and infected with I-SceI or I-SceI* control retroviruses. 100,000 cells were assayed each in lane. Three independent experiments.

AID induces DSBs at *c-myc*

To test whether AID is responsible for the generation of DSBs in *c-myc* we infected $Myc^{I/+}AID^{-/-}$, $IgH^{I/+}AID^{-/-}$ or control $Myc^{I/+}IgH^{I/+}AID^{-/-}$ B cells with I-SceI or I-SceI* (Figure 2.7). While I-SceI infection of $Myc^{I/+}IgH^{I/+}AID^{-/-}$ B cells leads to efficient *c-myc*/*IgH* translocations, none were detected in I-SceI infected $Myc^{I/+}AID^{-/-}$ or $IgH^{I/+}AID^{-/-}$ B cells (Figure 2.7). We conclude that AID induced DSB formation at both *IgH* and *c-myc* is required to generate *c-myc*/*IgH* translocations.

Figure 2.7. AID is essential for the lesion in *c-myc* that leads to *c-myc/IgH* translocation.

(A) Top: schematic representation of the Myc^{I}, Myc^{+} and IgH^{+} alleles with the PCR primers for detecting der12 and der15 *c-myc/IgH* translocations. Circle indicates I-SceI site. Bottom: a representative ethidium bromide (EtBr) stained agarose gel was also Southern blotted and probed for *c-myc* and *IgH*, as indicated, to verify translocations. $Myc^{I/+}AID^{-/-}$ B cells were stimulated with LPS and IL-4 and infected with an I-SceI encoding retrovirus. 100,000 cells were assayed in each lane. No translocations were identified out of $3.4x10^{7}$ cells analyzed. Three independent experiments.

(B) Top: schematic representation of the Myc^{+} and IgH^{I} alleles with the PCR primers for detecting der15 *c-myc/IgH* translocations. Circle indicates I-SceI site. Bottom: a representative ethidium bromide (EtBr) stained agarose gel was also Southern blotted and probed for *c-myc* and *IgH*, as indicated to verify translocations. $IgH^{I/+}AID^{-/-}$ B cells were stimulated with LPS and IL-4 and infected with I-SceI. 100,000 cells were assayed in each lane. No translocations were identified in $6.9x10^{7}$ cells. Seven independent experiments.

A

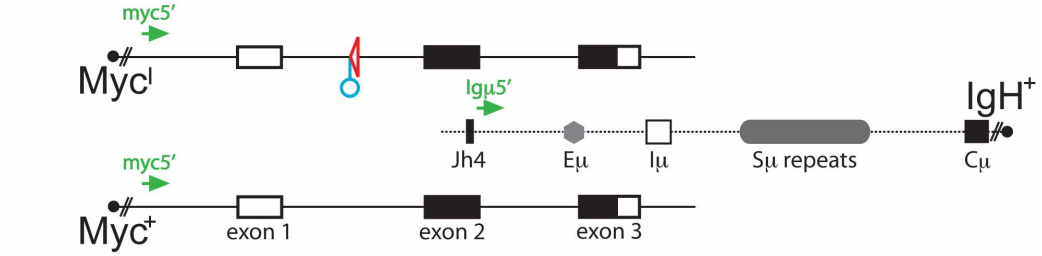
myc5′
Myc^{I}
Igμ5′
IgH^{+}
Jh4
Eμ
Iμ
Sμ repeats
Cμ
myc5′
Myc^{+}
exon 1
exon 2
exon 3

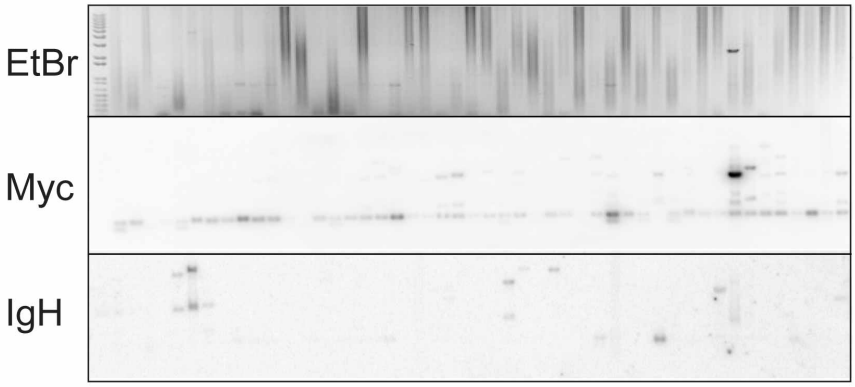
EtBr
Myc
IgH

B

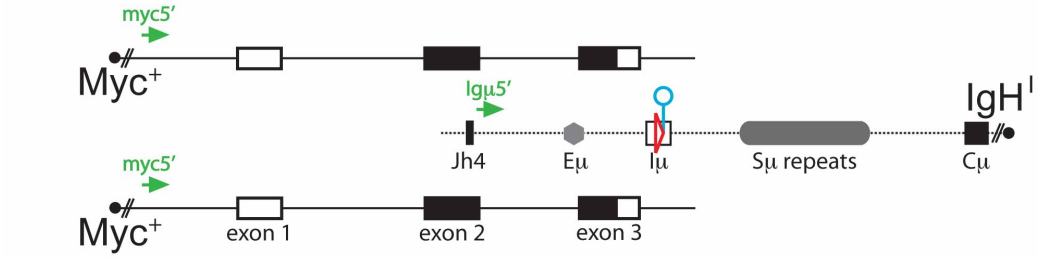
myc5′
Myc^{+}
Igμ5′
IgH^{I}
Jh4
Eμ
Iμ
Sμ repeats
Cμ
myc5′
Myc^{+}
exon 1
exon 2
exon 3

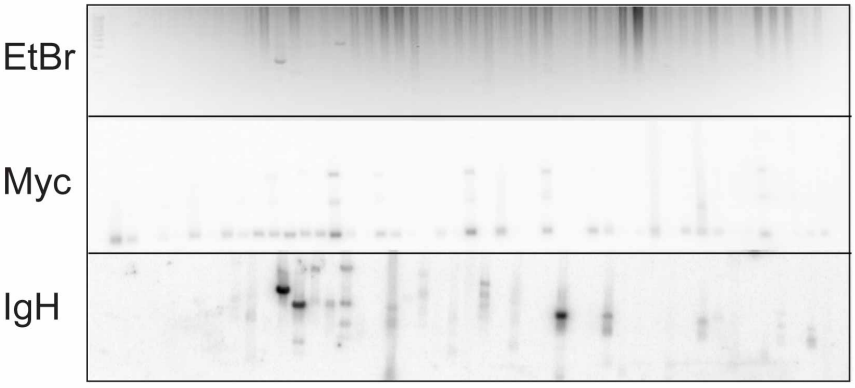
EtBr
Myc
IgH

CHAPTER 3:

Role of Distance in DSB Joining

DSBs are dangerous lesions that can lead to genomic rearrangements. Joining of DSBs within one chromosome can lead to chromosomal deletions, while joining of paired DSBs on separate chromosomes can lead to chromosome translocations. However, paired intra-chromosomal DSBs are necessary intermediates in immune cell diversification reactions such as V(D)J recombination and CSR. During CSR, AID produces tandem DSBs in IgH switch regions separated by 60-200 kb, which are rejoined while the intervening DNA is lost from the genome. DNA damage response factors are required for the efficient joining between IgH switch breaks. Among DNA damage response factors, the absence of 53BP1 leads to the most dramatic CSR defect (194-196). Similarly, joining of DSBs during V(D)J recombination of the TCRα receptor locus and of de-protected telomeres due to the absence of TRF2 is dependent on 53BP1 (124, 152). However, absence of 53BP1 does not lead to a joining defect per se, as proximal breaks within one switch region can be joined, leading to the hypothesis that the requirement for 53BP1 in the joining of DSBs is distance dependent (196).

The systematic study of the role of distance and the effect of 53BP1 on the joining of DSBs necessitates a method that allows for temporal and spatial control of DSB formation. In this Chapter we use the previously established I-SceI endonuclease system to study the joining of paired DSBs different distances

apart from each other on the same chromosome, and the role of 53BP1 in the joining process.

Genetic modifications of chromosome 12

To study the role of distance in DSB joining, we used gene targeting to introduce paired I-SceI recognition sites separated by various distances on mouse chromosome 12 (Figure 3.1).

To determine short-range intra-chromosomal joining frequencies, ES cells were targeted with a construct containing two I-SceI sites separated by 1.2 kb of spacer sequence at the *IghG1* locus ($IgH^{I\text{-}1k}$, Figure 3.1 A, for details see methods section). Joining of paired DSBs separated by 1.2 kb resembles the distance involved in the joining of DSBs within the same S-region.

To examine the joining of DSBs separated by distances occurring during CSR, we retargeted the IgH^{I} ES cell clone already containing an I-SceI site at Sμ and inserted a second I-SceI site 3′ of Sγ1. This yielded ES cells with two I-SceI sites spaced 96 kb apart from each other ($IgH^{I\text{-}96k}$, Figure 3.1 B, for details see methods section). This setting should recapitulate the physiological switch recombination reaction to IgG1.

To determine how DSBs situated long distances apart from each other are joined we introduced an I-SceI site into the *c-fos* locus, which lies 27 Mb centromeric of the *IgH* locus on chromosome 12. For this targeting, the ES cell clone already containing an I-SceI site at Sμ was used, resulting in paired I-SceI sites spaced by 27 Mb on chromosome 12 ($IgH^{I\text{-}27M}$, Figure 3.1 C, for details see methods section).

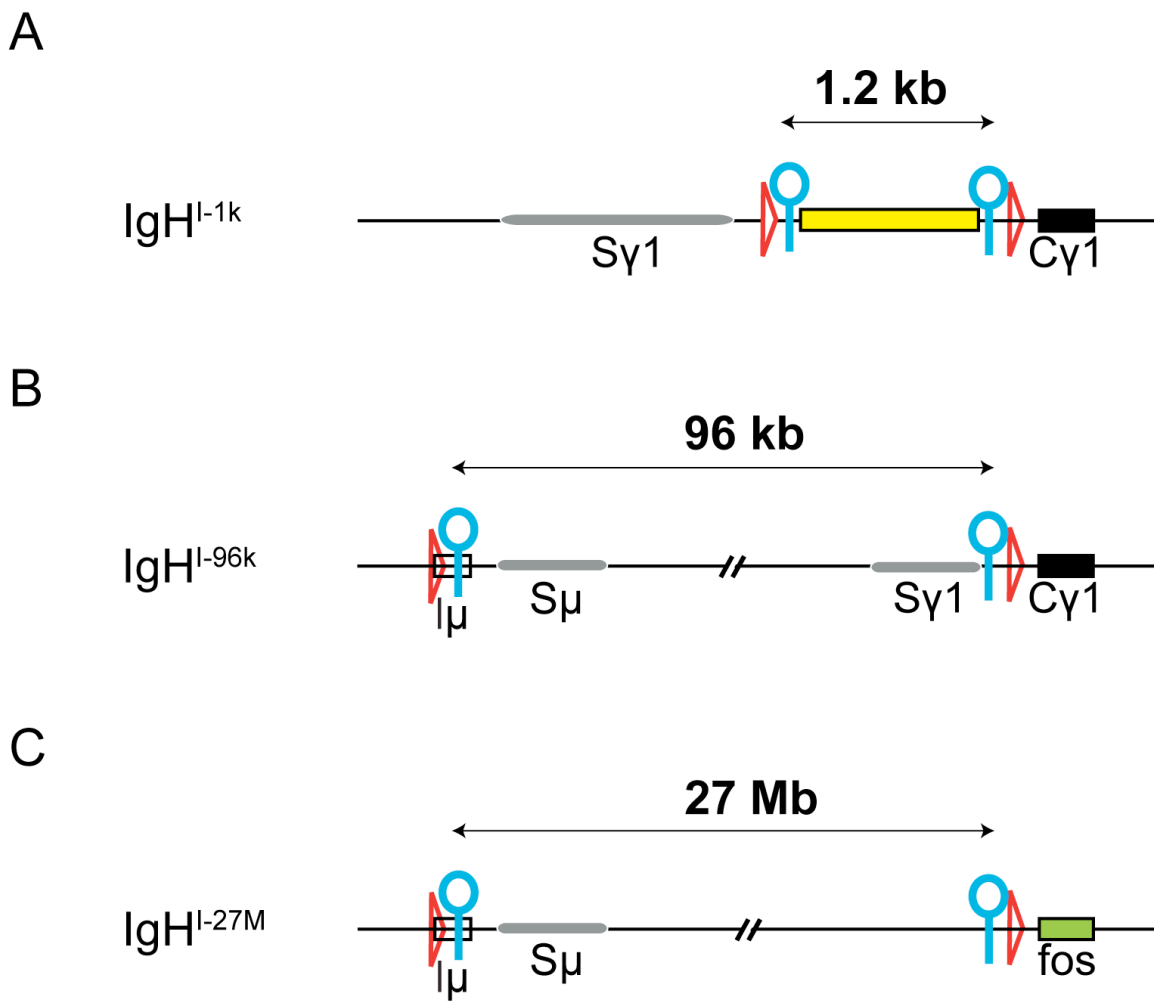

Figure 3.1. Schematic of genetic modifications of chromosome 12.

(A) Schematic representation of $IgH^{I\text{-}1k}$ allele, bearing two I-SceI sites separated by 1.2 kb. Spacer sequence is indicated as yellow rectangle.

(B) Schematic representation of $IgH^{I\text{-}96k}$ allele, bearing two I-SceI sites separated by 96 kb.

(C) Schematic representation of $IgH^{I\text{-}27M}$ allele, bearing two I-SceI sites separated by 27 Mb.

In all panels: I-SceI sites are indicated as blue circles, loxP sites as red triangles.

Loss of 53BP1 does not affect proximal DSB joining

To assess the effect of 53BP1 on the joining efficiency of proximal DSBs, we first assayed $IgH^{I\text{-}1k}$ mice, which bear I-SceI sites separated by 1.2 kb (Figure 3.2 A). $IgH^{I\text{-}1k}$ B cells showed normal development, proliferation and CSR to IgG1 upon stimulation with LPS and IL-4 (Figure 3.2 B). To ensure that DSB joining is exclusively mediated by I-SceI and is not confounded through randomly generated AID dependent breaks in the same region, we crossed $IgH^{I\text{-}1k}$ mice into $AID^{-/-}$. We infected $IgH^{I\text{-}1k/+}AID^{-/-}$ and $IgH^{I\text{-}1k/+}AID^{-/-}53BP1^{-/-}$ B cells with an I-SceI expressing virus or an inactive I-SceI* control and measured recombination frequencies by sample dilution PCR. Infection with the inactive control virus led to no detectable recombination (Figure 3-2 C, lower panel). In agreement with the finding that proximal, switch region internal DSBs are not affected by the absence of 53BP1, we found that loss of 53BP1 did not significantly affect the joining frequency of DSBs separated by 1.2 kb ($0.17x10^{-2}$ $IgH^{I\text{-}1k}AID^{-/-}$ and $0.29x10^{-2}$ in $IgH^{I\text{-}1k}AID^{-/-}53BP1^{-/-}$, Figure 3-2 D).

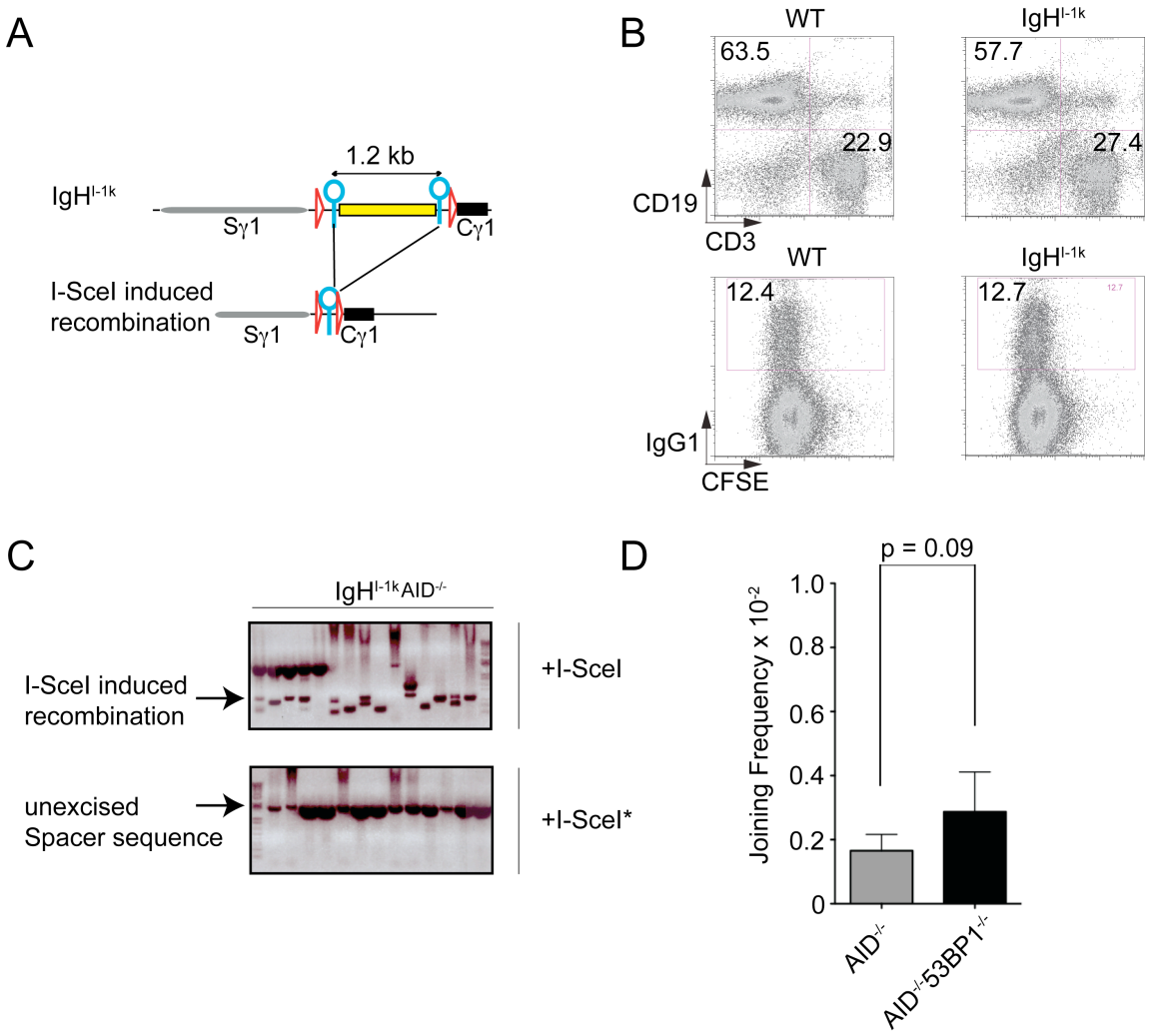

Figure 3.2. Effect of 53BP1 on joining efficiency of proximal DSBs.

(A) Schematic representation of $IgH^{I\text{-}1k}$ allele before (top) and after (bottom) I-SceI induced recombination. I-SceI sites are indicated as blue circles, loxP sites as red triangles. Spacer sequence of 1.2 kb is indicated as yellow rectangle.

(B) Flow cytometric analysis of spleen cells from age-matched wild type and mutant $IgH^{I\text{-}1k/+}$ mice reveals normal B cell development, CSR to IgG1 and proliferation (by labeling with the dye CFSE). Numbers indicate percentage of live cells within the indicated gates.

(C) Representative ethidium bromide stained agarose gel showing PCR products obtained after I-SceI and I-SceI* induced recombination in $IgH^{I\text{-}1k/+}AID^{-/-}$ B cells.

(D) Bar graph shows I-SceI induced recombination frequency of $IgH^{I\text{-}1k/+}AID^{-/-}$ B cells in the presence or absence of 53BP1. Error bars indicate standard deviation. P value was calculated using a paired two tailed students t-test. Seven independent measurements.

Loss of 53BP1 decreases joining efficiency of DSB separated by 96 kb

We next determined whether loss of 53BP1 affects the joining efficiency of I-SceI breaks separated by 96 kb. $IgH^{I\text{-}96k}$ mice (Figure 3.3 A) displayed normal B cell development, proliferation and CSR upon stimulation with LPS and IL-4 (Figure 3.3 B). As with proximal break joining, we performed all experiments in the absence of AID. Infection of $IgH^{I\text{-}96k/+}AID^{-/-}$ B cells with an I-SceI expressing retrovirus should recapitulate physiologic CSR and yield IgG1 expression upon successful recombination. To test if this is the case, we infected $IgH^{I\text{-}96k/+}AID^{-/-}$ B cells with I-SceI or an inactive control I-SceI*. Indeed, I-SceI expression led to IgG1 surface expression, while the catalytically inactive I-SceI* did not induce recombination (Figure 3.3 C and D). We then used surface IgG1 expression as a proxy for I-SceI joining efficiency and measured recombination frequencies in the presence and absence of 53BP1. Joining was significantly reduced from 0.54% in $IgH^{I\text{-}96k/+}AID^{-/-}$ to 0.31% in $IgH^{I\text{-}96k/+}AID^{-/-}53BP1^{-/-}$ B cells (Figure 3.3 E and F). To obtain an independent measure of recombination frequency we examined the joining between I-SceI sites by sample dilution PCR. In agreement with the flow cytometry analysis we found that with this method the joining efficiency in stimulated $IgH^{I\text{-}96k/+}AID^{-/-}$ B lymphocytes was significantly reduced from 0.76% to 0.48% in the absence of 53BP1 (Figure 3.2 G). We conclude that loss of 53BP1 decreases the efficiency of recombination between I-SceI sites in $IgH^{I\text{-}96k/+}AID^{-/-}$ B cells; however, the effect is far less pronounced than it is for physiologic CSR, where the reduction of in the absence of 53BP1 is to approximately 10% of wild type levels.

Figure 3.3. Loss of 53BP1 decreases joining efficiency of DSBs separated by 96 kb.
(A) Schematic representation of the $IgH^{I\text{-}96k}$ allele (upper panel) and the I-SceI induced recombinant that encodes IgG1 (lower panel). LoxP sites are indicated as red triangles and I-SceI sites as blue circles.
(B) Flow cytometric analysis of spleen cells from age-matched wild type and mutant $IgH^{I\text{-}96k}$ mice reveals normal B cell development and CSR to IgG1 after stimulation with LPS and IL-4. B cells were labeled with CFSE to track cell division.
(C) Representative flow cytometry experiment shows CSR to IgG1 of $IgH^{I\text{-}96k}AID^{-/-}$ B cells 72 hrs after the first infection with I-SceI or catalytically inactive I-SceI* encoding retrovirus.
(D) Graph shows the results of six independent flow cytometry measurements for IgG1 expression of I-SceI or I-SceI* infected $IgH^{I\text{-}96k}AID^{-/-}$ B cells. P value was calculated using Student's t-test (two-tailed). Error bars indicate standard deviation.
(E) Representative flow cytometry experiment shows CSR to IgG1 of $IgH^{I\text{-}96k}AID^{-/-}$ and $IgH^{I\text{-}96k}AID^{-/-}53BP1^{-/-}$ B cells 72 hrs after the first infection with an I-SceI encoding retrovirus.
(F) Graph shows I-SceI recombination efficiency of $IgH^{I\text{-}96k}AID^{-/-}$ and $IgH^{I\text{-}96k}AID^{-/-}53BP1^{-/-}$ B cells, determined in five independent flow cytometry experiments, each dot representing an individual experiment. P value was calculated using Student's paired t-test (two-tailed). The means are shown as a line in the graph.
(G) Bar graph shows I-SceI recombination efficiency of $IgH^{I\text{-}96k}AID^{-/-}$ and $IgH^{I\text{-}96k}AID^{-/-}53BP1^{-/-}$ B cells, determined by nine independent PCR experiments. Error bars indicate standard deviation. P value was calculated using Student's paired t-test (two-tailed).

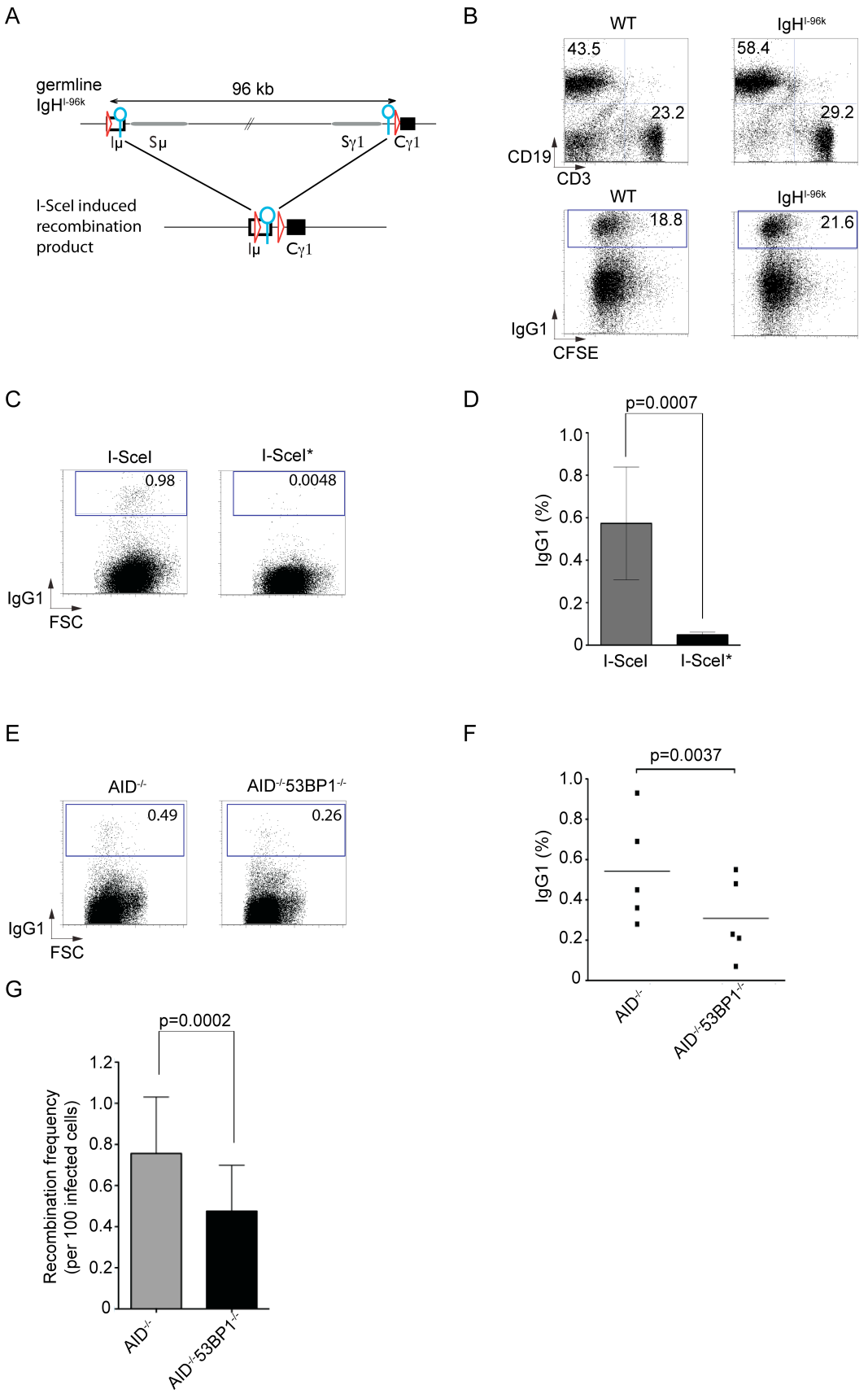
A
germline
IgH^I-96k
96 kb
Iμ
Sμ
Sγ1
Cγ1
I-SceI induced
recombination
product
Iμ
Cγ1
B
WT
IgH^I-96k
43.5
23.2
58.4
29.2
CD19
CD3
WT
IgH^I-96k
18.8
21.6
IgG1
CFSE
C
I-SceI
I-SceI*
0.98
0.0048
IgG1
FSC
D
p=0.0007
IgG1 (%)
1.0
0.8
0.6
0.4
0.2
0
I-SceI
I-SceI*
E
AID-/-
AID-/-53BP1-/-
0.49
0.26
IgG1
FSC
F
p=0.0037
IgG1 (%)
1.0
0.8
0.6
0.4
0.2
0
AID-/-
AID-/-53BP1-/-
G
p=0.0002
Recombination frequency
(per 100 infected cells)
1.2
1.0
0.8
0.6
0.4
0.2
0
AID-/-
AID-/-53BP1-/-

Loss of 53BP1 does not affect joining efficiency of distal DSBs separated by 27 Mb

To determine the effect of 53BP1 on long-range joining across 27 Mb, we assayed $IgH^{I\text{-}27M}$ mice (Figure 3.4 A). $IgH^{I\text{-}27M}$ mice displayed normal B cell development and CSR upon stimulation with LPS and IL-4 (Figure 3.4 B). We infected $IgH^{I\text{-}27M/+}AID^{-/-}53BP1^{-/-}$ B cells and the respective 53BP1 proficient control with an I-SceI retrovirus. In contrast to joining across 96 kb and similar to joining of DSB separated by short distances, loss of 53BP1 leads to an increase in recombination frequency from $0.0048x10^{-2}$ in $IgH^{I\text{-}27M/+}AID^{-/-}$ to $0.0062x10^{-2}$ in $IgH^{I\text{-}27M}AID^{-/-}53BP1^{-/-}$ (Figure 3.4 D). Strikingly, the efficiency of joining DSBs separated by 27 Mb was >30 fold lower than that of DSBs separated by 1.2 kb or 96 kb ($0.0048x10^{-2}$ versus $0.17\ x10^{-2}$ and $0.7x10^{-2}$ respectively, grey bars in Figures 3.4 C, 3.3 E and 3.2 D). We conclude that in contrast to facilitating the joining of DSBs separated by 96 kb, 53BP1 does not alter the joining frequency of more proximal or distal DSBs.

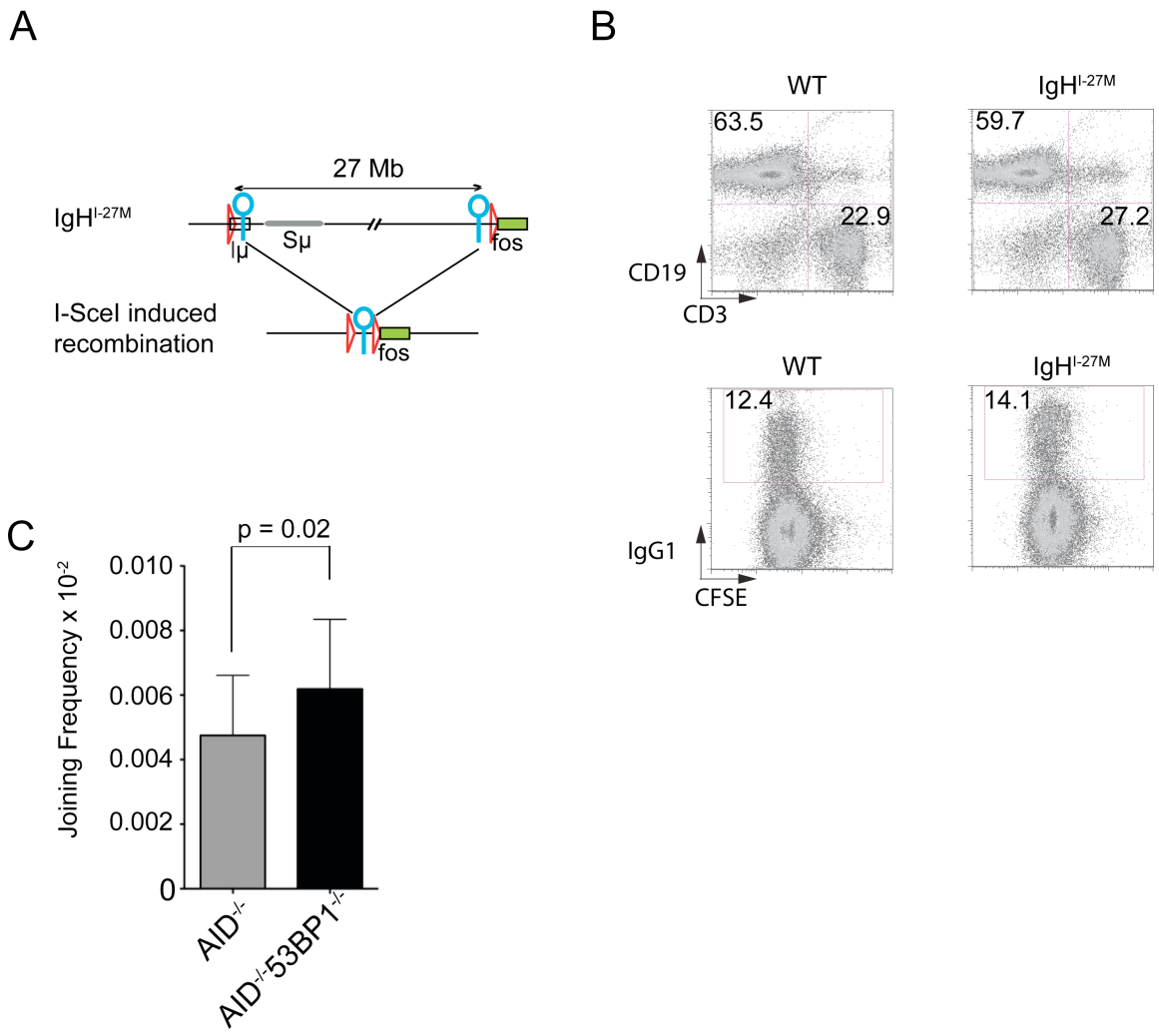

Figure 3.4. Loss of 53BP1 does not affect joining of distal DSBs separated by 27 Mb.

(A) Schematic representation of $IgH^{I\text{-}27M}$ allele before (top) and after (bottom) I-SceI induced recombination.

(B) Flow cytometric analysis of spleen cells from age-matched wild type and mutant $IgH^{I\text{-}27M/+}$ mice reveals normal B cell development, CSR to IgG1 and proliferation.

(C) Bar graph shows I-SceI induced recombination frequency of $IgH^{I\text{-}27M/+}AID^{-/-}$ B cells in the presence or absence of 53BP1. Error bars are standard deviations. P value was calculated using a paired two tailed students t-test. Eight independent measurements.

Loss of 53BP1 does not affect joining of trans-chromosomal DSBs

To determine how distal intra-chromosomal joining compares with trans-chromosomal joining, we produced mice with paired I-SceI sites on chromosomes 12 and 15 (IgH^{I} and Myc^{I}, respectively) and generated translocations by infecting cells with I-SceI viruses. The joining frequency of I-SceI infected $IgH^{I/+}Myc^{I/+}AID^{-/-}$ B cells was $0.0027x10^{-2}$, which is comparable to the joining between I-SceI sites separated by 27 Mb in $IgH^{I\text{-}27M/+}AID^{-/-}$ (Figures 3.4 C and Figures 3.5 B, grey bars). We then measured the effect of 53BP1 on the joining of trans-chromosomal DSBs. We infected $Myc^{I/+}IgH^{I/+}AID^{-/-}53BP1^{-/-}$ B cells with an I-SceI retrovirus. Similarly to the joining of intra-chromosomal DSB separated by 27 Mb, loss of 53BP1 leads to an increase in recombination frequency from $0.0027x10^{-2}$ in $Myc^{I/+}IgH^{I/+}AID^{-/-}$ B cells to $0.004x10^{-2}$ in $Myc^{I/+}IgH^{I/+}AID^{-/-}53BP1^{-/-}$ B cells (Figure 3.5 B).

We conclude that the joining of distal (27 Mb) intra-chromosomal DSBs is similar to the trans-chromosomal joining.

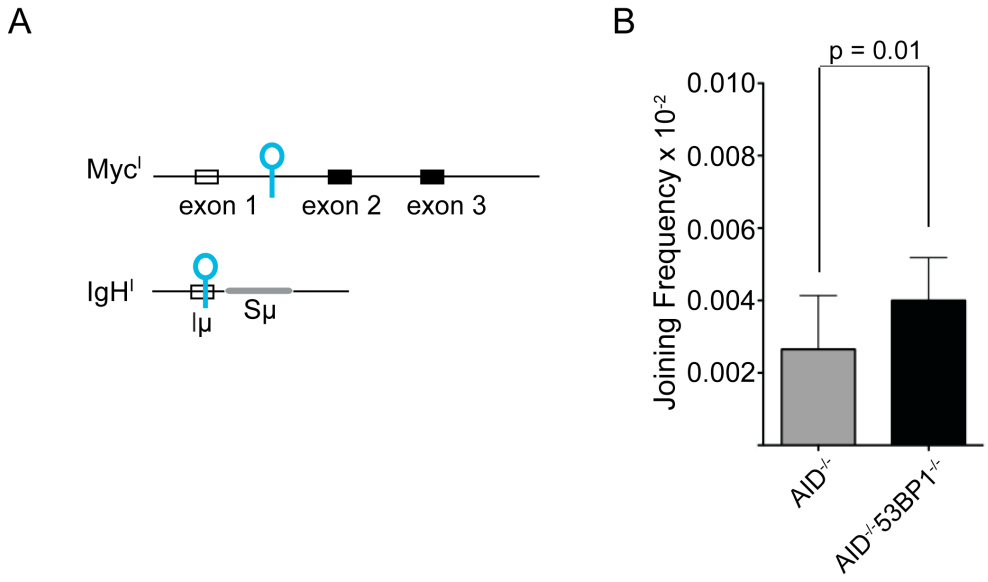

Figure 3.5. 53BP1 does not affect joining efficiency of trans-chromosomal DSBs.

(A) Schematic representation of the Myc^{I} and IgH^{I} alleles.

(B) Bar graph shows I-SceI induced recombination frequency of $IgH^{I/+}Myc^{I/+}AID^{-/-}$ B cells in the presence or absence of 53BP1. Error bars indicate standard deviations. P value was calculated using a paired two tailed students t-test. Four independent measurements.

Spreading of DNA damage response along chromatin

53BP1 selectively facilitates end-joining of DSBs in cis separated by 96 kb. Loss of 53BP1 does not reduce the joining frequency of proximal, very distal or trans-chromosomal DSBs. This selective effect of 53BP1 on the joining of paired breaks coincides with the proposed spread of DNA damage response to chromatin surrounding the DSB (33, 228). We hypothesized that DNA damage response factors could facilitate DSB joining in areas that are affected by the spreading. To test whether in our system we could detect spreading of the DNA damage response we performed a γH2AX ChIP after DSB formation by I-SceI in $IgH^{I\text{-}96k/+}AID^{-/-}$ B cells. Indeed, we could detect γH2AX in areas surrounding the I-SceI induced DSBs at the IgH locus with an ensuing spread of 100-300 kb (Figure 3.6). No γH2AX was detected beyond 1 Mb of the DSBs. As a control, we measured γH2AX density at 27 Mb and as expected did not detect a signal above background. We conclude that the DNA damage induced γH2AX signal reaches a maximum at ~100-300 kb from the DSB, but that distal sites are not affected.

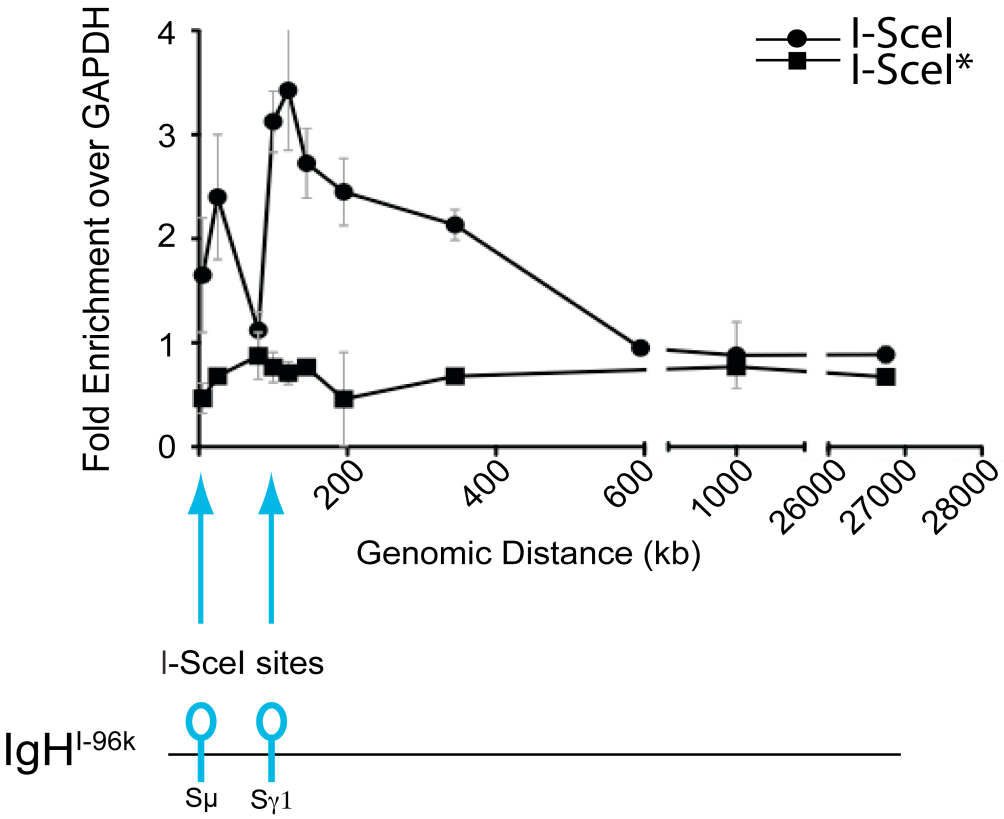

Figure 3.6. γH2AX spreading to areas surrounding the I-SceI induced DSBs.
γH2AX density measured by Chromatin IP at the $IgH^{I\text{-}96k}$ allele upon I-SceI induced DSB formation (blue circles) by infection of $IgH^{I\text{-}96k/+}AID^{-/-}$ B cells or $IgH^{I\text{-}96k/I\text{-}96k}AID^{-/-}$ B cells with I-SceI or I-SceI* control. To calculate γH2AX density (y-axis), the γH2AX signal at different genomic locations on chromosome 12 (indicated by x-axis) was normalized to the signal at the (non-broken) GAPDH locus. Two independent experiments. Error bars indicate standard errors.

Switching by Cre mediated recombination

The mechanism that mediates joining of DSBs between switch regions during CSR includes DNA damage response factors. However, chromosome conformation capture PCR experiments suggest that AID may contribute to long-range interactions between switch regions (229). To determine whether AID

plays a role in modulating chromosome conformation we made use of the Cre/loxP system. Cre is a bacteriophage enzyme that mediates recombination between loxP sites via Holliday junction intermediates (230). Synapsis between two molecules of Cre bound to separate loxP sites precedes and is required for catalysis (231). Because synapsis is limiting in this reaction, the rate of recombination between loxP sites in mammalian cells expressing Cre is inversely proportional to the distance between the sites and can therefore serve as a measure of chromosome topography (232, 233).

To determine whether AID expression alters *IgH* topology sufficiently to change the rate of Cre mediated recombination between switch regions, we compared Cre induced CSR in AID deficient $IgH^{I\text{-}96k}$ B cells and control $IgH^{I\text{-}96k}$ B cells (Figure 3.7). B cells were stimulated with LPS and IL-4 and infected with a Cre encoding retrovirus or an inactive retrovirus Cre*. Infected cells were identified by GFP expression and CSR was measured by flow cytometry. Cre expression in AID sufficient $IgH^{I\text{-}96k}$ B lymphocytes increased CSR to IgG1 from 3.8% to 14.4% and 16.2% to 32.2% at 72 hrs and 96 hrs after stimulation respectively (Fig 3.7 B and C). However, the rate of CSR in $IgH^{I\text{-}96k}$ B cells was similar in the presence or absence of AID 96 hrs after stimulation (Figure 3.7 B and C).

To determine whether the loss of 53BP1 alters the efficiency of Cre mediated CSR we compared the frequency of recombination between $IgH^{I\text{-}96k/+}AID^{-/-}53BP1^{-/-}$ and $IgH^{I\text{-}96k/+}AID^{-/-}$ B cells. We found that CSR in Cre infected $IgH^{I\text{-}96k/+}AID^{-/-}$ $53BP1^{-/-}$ B cells was indistinguishable from 53BP1 proficient cells (Figure 3.7 C and D). We conclude that neither AID nor 53BP1 alter the overall structure of the *IgH* locus sufficiently to change the rate of synapsis between the loxP sites in $IgH^{I\text{-}96k}$.

Figure 3.7. Cre recombinase induces efficient CSR to IgG1 independently of AID and 53BP1.

(A) Schematic representation of the $IgH^{I\text{-}96k}$ allele (upper panel) and the Cre induced recombinant that encodes IgG1 (lower panel). LoxP sites are indicated as red triangles, I-SceI sites are shown as blue circles.

(B) Representative flow cytometry experiments showing CSR to IgG1 of $IgH^{I\text{-}96k}$ B cells infected with retroviruses encoding Cre or catalytically inactive Cre*. IgG1 expression was analyzed at 72 hrs and 96 hrs after LPS and IL-4 stimulation.

(C) Representative flow cytometry experiments showing CSR to IgG1 for $IgH^{I\text{-}96k/+}AID^{-/-}$ and $IgH^{I\text{-}96k/+}AID^{-/-}53BP1^{-/-}$ B cells analyzed at 96 hrs after LPS and IL-4 stimulation.

(D) Graph shows the results of three independent flow cytometry experiments measuring CSR to IgG1 after Cre infection of $IgH^{I\text{-}96/+}AID^{-/-}$ and $IgH^{I\text{-}96k/+}AID^{-/-}53BP1^{-/-}$ B cells.

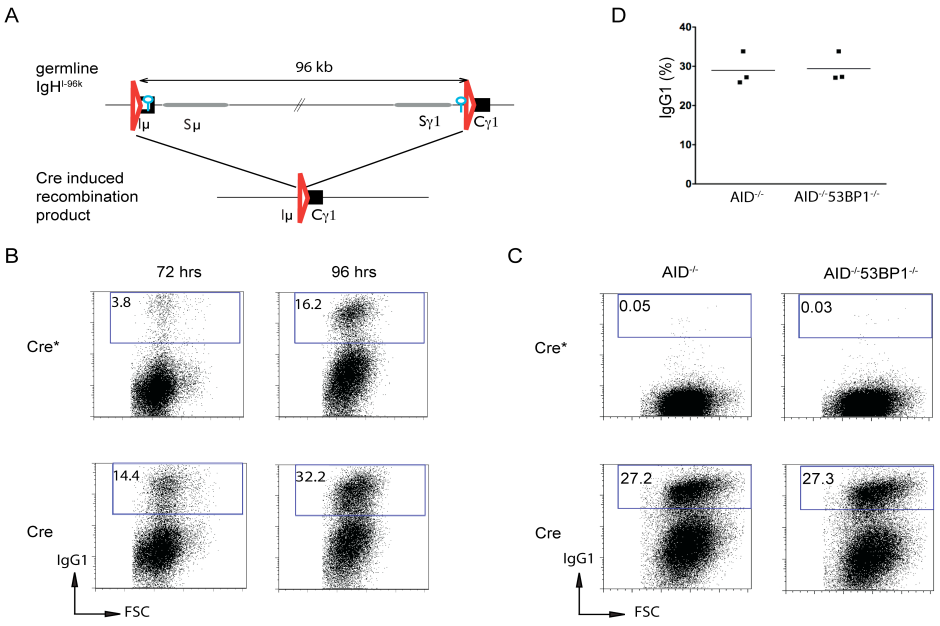
A
germline
IgH^I-96k
96 kb
Iμ
Sμ
Sγ1
Cγ1
Cre induced
recombination
product
Iμ
Cγ1
D
IgG1 (%)
40
30
20
10
0
AID-/-
AID-/-53BP1-/-
B
72 hrs
96 hrs
Cre*
3.8
16.2
Cre
IgG1
14.4
32.2
FSC
C
AID-/-
AID-/-53BP1-/-
Cre*
0.05
0.03
Cre
IgG1
27.2
27.3
FSC

CHAPTER 4:

The Role of 53BP1 in DNA Repair Pathway Choice

As shown in the previous chapter, we have established a system using the I-SceI enduclease to determine joining efficiencies of DSBs separated by different distances. This system allows us to examine joining and repair of two spatially separated I-SceI induced DSBs. Here we utilize this system to explore a role for 53BP1 in DSB repair.

Absence of 53BP1 results in more end processing

To address if 53BP1 plays a role in DNA repair, we analyzed the joining products of DSBs separated by 96 kb. $IgH^{I\text{-}96k/+}AID^{-/-}53BP1^{-/-}$ and $IgH^{I\text{-}96k}AID^{-/-}$ control B cells were infected with I-SceI and analyzed using the previously described dilutional PCR assay. We noticed the occurrence of PCR products with lower than expected molecular weight, which predominantly occurred in the absence of 53BP1. The expected size for precise I-SceI to I-SceI joining is a PCR product of 336 nt. Lower molecular weight products are a consequence of end processing at the sites of the DSBs, resulting in a deletion and loss of DNA. Our single event dilutional PCR assay allows us to directly score the appearance of lower molecular weight species (products running below 300 nt i.e. more than ~30 nt total end resection). By visual inspection of the agarose gels we found that PCR products with minimal deletions (running above > 300 nt) were the predominant species in control $IgH^{I\text{-}96k/+}AID^{-/-}$ B cells (Figure 4.1 B and C). The loss of 53BP1 resulted in an overall increase in the number of PCR products with lower than expected molecular weight to 51.6% of all products. (Figure 4.1 B and C).

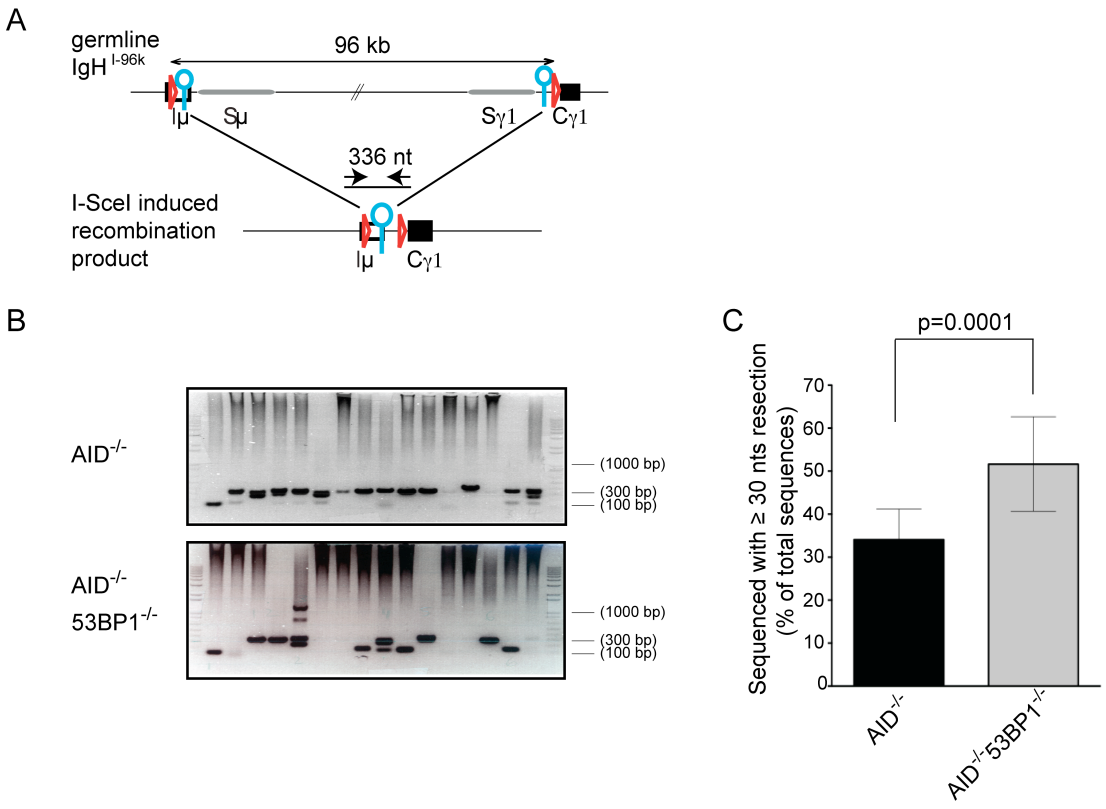

Figure 4.1. Loss of 53BP1 leads to increased end resection.

(A) Schematic representation of $IgH^{I\text{-}96k}$ allele (upper panel) with the PCR primers (arrows) used to amplify a 336 nt recombination product (lower panel).

(B) Representative ethidium bromide stained agarose gels showing PCR products obtained after I-SceI induced recombination in $IgH^{I\text{-}96k/+}AID^{-/-}$ and $IgH^{I\text{-}96k/+}AID^{-/-}53BP1^{-/-}$ B cells.

(C) Bar graphs showing the frequency of I-SceI induced recombination products running at or below 300 nts, for $IgH^{I\text{-}96k/+}AID^{-/-}$ and $IgH^{I\text{-}96k/+}AID^{-/-}53BP1^{-/-}$ B cells. Error bars indicate standard deviation. P value was calculated using Student's t-test (two-tailed).

Molecular structure of joins

To determine the precise molecular structure of the joins we sequenced all recombination products. I-SceI induced cleavage of its recognition site leaves a 4 nt 3′ overhang which needs to be removed during the joining process. The extent of resection was scored as the number of nucleotides lost from the 5′ end (i.e. only 5′-3′ resection was scored, not loss of 4 nt overhang, Figure 4.2 A). We found that the average extent of end processing was 34.7 nucleotides for $IgH^{I\text{-}96k/+}AID^{-/-}$ B cells while the average number of nucleotides lost from the junction increased almost two-fold to 66.8 nucleotides in the absence of 53BP1, confirming our visual scoring of resection on the agarose gel (Figure 4.2 C). If no end processing occurs, an intact I-SceI site will be reconstituted. Hence, scoring the frequency of this precise event is an alternative and complementary measure of end processing. We found that consistent with the idea that ends are more frequently processed in the absence of 53BP1, the number of precise joins decreased from 30.9% to 13.3% in $53BP1^{-/-}$ B cells (Figure 4.2 C).

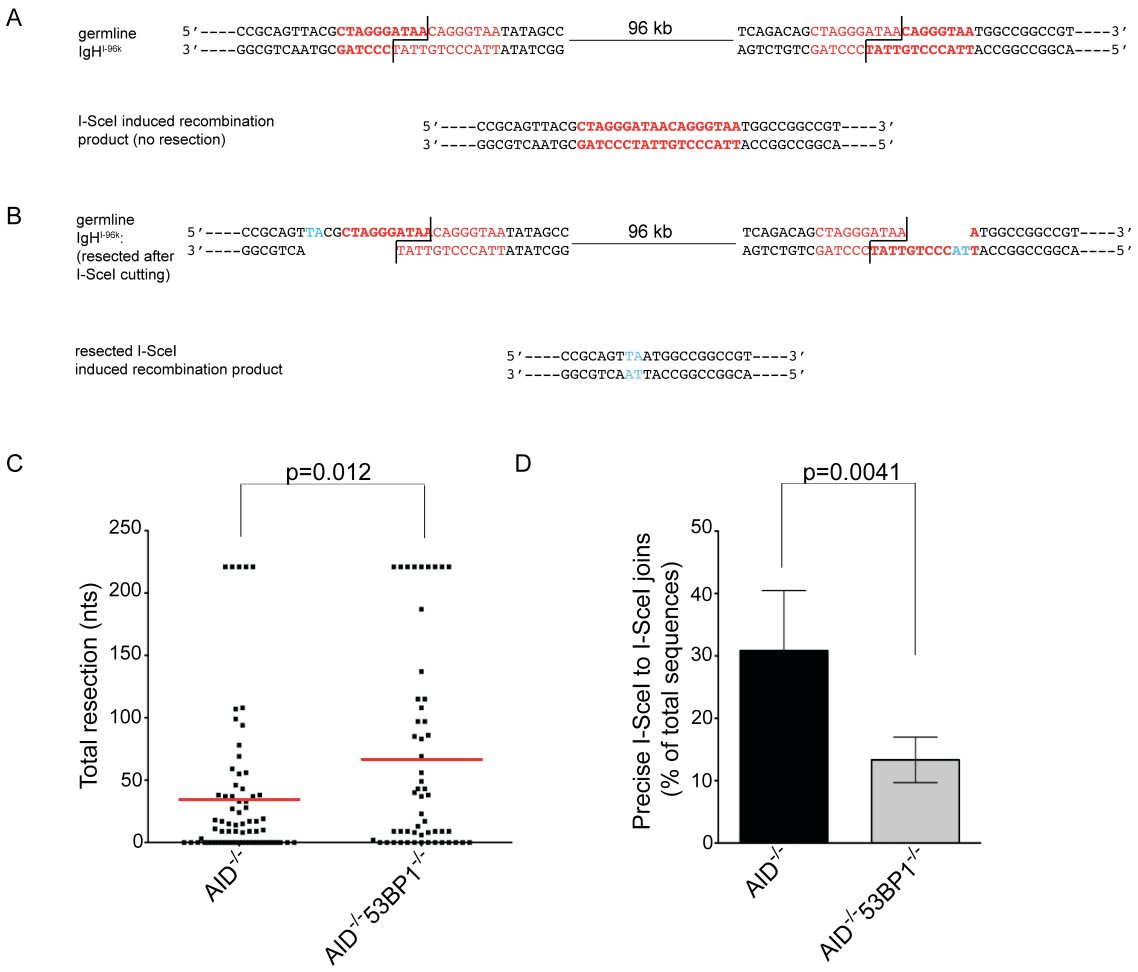

Figure 4.2. Loss of 53BP1 leads to increased end resection.

(A) Top: Sequence of I-SceI site in Iμ and 3′ of Sγ (red). I-SceI cutting (black lines) will result in a 4 nt 3′ overhang. Bottom: Joining without end-processing results in reconstitution of a complete, recleavable I-SceI site (red).

(B) Top: Resection of the 3′ strand after I-SceI cutting exposes microhomology (blue). Bottom: Joining product after resection and loss of the I-SceI sequence, indicating the microhomology used (blue).

(C) Dot plot showing total resection of I-SceI infected $IgH^{I\text{-}96k/+}AID^{-/-}$ and $IgH^{I\text{-}96k/+}AID^{-/-}53BP1^{-/-}$ B cells. Each dot represents one sequence. The means are indicated as red lines in the graph. The p-value was calculated using the Student's t-test (two-tailed).

(D). Bar graph shows the average frequency of perfect I-SceI joins in I-SceI infected $IgH^{I\text{-}96k/+}AID^{-/-}$ and $IgH^{I\text{-}96k}AID^{-/-}53BP1^{-/-}$ B cells of five independent experiments. Error bars indicate standard deviation. The p-value was calculated using the Student's t-test (two-tailed).

Resection of DNA Ends correlates with microhomology at the junction

Besides determining the extent of nucleotide loss (resection) during DSB joining , sequencing repair joins yields additional information about microhomology usage at the junction. All of the minimally processed joins showing less than 30 nt end resection, displayed 0-4 nt of junctional microhomology, with an average of 1.5 and 2.0 nt, for $AID^{-/-}$ and $AID^{-/-}53BP1^{-/-}$ B cells respectively (Figure 4.3). Minimal end processing in combination with little junctional homology is characteristic of C-NHEJ. In contrast, the majority of joining events that involved extensive resection (≥ 30 nt) used 3 nt or more of junctional microhomology, with an average of 3.6 and 4.0 nt, for $AID^{-/-}$ and $AID^{-/-}53BP1^{-/-}$ B cells respectively (Figure 4.3, $p<0.0001$ for $AID^{-/-}$ and $p=0.0004$ for $AID^{-/-}53BP1^{-/-}$). Extensive end processing and junctional microhomologies are indicative of A-NHEJ. Interestingly, end resection leads to microhomology mediated end joining regardless of 53BP1 status. We therefore conclude that loss of 53BP1 leads to a greater likelihood of resection of DNA ends, which then leads to increased microhomology usage at the repair junction.

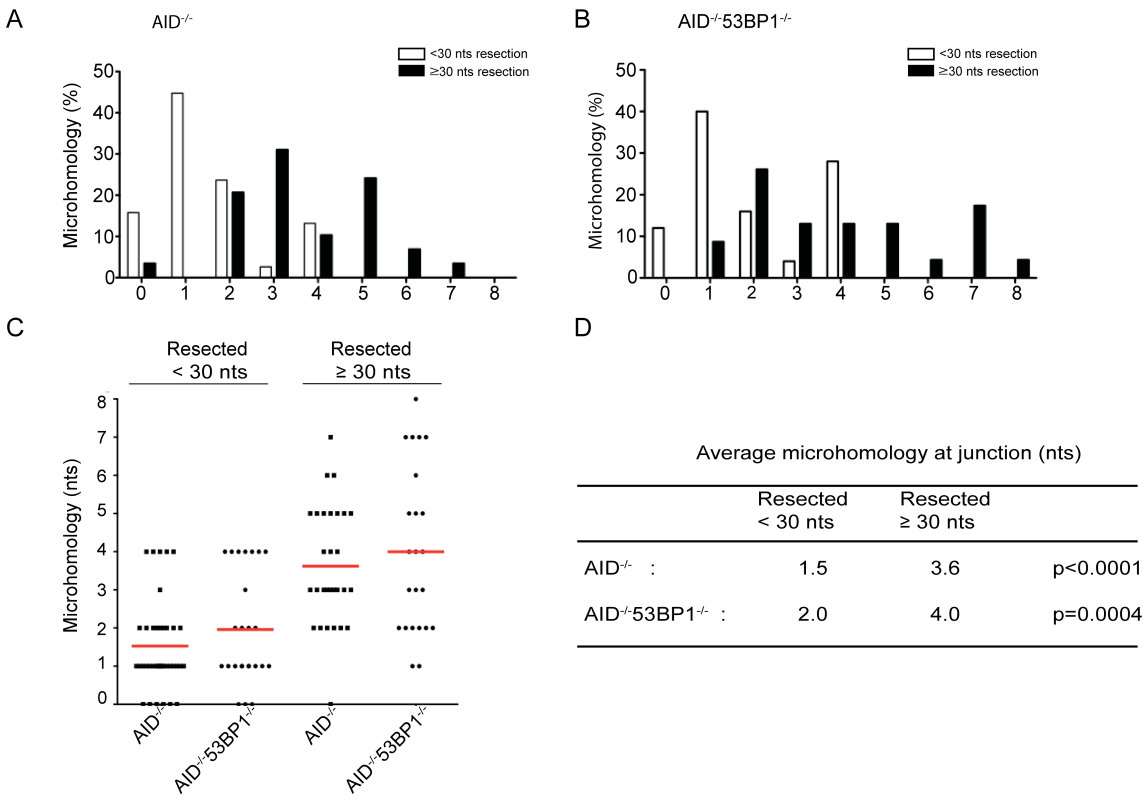

Figure 4.3. Resected DSBs are joined using microhomology-mediated end-joining, independently of 53BP1.

(A) Bar graph shows microhomology at junctions of PCR products from I-SceI infected $IgH^{I\text{-}96k/+}AID^{-/-}$ B cells. Black bars indicate sequences with little resection (< 30nt), white bars indicate sequences with resection ≥ 30nt.

(B) Bar graph shows microhomology at junctions of PCR products from I-SceI infected $IgH^{I\text{-}96k/+}AID^{-/-}53BP1^{-/-}$ B cells. Black bars indicate sequences with little resection (< 30 nt), white bars indicate sequences with resection ≥ 30 nt.

(C) Graph shows extent of microhomology at junctions of PCR products from I-SceI infected $IgH^{I\text{-}96k/+}AID^{-/-}$ and $IgH^{I\text{-}96k/+}AID^{-/-}53BP1^{-/-}$ B cells. Sequences are divided into those displaying fewer than 30 nt processing (left) and those with more than 30 nt (right). Horizontal line shows the mean. A total of 67 and 48 sequences were analyzed for $IgH^{I\text{-}96k/+}AID^{-/-}$ and $IgH^{I\text{-}96k/+}AID^{-/-}53BP1^{-/-}$ B cells, respectively.

(D) Table indicates the average number of nt of microhomology at junctions in I-SceI infected $IgH^{I\text{-}96k/+}AID^{-/-}$ and $IgH^{I\text{-}96k/+}AID^{-/-}53BP1^{-/-}$ B cells.

Increased end-resection in the absence of 53BP1 is independent of distance

Next we asked whether the increased end resection in the absence of 53BP1 is specific for joining of DSBs across 96 kb. We first applied our PCR assay to measure resection frequency of DSBs separated by 1.2 kb utilizing B cells of $IgH^{I\text{-}1k/+}AID^{-/-}53BP1^{-/-}$ mice and the respective 53BP1 proficient control (Figure 4.4 A). Joins with deletions of more than 30 nt (indicative of extensive end-processing) increased from 37.2 % in $IgH^{I\text{-}1k/+}AID^{-/-}$ to 52.4 % in $IgH^{I\text{-}1k/+}AID^{-/-}53BP1^{-/-}$. Sequencing of joins showed a corresponding increase in the average amount of end resection from 54.8 nt in $IgH^{I\text{-}1k/+}AID^{-/-}$ to 90.4 nt in $IgH^{I\text{-}1k/+}AID^{-/-}53BP1^{-/-}$ (Figure 4.4 C).

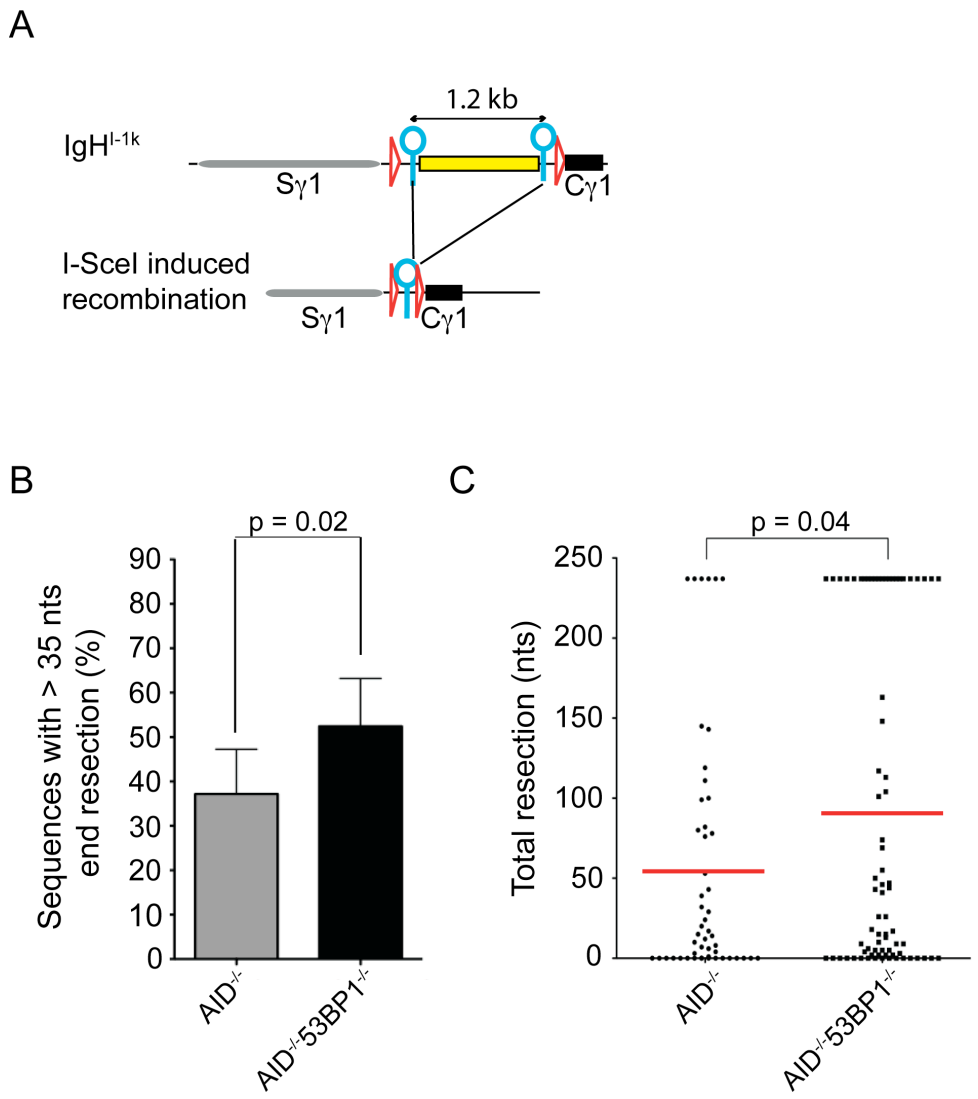

Figure 4.4. 53BP1 effects on end resection during proximal DSBs joining.

(A) Schematic representation of $IgH^{I\text{-}1k}$ allele before (top) and after (bottom) I-SceI induced recombination. I-SceI sites are indicated as blue circles, loxP sites as red triangles. PCR primers to amplify recombination products are shown as arrows.

(B) Bar graph showing the frequency of I-SceI induced recombination products with more than 30 nt end processing for $IgH^{I\text{-}1k/+}AID^{-/-}$ and $IgH^{I\text{-}1k/+}AID^{-/-}53BP1^{-/-}$ B cells. Error bars indicate standard deviations. The p-value was calculated using the Student's t-test (two-tailed). Average of seven independent measurements.

(C) Dot plot showing resection in sequences from I-SceI infected $IgH^{I\text{-}1k/+}AID^{-/-}$ and $IgH^{I\text{-}1k/+}AID^{-/-}53BP1^{-/-}$ B cells, with each dot representing one sequence. Average is indicated as a red line. The p-value was calculated using the Student's t-test (two-tailed).

Next we tested whether loss of 53BP1 leads to increased end resection upon joining of DBSs across long distances utilizing our $IgH^{I\text{-}27M}$ mice. Similarly to our observations for joining of DSBs separated by 1.2 kb and 96 kb the extent of end processing increased from 55.5 % in $IgH^{I\text{-}27M/+}AID^{-/-}$ to 75.5 % in $IgH^{I\text{-}27M/+}AID^{-/-}53BP1^{-/-}$ (Figure 4.5 B), with the precise loss of sequence increasing from 103.2 nt to 142 nt in $IgH^{I\text{-}27M/+}AID^{-/-}$ and $IgH^{I\text{-}27M/+}AID^{-/-}53BP1^{-/-}$, respectively (Figures 4.5 C).

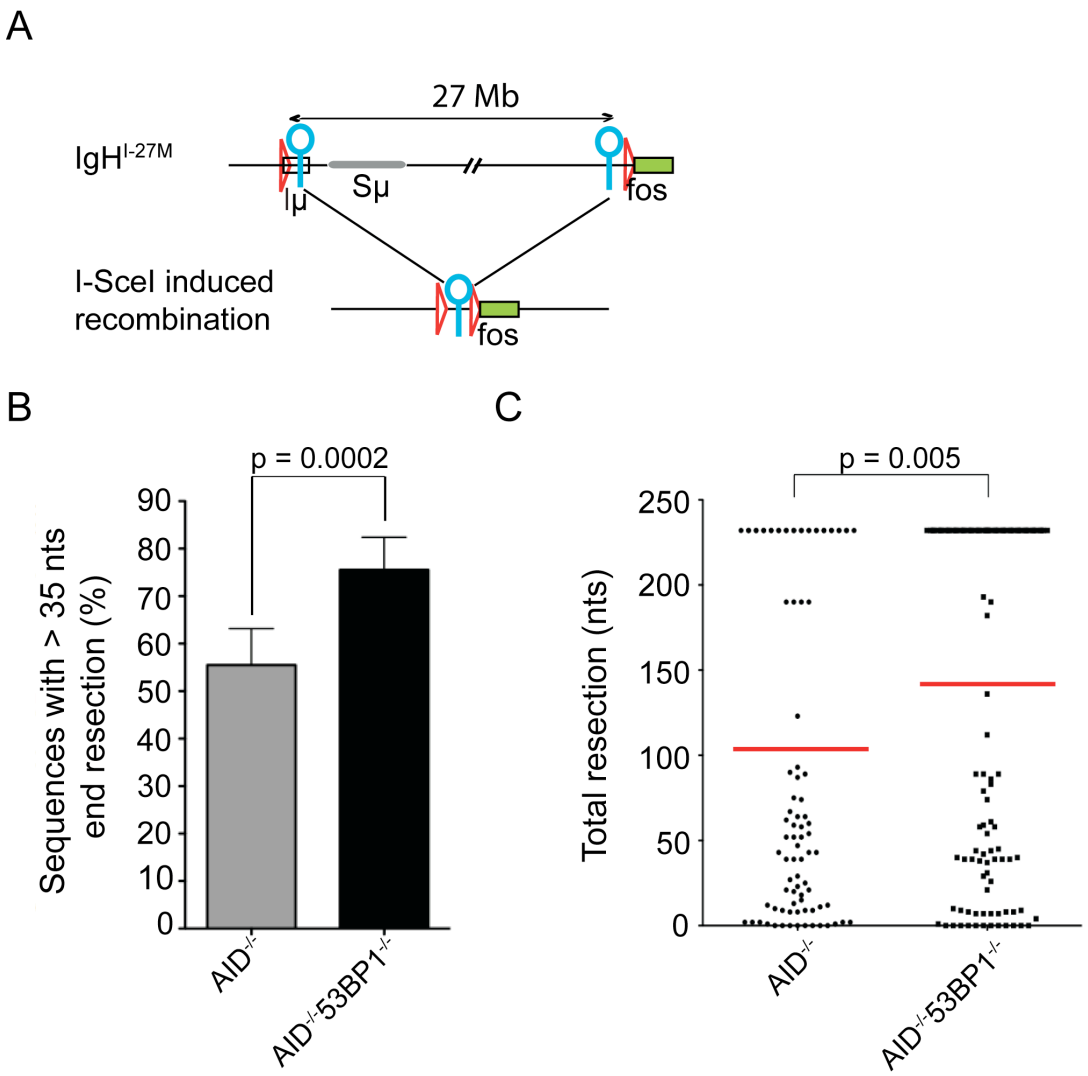

Figure 4.5. 53BP1 effects on end resection during distal (27 Mb) DSB joining.

(A) Schematic representation of $IgH^{I\text{-}27M}$ allele before (top) and after (bottom) I-SceI induced recombination. I-SceI sites are indicated as blue circles, loxP sites as red triangles. PCR primers to amplify recombination products are shown as arrows.

(B) Bar graph showing the frequency of I-SceI induced recombination products with more than 30 nt end processing for $IgH^{I\text{-}27M/+}AID^{-/-}$ and $IgH^{I\text{-}27M/+}AID^{-/-}53BP1^{-/-}$ B cells. Error bars indicate standard deviations. The p-value was calculated using the Student's t-test (two-tailed). Average of seven independent measurements.

(C) Dot plot showing resection in sequences from I-SceI infected $IgH^{I\text{-}27M/+}AID^{-/-}$ and $IgH^{I\text{-}27M/+}AID^{-/-}53BP1^{-/-}$ B cells, with each dot representing one sequence. The p-value was calculated using the Student's t-test (two-tailed). Means are indicated as red lines.

Next we asked whether loss of 53BP1 also affects the repair process of DSBs on different chromosomes, utilizing the I-SceI inducible *c-myc/IgH* translocation system described in Chapter 2 (Figure 4.6 A). While the average amount of nucleotides lost from $Myc^{I/+}IgH^{I/+}AID^{-/-}$ B cells is 448.2, the average amount of end resection increased almost two-fold to 742.3 nt in $Myc^{I/+}IgH^{I/+}AID^{-/-}53BP1^{-/-}$ B cells (Figure 4.6 B). Hence, we find that the absence of 53BP1 leads to increased DNA end resection even when DSBs are joined across different chromosomes

We conclude that 53BP1's ability to prevent end resection is independent of distance between paired DSBs.

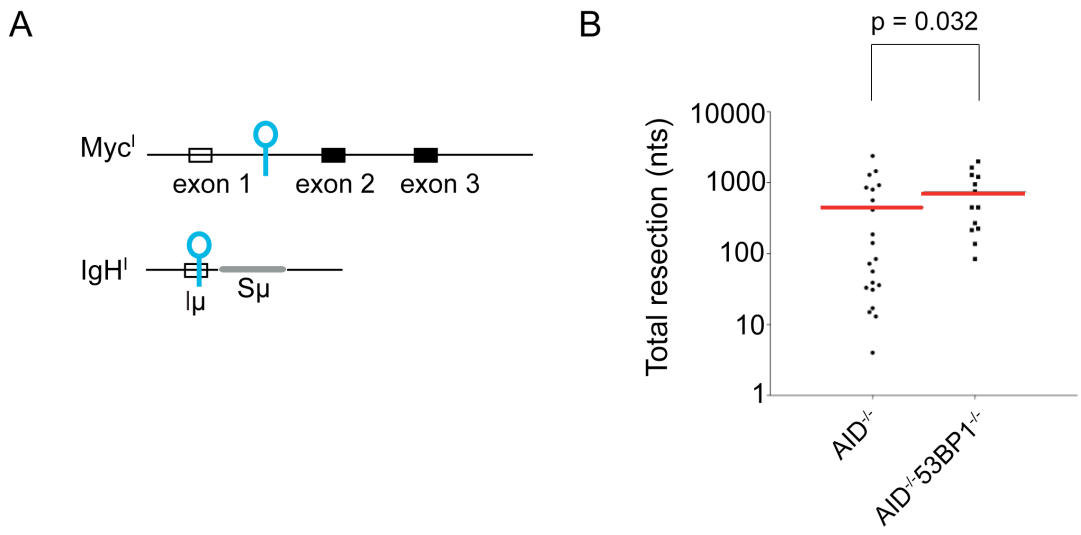

Figure 4.6. 53BP1 effect on trans-chromosomal joining of DSBs.

(A) Schematic representation of the Myc^{I} and IgH^{I} alleles.

(B) Dot plot showing resection in sequences from I-SceI infected $Myc^{I/+}IgH^{I/+}AID^{-/-}$ B cells in the presence or absence of 53BP1. The p-value was calculated using a two-tailed students t-test. Means are indicated as red lines.

Inhibition of ATM kinase decreases resection

Optimal resection and formation of the single-stranded DNA substrate for HR requires ATM kinase activity as it facilitates the recruitment and activation of the nucleases that attack DNA ends (83, 234). Although HR does not appear to be involved in CSR, we investigated whether a related mechanism is involved in processing DNA ends for microhomology based A-NHEJ.

To this end, we treated I-SceI infected $IgH^{I\text{-}96k/+}AID^{-/-}$ and $IgH^{I\text{-}96k/+}AID^{-/-}53BP1^{-/-}$ B cells with a small molecule inhibitor of ATM (ATMi). Indeed, ATMi treated $IgH^{I\text{-}96k/+}AID^{-/-}$ B cells showed significantly reduced DNA end resection (17.8% ATMi vs. 34.1% control, Figure 4.7 A and B) and a concomitant increase in the number of precise I-SceI joins (47.6 % in ATMi treated vs. 30.9% in control, Figure 4.7 C). Thus, the increase in I-SceI induced DNA end processing observed in the absence of 53BP1 is dependent on ATM.

Figure 4.7. Increased DNA end resection in the absence of 53BP1 is dependent on ATM.

(A) Representative ethidium bromide stained agarose gels showing the PCR amplification products after I-SceI induced recombination of $IgH^{I\text{-}96k/+}AID^{-/-}$ and $IgH^{I\text{-}96k/+}AID^{-/-}53BP1^{-/-}$ B cells in the presence or absence of ATMi.

(B) Bar graph showing the frequency of I-SceI induced recombination products running at or below 300 nt, for $IgH^{I\text{-}96k/+}AID^{-/-}$ and $IgH^{I\text{-}96k/+}AID^{-/-}53BP1^{-/-}$ B cells in the presence or absence of ATMi. Error bars indicate standard deviation. P-value was calculated using Student's t-test (two-tailed), three independent experiments.

(C) Frequency of direct I-SceI joins, reconstituting an I-SceI site, as determined by sequencing of individual amplification products of I-SceI infected $IgH^{I\text{-}96k/+}AID^{-/-}$ and $IgH^{I\text{-}96k/+}AID^{-/-}$ $53BP1^{-/-}$ B cells in the presence or absence of ATMi. Error bars indicate standard deviation. P-value was calculated using Student's t-test (two-tailed), three independent sequencing experiments.

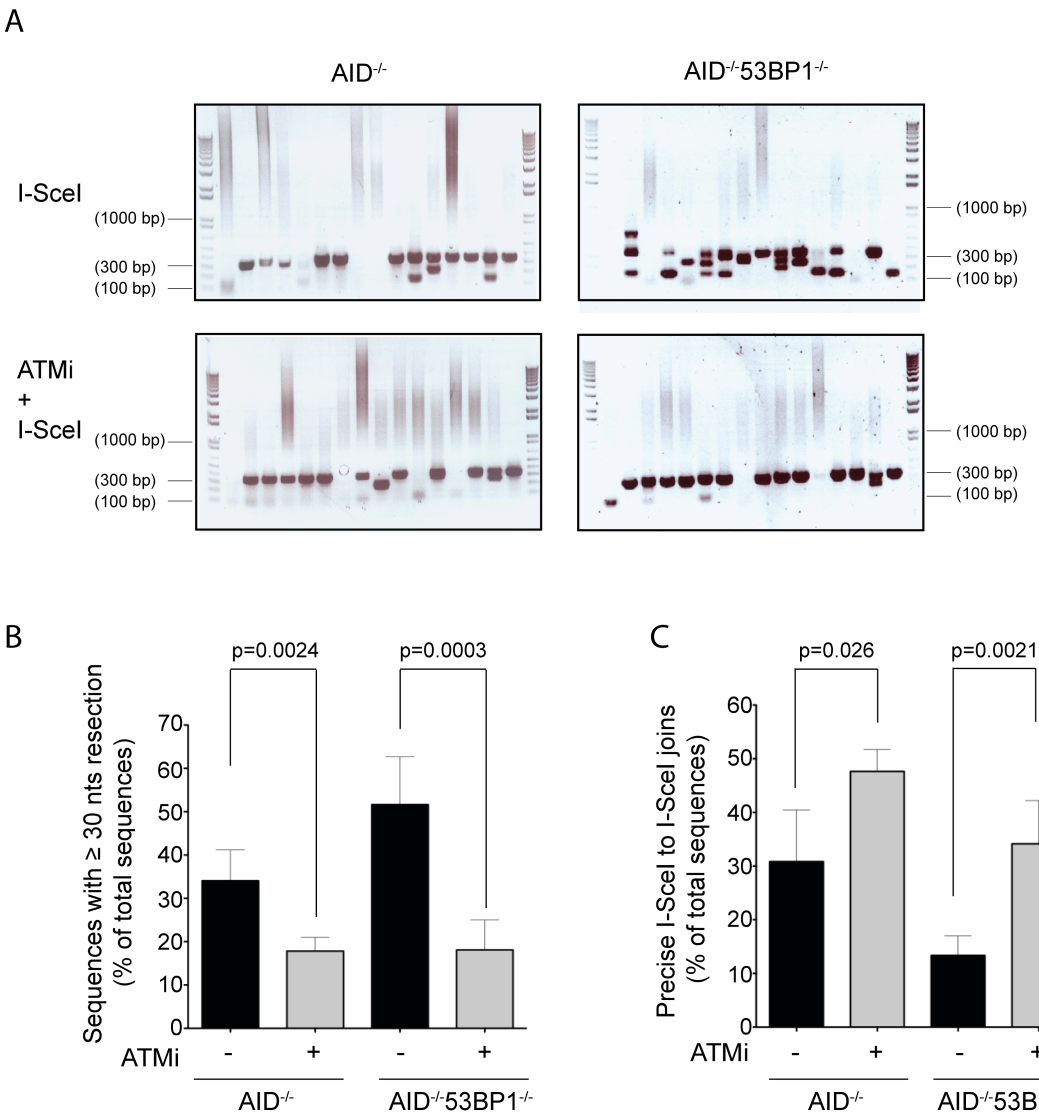
A
AID-/-
AID-/-53BP1-/-
I-SceI
(1000 bp)
(300 bp)
(100 bp)
ATMi
+
I-SceI
B
p=0.0024
p=0.0003
Sequences with ≥ 30 nts resection
(% of total sequences)
ATMi
AID-/-
AID-/-53BP1-/-
C
p=0.026
p=0.0021
Precise I-SceI to I-SceI joins
(% of total sequences)

Partial rescue of CSR in 53BP1 deficient B cells treated with ATMi

Loss of 53BP1 interferes with CSR, but enhances recombination between repeat DNA within switch regions (194-196, 208). Since the latter requires DNA end processing we examined whether inhibition of DNA end processing by ATMi enhances CSR in 53BP1$^{-/-}$ B cells. In agreement with published studies (191, 192, 235), ATMi reduces CSR to IgG1 in wild type B cells from 21.5% to 11.6% (Figure 4.8 A). In striking contrast, ATMi enhanced CSR in 53BP1$^{-/-}$ B cells from 1.3% to 3.2% (Figure 4.8 B). We conclude that ATMi ameliorates the severe defect in CSR observed in the absence of 53BP1.

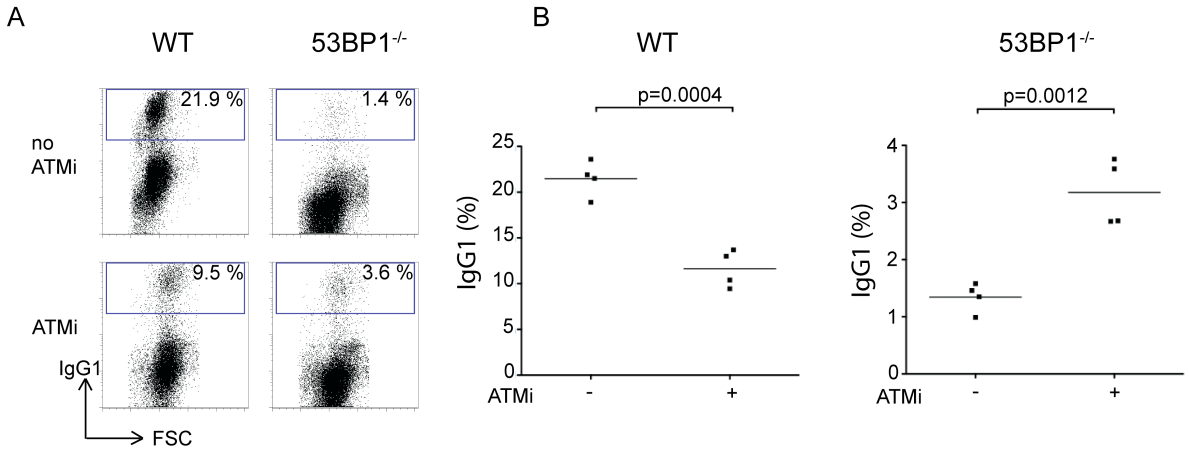

Figure 4.8. Inhibition of ATM partially rescues the CSR defect in 53BP1$^{-/-}$ B cells.

(A) Representative flow cytometry experiment showing CSR to IgG1 by wild type and 53BP1$^{-/-}$ B cells, 96 hrs after LPS, IL-4 and RP105 stimulation in the presence or absence of ATMi.

(B) Graph summarizes CSR to IgG1 by wild type and 53BP1$^{-/-}$ B cells in four independent experiments in the presence or absence of ATMi. Means are shown as a line in the graph and in the table below the graph. P-value was calculated using Student's t-test (two-tailed).

CHAPTER 5:

53BP1 Structure/Function Analysis

53BP1 is a DNA damage response protein that rapidly forms nuclear foci in response to DNA damage (60-62). This process is dependent on PIKK-(ATM/ATR/DNA-PKcs) induced phosphorylation of histone H2AX (γH2AX, (70-73)). γH2AX in turn recruits the E3 ubiquitin ligases RNF8 and RNF168 (51, 52, 55, 56, 236) which promote histone ubiquitylation at sites of DSBs. The way in which ubiquitylation facilitates the accumulation of 53BP1 at sites of DSBs has not yet been defined; but one possible scenario is that ubiquitylation exposes constitutive chromatin marks, such as H4K20me2, to which 53BP1 then binds via its tandem tudor domain (52, 65).

In addition to its chromatin binding tudor domain, 53BP1 contains an oligomerization domain, tandem BRCT domains, and numerous sites that can be modified post-translationally (237). Homo-oligomerization and interaction between the tudor domains and H4K20me2 are required for 53BP1 focus formation in response to DNA damage (63, 65, 72, 75, 76). In contrast, the C-terminal tandem BRCT domains are not essential for focus formation, but mediate the interaction between 53BP1 and EXPAND1, a protein shown to promote chromatin changes after DNA damage and to facilitate repair (50, 75). Finally, the N-terminal portion of 53BP1 lacks defined structural domains but contains multiple S/T-Q sites, which are phosphorylation targets of ATM. Although mutating these residues to alanine alters the kinetics of resolution of DNA damage foci, it does not affect the formation of 53BP1 foci in response to

DNA damage (75, 78, 238). In addition to DNA damage dependent focus formation, 53BP1 is required to protect DSBs from end resection.

In this chapter we analyze the contribution of 53BP1's functional domains towards the protection of broken ends from resection, CSR, chromatin binding and focus formation upon DNA damage.

The BRCT domains are dispensable for CSR and the prevention of end resection

To investigate the function of the BRCT domains of 53BP1 in CSR and for the protection of DNA ends from resection, we deleted the region corresponding to amino acids 1708-1969 from the mouse germline (53BP1$^{\Delta BRCT}$; Figure 5.1 A). Lymphocyte development was normal in 53BP1$^{\Delta BRCT}$ mice (Figure 5.1 B), despite lower than wild type levels of the mutant protein (Figure 5.1 C).

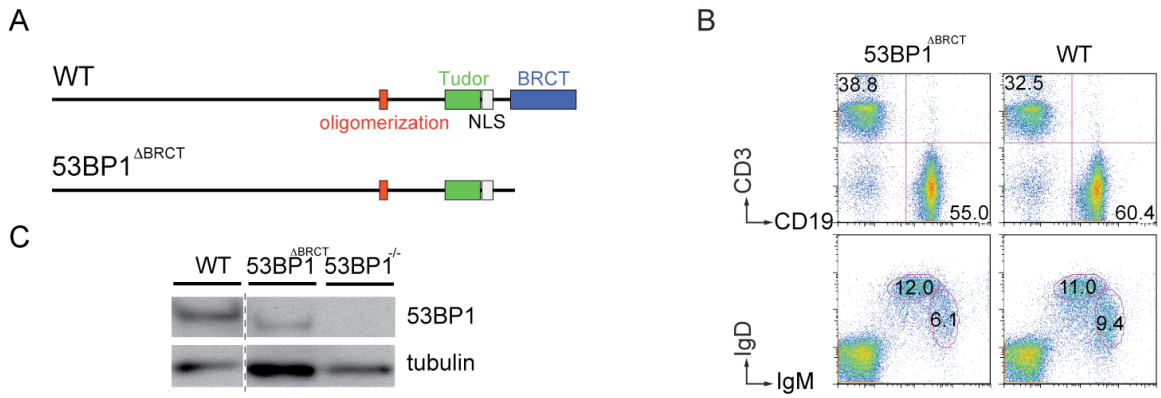

Figure 5.1. B cell development is unaltered in 53BP1$^{\Delta BRCT}$ mice but expression of the truncated protein is reduced.

(A) Schematic representation of wild type (WT) 53BP1 protein (top) and (53BP1$^{\Delta BRCT}$) lacking the BRCT domains (bottom).

(B) Flow cytometric analysis of splenocytes from age-matched wild type and 53BP1$^{\Delta BRCT}$ mutant mice showing normal B lymphocyte development. Immuno-staining was performed with the indicated markers on total spleen cells. Representative of three independent experiments.

(C) Western blot on total cell lysates showing 53BP1 expression levels in WT and 53BP1$^{\Delta BRCT}$ B cells.

We next tested whether the absence of the BRCT domains affects CSR. 53BP1$^{\Delta BRCT}$ B cells were stimulated with LPS, IL-4 and RP105 to induce CSR to IgG1. We found that CSR in 53BP1$^{\Delta BRCT}$ B cells occurs at levels comparable to WT control cells and conclude that the BRCT domains are dispensable for CSR. (Figure 5.2).

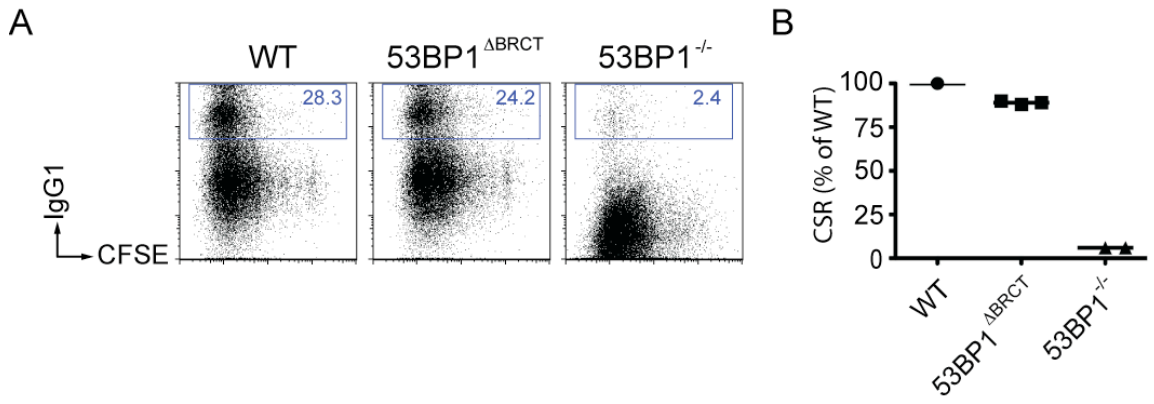

Figure 5.2. The tandem BRCT domains of 53BP1 are not required for CSR.
(A) Representative flow cytometry plots measuring CSR to IgG1 after stimulation of WT, 53BP1$^{\Delta BRCT}$ and 53BP1$^{-/-}$ B cells.
(B) Summary dot plot indicating CSR as a percentage of WT. The bar indicates the mean. Each dot represents an independent experiment.

To determine whether the BRCT domains are required for DSB end protection, we produced 53BP1$^{\mathbf{\Delta BRCT}/-}IgH^{I\text{-}96k/+}$ mice and assayed the resection of paired I-SceI breaks. We found a minor increase in the number of PCR products that showed extensive end resection (> 35 nt) in 53BP1$^{\mathbf{\Delta BRCT}/-}IgH^{I\text{-}96k/+}$ B cells compared to control IgH$^{I\text{-}96k/+}$, B cells, which can probably be attributed to the decreased expression level of the mutant protein (Figure 5.3 B). However, sequencing of PCR products did not reveal a major difference in the total number of nucleotides resected between IgH$^{I\text{-}96k/+}$ and 53BP1$^{\mathbf{\Delta BRCT}/-}IgH^{I\text{-}96k/+}$ B cells. We conclude that the BRCT domains of 53BP1 are dispensable the protection of DNA ends from resection.

Figure 5.3. The tandem BRCT domains of 53BP are not required to protect DSBs from end resection.

(A) Representative ethidium bromide stained agarose gels showing PCR products obtained after I-SceI induced recombination in $IgH^{I\text{-}96k/+}$, $IgH^{I\text{-}96k/+}53BP^{\Delta BRCT}$ and $IgH^{I\text{-}96k}53BP1^{-/-}$ B cells. Red arrows point to the expected product size of 336 nts.

(B) Bar graph quantitating the frequency of I-SceI induced recombination products with more than 35 nt end processing. Error bars indicate standard deviations. The p-value was calculated using the Student's t-test (two-tailed). Average of at least six independent measurements using B cells from two mice.

(C) Dot plot showing resection with each dot representing one sequence. Average is indicated as a red line. The p-value was calculated using the Student's t-test (two-tailed). Recombination junctions from two mice were analyzed.

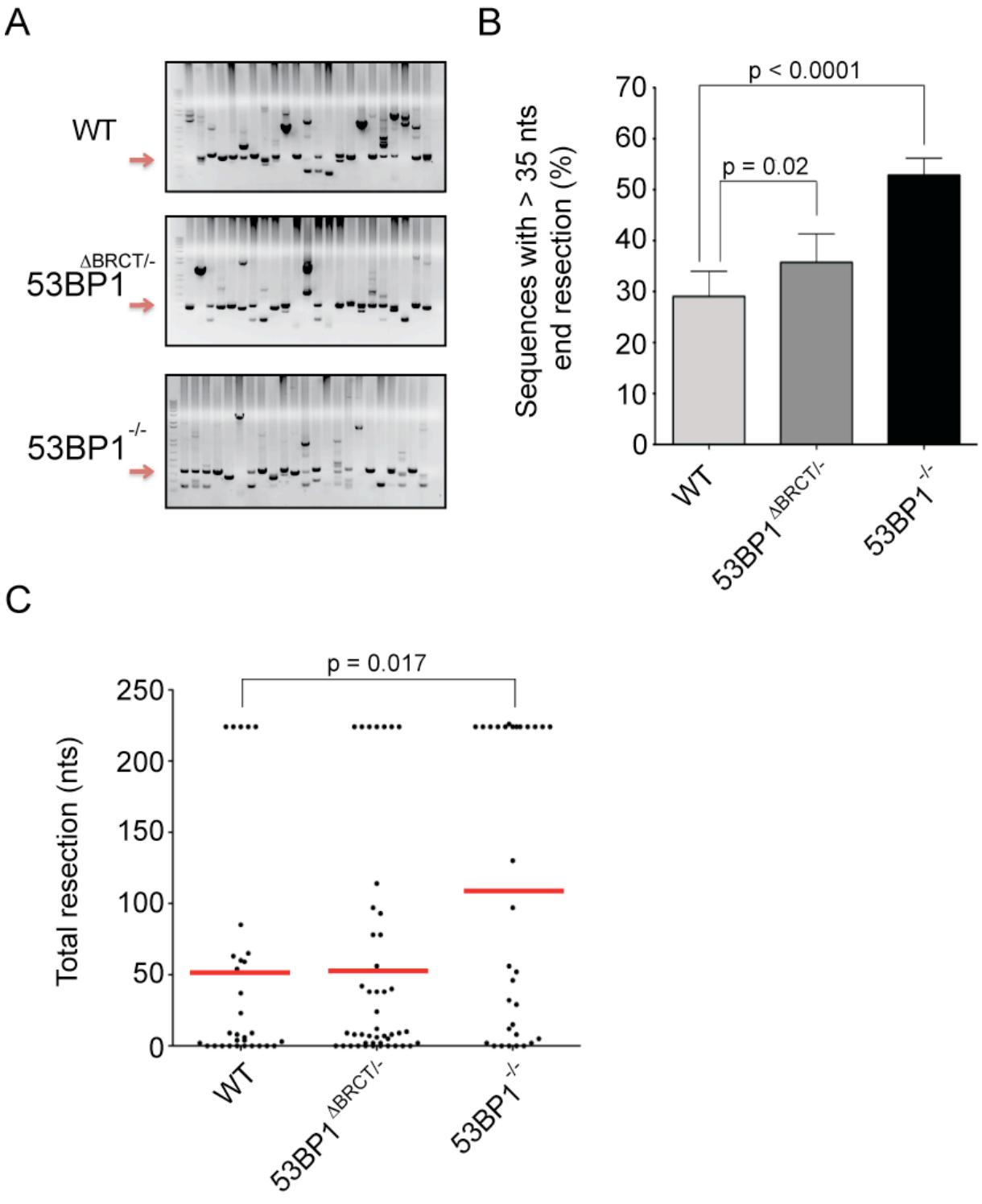
A
WT
ΔBRCT/-
53BP1
53BP1 -/-
B
Sequences with > 35 nts end resection (%)
p < 0.0001
p = 0.02
70
60
50
40
30
20
10
0
WT
53BP1 ΔBRCT/-
53BP1 -/-
C
Total resection (nts)
p = 0.017
250
200
150
100
50
0
WT
53BP1 ΔBRCT/-
53BP1 -/-

53BP1 is constitutively associated with chromatin

53BP1 is a predominantly nuclear protein and forms nuclear foci in response to DNA damage (60, 65). Focus formation was shown to require the interaction of the 53BP1 tandem tudor domains with H4K20me2. It is unclear whether or not this interaction is inducible or constitutive, as the global level of H4K20me2 does not seem to change upon DNA damage. To determine the cellular distribution of 53BP1 and whether it changes upon DNA damage we biochemically fractionated WT day 0 B cells (no stimulation). We confirmed the previous finding that 53BP1 is a predominantly nuclear protein, as virtually no signal could be detected in the cytoplasmic fraction (Figure 5.4 left panel). The majority of 53BP1 is present in the nuclear soluble fraction; however, we could reproducibly detect the association of 53BP1 with chromatin in an undamaged state (Figure 5.4, left panel). Upon treatment of IR, we could not detect a measurable increase in 53BP1 chromatin association, with the majority of the protein remaining in the nuclear soluble fraction (Figure 5.4, right panel). We conclude that a fraction of 53BP1 is constitutively chromatin associated and that upon treatment with 10 Gy of IR, 53BP1 chromatin association is not increased globally.

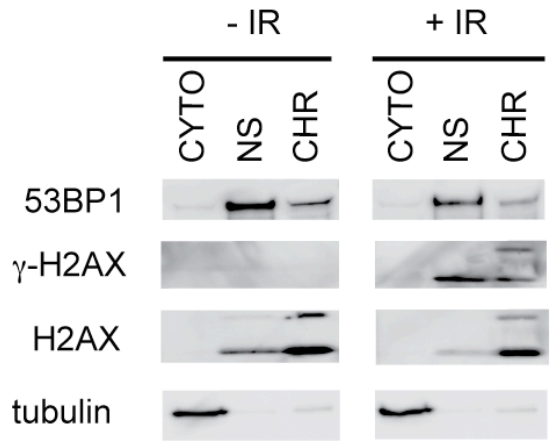

Figure 5.4. 53BP1 is constitutively associated with chromatin in the absence of IR induced DNA damage. Western blots of fractionated WT B cells on day 0 with (+) or without (-) 10 Gy of IR, probed with antibodies shown on left. CYTO, cytoplasmic fraction; NS, nuclear soluble fraction; CHR, chromatin fraction.

The tudor domain is required for CSR and the prevention of end resection

The aspartic acid residue D1521 in the tudor domain of human 53BP1 is required for its binding to H4K20me2 (65). To test the significance of this interaction in CSR and the prevention of DNA resection, we produced D1518R mutant mice (53BP1^{DR}) bearing a single amino acid substitution that is equivalent to D1521R in humans (Figure 5.5 A). Lymphocyte development was similar to wild type in 53BP1^{DR} mice (Figure 5.5 B), and the mutant 53BP1^{DR} protein was normally phosphorylated at Ser^{25} upon IR (Figure 5.5 C).

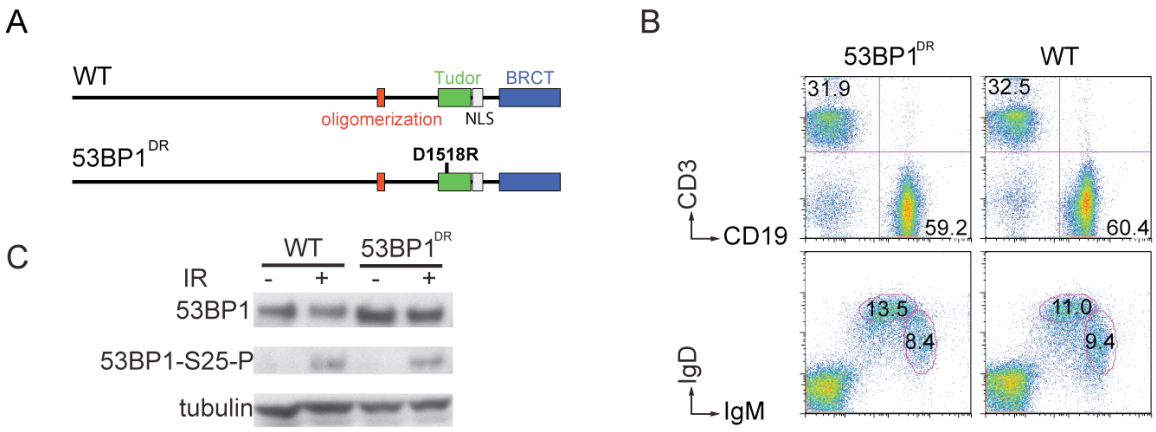

Figure 5.5. B cell development and 53BP1 phosphorylation are unaltered in 53BP1 tudor domain mutant mice.

(A) Schematic representation of WT 53BP1 (top) and 53BP1 with tudor domain mutation D1518R (bottom).

(B) Flow cytometric analysis of splenocytes from age-matched wild type and 53BP1^{DR} mutant mice reveals normal B lymphocyte development. Immuno-staining was performed with the indicated markers on total spleen cells. Representative of three independent experiments.

(C) Western blots showing 53BP1 expression levels and phosphorylation at Ser^{25} in response to 10 Gy of IR (90 min recovery) in WT and 53BP1^{DR} B cells.

In agreement with previous studies, 53BP1^{DR} failed to form IR-induced foci in mouse embryonic fibroblasts (MEFs; Figures 5.6 A, (64, 65)). In addition, 53BP1^{DR} was not chromatin associated in B cells (Figure 5.6 B). In fact, we noticed that in contrast to wild type 53BP1 the majority of 53BP1^{DR} was located in the cytoplasm. Though the nuclear localization signal remains intact in this mutant, we cannot exclude that defects in nuclear localization are responsible for the observed deficiency in chromatin association. We conclude that chromatin association is required for focus formation but dispensable for DNA damage inducible 53BP1 phosphorylation.

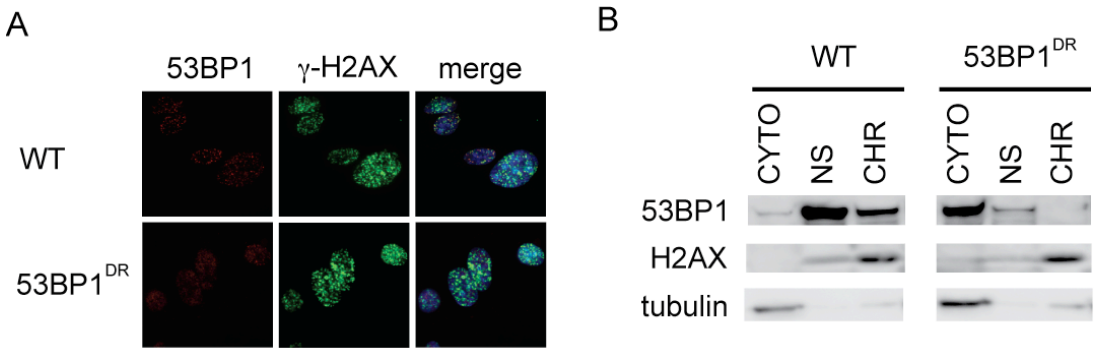

Figure 5.6. The tudor domain of 53BP1 is required for focus formation and constitutive interaction with chromatin.

(A) 53BP1 and γ-H2AX IRIF in WT and 53BP1^{DR} MEFs after 10 Gy of IR, recovery 90 min *(contributed by Jacqueline Barlow)*.

(B) Western blots of fractionated WT and 53BP1^{DR} B cells on day 0. CYTO, cytoplasmic fraction; NS, nuclear soluble fraction; CHR, chromatin fraction.

To determine whether chromatin association is required for CSR, we stimulated 53BP1^{DR} B cells *in vitro*. Mutant B cells assayed for IgG1 expression on day 4 of LPS, IL-4 and RP105 stimulation showed class switching at about 10% of wild type levels, phenocopying 53BP1$^{-/-}$ (Figure 5.7).

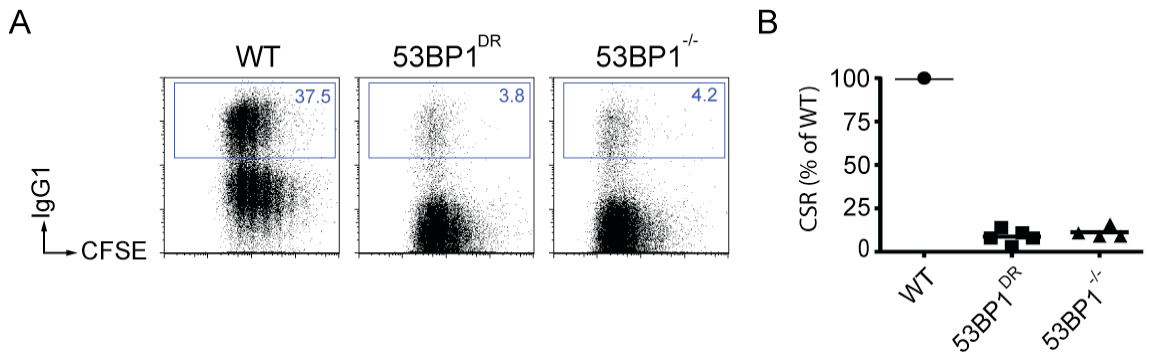

Figure 5.7. The tudor domain of 53BP1 is required for CSR.

(A) Representative flow cytometry plots measuring CSR to IgG1 after stimulation of WT, 53BP1^{DR} and 53BP1$^{-/-}$ B cells.

(B) Summary dot plot indicating CSR as a percentage of WT. The bar indicates the mean. Each dot represents an independent experiment.

We next determined the effect of the tudor domain mutation on the ability of 53BP1 to prevent the occurrence of end resection. We crossed 53BP1^{DR} mice to the resection reporter system IgH$^{I\text{-}96k}$ to produce IgH$^{I\text{-}96k/+}$53BP1^{DR} mice. We infected IgH$^{I\text{-}96k/+}$53BP1^{DR} B cells with I-SceI, inducing DSB formation at both IgH$^{I\mu}$ and IgH$^{I\gamma}$. DSB joining was measured using the previously described dilution PCR assay. We detected an increase in DNA end resection in 53BP1^{DR}IgH$^{I\text{-}96k/+}$ B cells comparable to 53BP1$^{-/-}$IgH$^{I\text{-}96k/+}$ controls (Figure 5.8). We conclude that 53BP1 is constitutively chromatin associated and that this association is required for the protection of DNA ends from resection. Furthermore, loss of chromatin association leads to a severe CSR defect.

Figure 5.8. The tudor domain of 53BP is required to protect broken ends from resection.

(A) Representative ethidium bromide stained agarose gels showing PCR products obtained after I-SceI induced recombination in $IgH^{I\text{-}96k/+}$, $IgH^{I\text{-}96k/+}53BP^{DR}$ and $IgH^{I\text{-}96k}53BP1^{-/-}$ B cells. Red arrows point to the expected product size of 336 nts.

(B) Bar graph quantitating the frequency of I-SceI induced recombination products with more than 35 nt end processing. Error bars indicate standard deviations. The p-value was calculated using the Student's t-test (two-tailed). Average of at least six independent measurements using B cells from two mice.

(C) Dot plot showing resection with each dot representing one sequence. The p-value was calculated using the Student's t-test (two-tailed). Recombination junctions from two mice were analyzed.

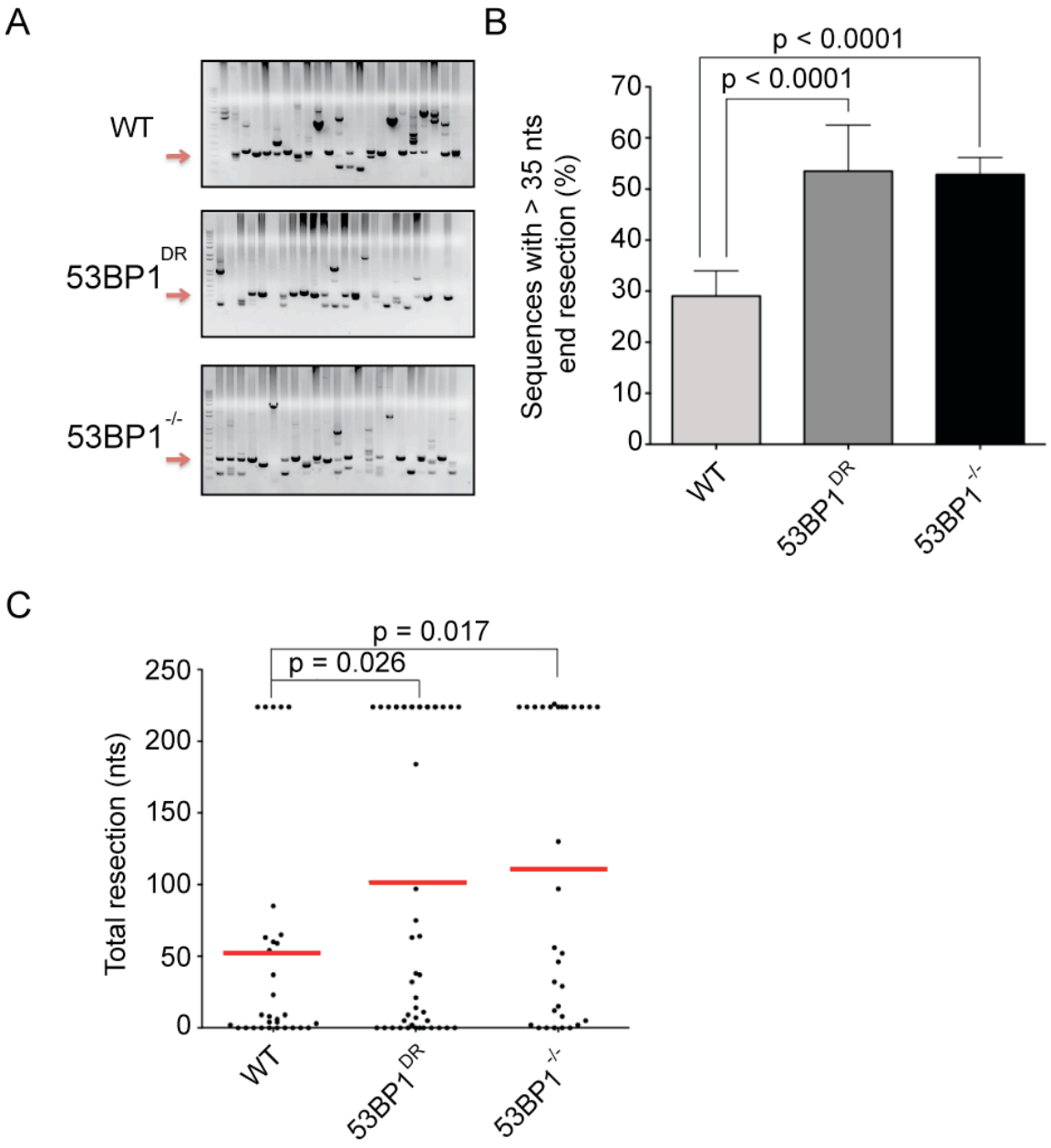
A
WT
53BP1 DR
53BP1 -/-
B
p < 0.0001
p < 0.0001
Sequences with > 35 nts end resection (%)
70
60
50
40
30
20
10
0
WT
53BP1 DR
53BP1 -/-
C
p = 0.017
p = 0.026
Total resection (nts)
250
200
150
100
50
0
WT
53BP1 DR
53BP1 -/-

53BP1 chromatin association is required but not sufficient for CSR and DNA end protection

H2AX is required for stable 53BP1 DNA damage focus formation, and its deficiency impairs CSR, but to a lesser extent than absence of 53BP1 (37, 71, 193). Moreover, 53BP1 was reported to interact with H2AX (72). To determine if the chromatin association of 53BP1 depends on this histone variant, we assayed H2AX deficient B cells. Although H2AX is required for 53BP1 foci, we found that H2AX is dispensable for constitutive 53BP1 chromatin association (Figure 5.9).

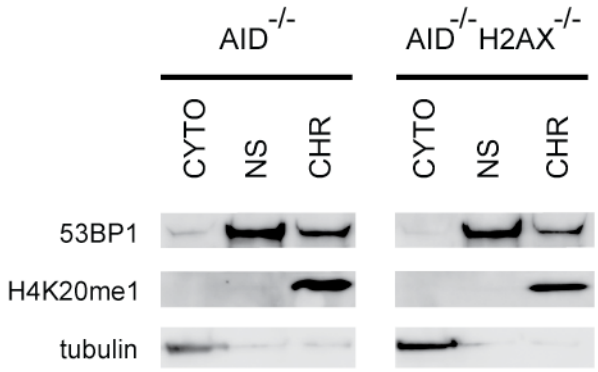

Figure 5.9. 53BP1 is chromatin associated in the absence of H2AX.
(A) Western blots of unstimulated fractionated $AID^{-/-}$ and $AID^{-/-}H2AX^{-/-}$ B cells. CYTO, cytoplasmic fraction; NS, nuclear soluble fraction; CHR, chromatin fraction.

To determine if H2AX is required to prevent DNA resection, we assayed $IgH^{I\text{-}96k/+}AID^{-/-}$ $H2AX^{-/-}$ B cells. We found that resection was increased in the absence of H2AX to levels comparable to $53BP1^{-/-}$ (51.7 % compared to 35.8 % in $IgH^{I\text{-}96k}AID^{-/-}$ control, Figure 5.10 A and B).

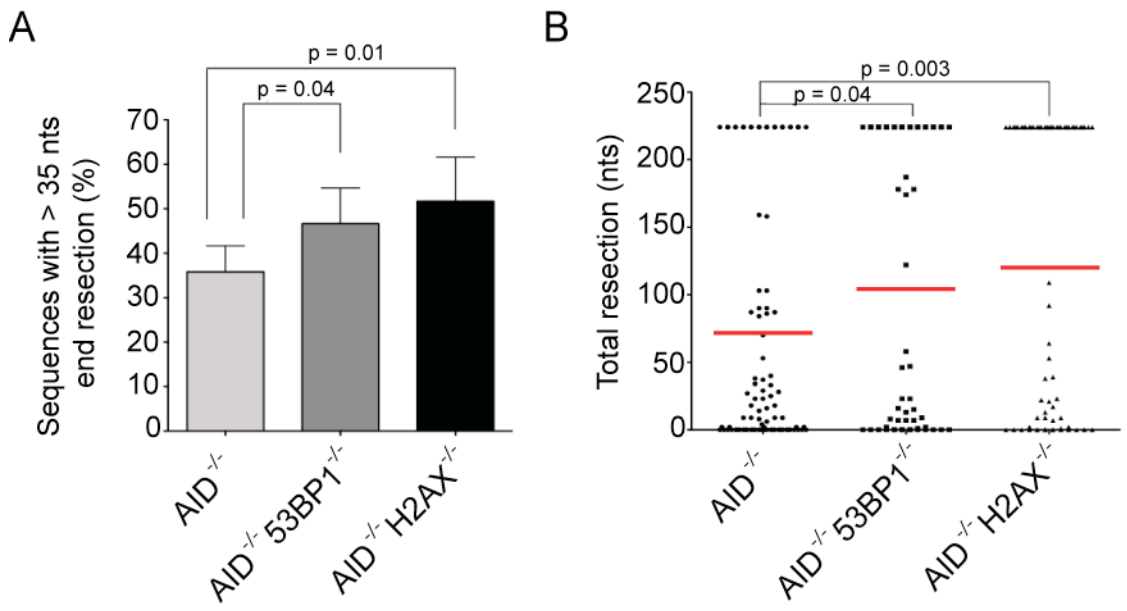

Figure 5.10. Chromatin associated 53BP1 is not sufficient for preventing end resection in the absence of H2AX.

(A) Bar graph showing the frequency of I-SceI induced recombination products with more than 35 nts end processing for $IgH^{I\text{-}96k/+}AID^{-/-}$, $IgH^{I\text{-}96k/+}AID^{-/-}53BP1^{-/-}$ and $IgH^{I\text{-}96k/+}AID^{-/-}H2AX^{-/-}$ B cells. Error bars indicate standard error of the mean. The p-value was calculated using the Student's t-test (two-tailed). Difference in resection between $IgH^{I\text{-}96k/+}AID^{-/-}53BP1^{-/-}$ and $IgH^{I\text{-}96k/+}AID^{-/-}H2AX^{-/-}$ B cells is not significant. Average of three independent measurements using B cells from two separate mice.

(B) Dot plot showing resection in sequences from I-SceI infected $IgH^{I\text{-}96k/+}AID^{-/-}$, $IgH^{I\text{-}96k/+}AID^{-/-}53BP1^{-/-}$ and $IgH^{I\text{-}96k/+}AID^{-/-}H2AX^{-/-}$ B cells. Red arrows point to the expected product size of 336 nts. The p-value was calculated using the Student's t-test (two-tailed). Recombination junctions from two mice were analyzed.

The oligomerization domain of 53BP1 is required for CSR

The central region of 53BP1 is required for 53BP1 oligomerization (75, 76) and contains residues that are phosphorylated by ATM (S1219; (239)), ubiquitylated by Rad18 (K1268; (240)), and methylated by PRMT1 (R1398, R1400, R1401; (241)).

To determine the role of this region *in vivo*, we produced mice that express a mutant form of 53BP1 lacking this region (Figures 5.11 A). 53BP1$^{\Delta 1210\text{-}1447}$ protein was expressed at normal levels, and lymphocyte development in 53BP1$^{\Delta 1210\text{-}1447}$ mice was similar to wild type (Figures 5.11 B and C).

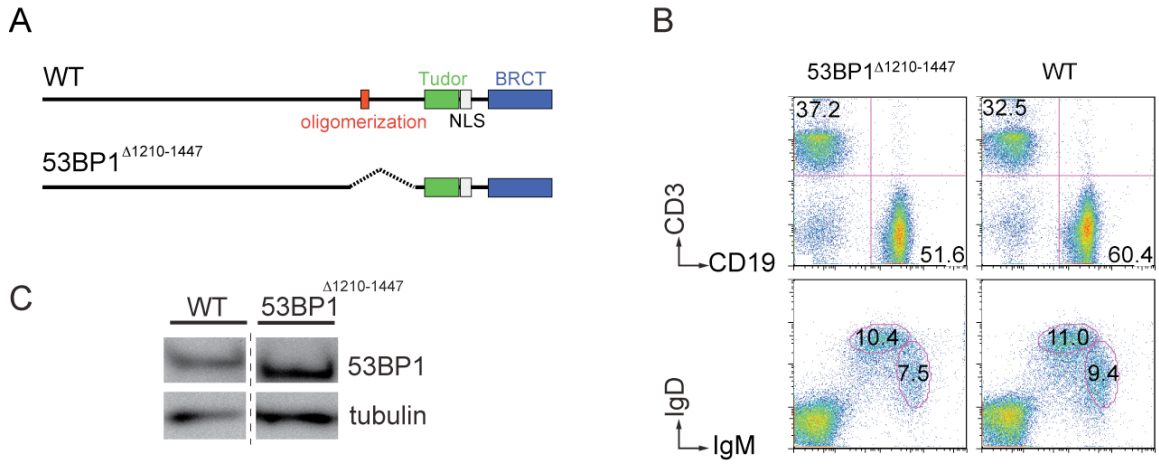

Figure 5.11. B cell development is unaltered in 53BP1$^{\Delta 1210\text{-}1447}$ mice and protein is expressed at normal.

(A) Schematic representation of wild type (WT) 53BP1 protein (top) and 53BP1 lacking the central domain (bottom).

(B) Flow cytometric analysis of splenocytes from age-matched wild type and 53BP1 $^{\Delta 1210\text{-}1447}$mutant mice reveals normal B lymphocyte development. Immuno-staining was performed with the indicated markers on total spleen cells. Representative of three independent experiments.

(C) Western blot showing 53BP1 expression levels in WT and 53BP1 $^{\Delta 1210\text{-}1447}$B cells.

However, 53BP1$^{\Delta 1210\text{-}1447}$ B cells similarly to 53BP1$^{-/-}$ B cells do not undergo CSR to IgG1 (Figure 5.12).

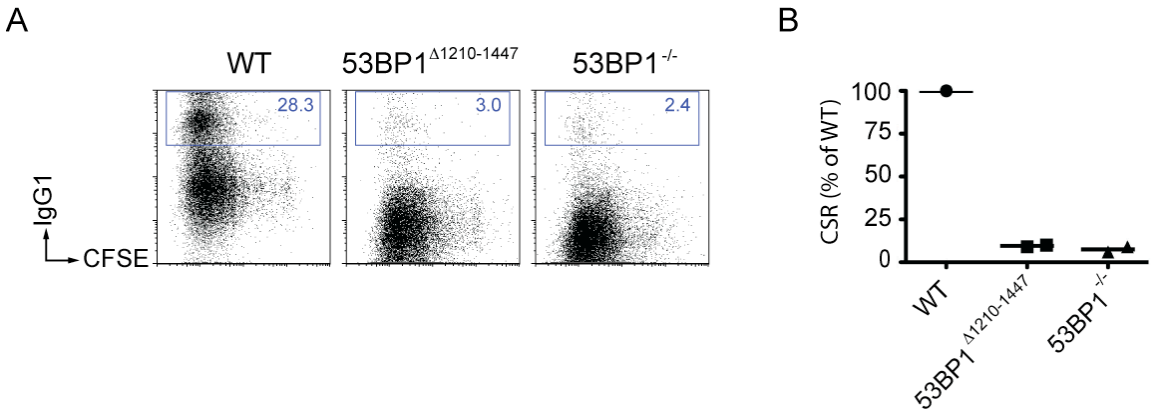

Figure 5.12. The central domain of 53BP1 is required for CSR.
(A) Representative flow cytometry plots measuring CSR to IgG1 after stimulation of WT, 53BP1$^{\Delta 1210\text{-}1447}$ and 53BP1$^{-/-}$ B cells.
(B) Summary dot plot indicating CSR as a percentage of WT. The bar indicates the mean. Each dot represents an independent experiment.

As the deletion of amino acids 1210-1447 of 53BP1 includes the oligomerization domain and several post-translational modification sites, we produced four region-specific mutant retroviruses and assayed them for their ability to rescue IgG1 switching in 53BP1$^{-/-}$ B cells (Figure 5.13 A) in order to identify which activity is required for CSR. All retroviruses were made without the tandem BRCT domains, since full-length 53BP1 is not expressed by retroviruses. Also, the retrovirus does not contain a GFP reporter gene, which compromises expression due to the size of the 53BP1 insert. We confirmed by

western blot that all retroviruses express the mutated 53BP1 proteins (Figure 5.13 B).

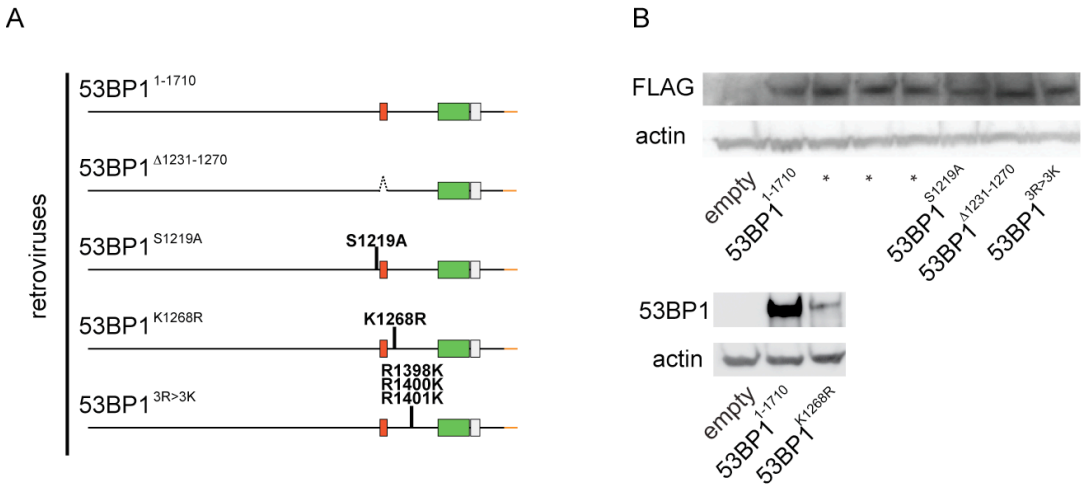

Figure 5.13. 53BP1 mutant retroviruses are expressed at normal levels after infection of 53BP1$^{-/-}$ B cells.
(A) Diagram of 53BP1 retroviral constructs with the indicated mutations and deletions.
(B) Western blot analysis on whole cell lysates to confirm that a protein of the expected size is produced upon retroviral infection. Asterisks denote lanes with unrelated samples, to be disregarded.

We then tested all four mutant 53BP1 retroviruses for their ability to rescue CSR upon infection in 53BP1$^{-/-}$ B cells (Figure 5.14 A). 53BP1$^{\Delta 1231\text{-}1270}$, which lacks the oligomerization domain, was the only mutant that failed to rescue CSR (Figure 5.14 A and B). We conclude that the oligomerization domain in 53BP1 is required for class switch recombination but that residues S1219, K1268 and R1398/R1400/R1401 are dispensable.

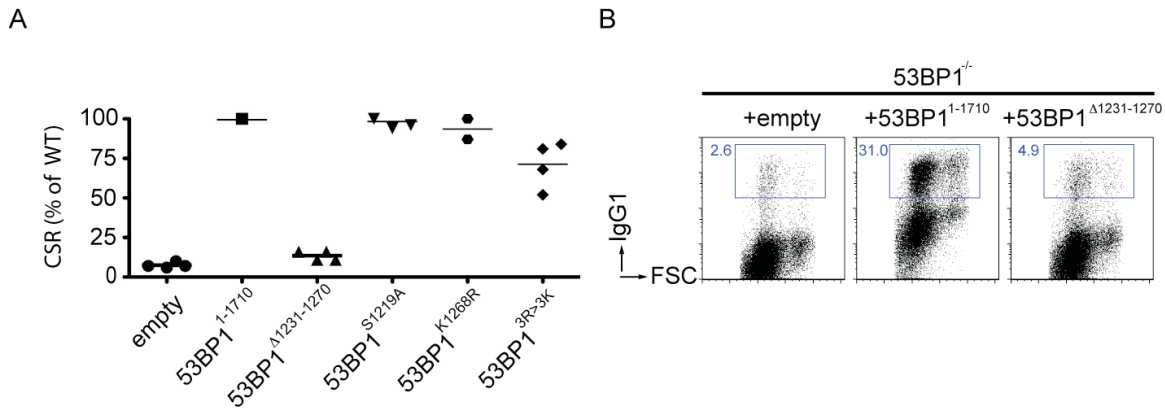

Figure 5.14. The oligomerization domain of 53BP1 is required for CSR.

(A) Summary dot plot indicating CSR as a percentage of WT value within the same experiment. The bar indicates the mean. Each dot represents an independent experiment.

(B) Representative flow cytometry plots measuring CSR after stimulation of 53BP1$^{-/-}$ B cells infected with the indicated retroviruses. Numbers indicate the percentage of IgG1 switched cells. CFSE dye tracks cell division.

We next tested whether the mutation in the oligomerization deletion affected the chromatin binding status of 53BP1. Interestingly, 53BP1$^{\Delta 1231\text{-}1270}$ partially retained the ability to bind chromatin (Figure 5.15 A, (76)). To test whether the oligomerization domain is required to protect DNA ends from resection, we reconstituted Brca1$^{\Delta 11/\Delta 11}$ 53BP1$^{-/-}$ B cells with the 53BP1$^{\Delta 1231\text{-}1270}$ retrovirus and measured the frequency of radial chromosome structures upon treatment with the PARP inhibitor (242). Loss of 53BP1 rescues homologous recombination in Brca1 mutant cells by facilitating the processing of DNA ends (242). Whereas 12 radial structures were found among 100 metaphases in Brca1$^{\Delta 11/\Delta 11}$53BP1$^{-/-}$ B cells infected with a negative control virus, 54 were present upon infection with 53BP1$^{1\text{-}1710}$ (average of two independent experiments, Figure 5.13 B). The

oligomerization mutant 53BP1$^{\Delta 1231\text{-}1270}$ showed on average 12/100 metaphases with radial fusions, which is similar to what we observed upon infection with an empty retrovirus (Figure 5.13 B). We therefore conclude that the oligomerization domain in 53BP1 is required for preventing DNA end resection.

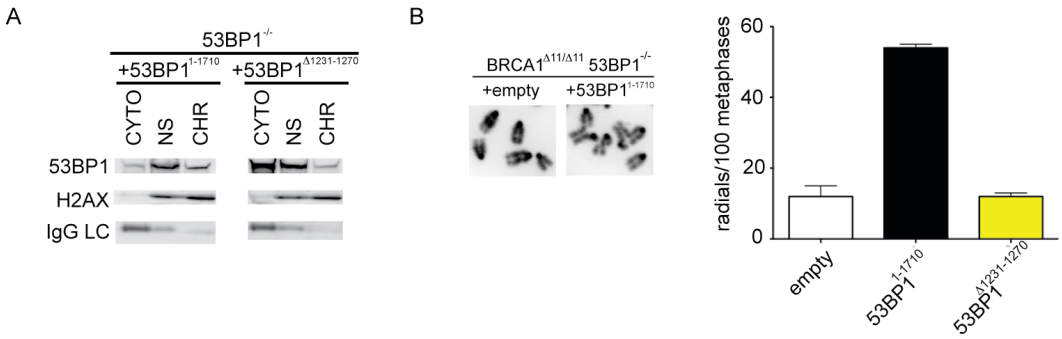

Figure 5.15. The oligomerization domain of 53BP1 is allows for partial chromatin association and is required for preventing end resection.

(A) Western blots of fractionated 53BP1$^{-/-}$ B cells stimulated and infected with 53BP1$^{1\text{-}1710}$ or 53BP1$^{\Delta 1231\text{-}1270}$. CYTO, cytoplasmic fraction; NS, nuclear soluble fraction; CHR, chromatin fraction.

(B) Left: Examples of normal metaphases (+empty) or metaphases containing radial chromosome structures (+53BP1$^{1\text{-}1710}$). Right: BRCA1$^{\Delta 11/\Delta 11}$53BP1$^{-/-}$ B cells reconstituted with 53BP1 mutant retroviruses. Histogram quantitating the number of radial structures upon infection with the indicated retroviruses. Error bars indicate standard error of the mean. Two independent experiments.

Minimal focus forming region is not sufficient for CSR

Residues 1052 to 1710 of 53BP1 include the tudor and oligomerization domains, which as shown above are required for efficient CSR and the prevention of end resection. We now asked whether oligomerization and chromatin binding are sufficient for 53BP1 function in those two processes and utilized 53BP1$^{1052\text{-}1710}$. A fragment that is can form DNA damage foci upon IR and contains those two

domains (Figure 5.16 A, (72, 76)). We confirmed expression of the mutant protein and found that expression levels are strongly elevated compared to the 53BP1$^{1-1720}$ control retrovirus Figure 5.16 B.

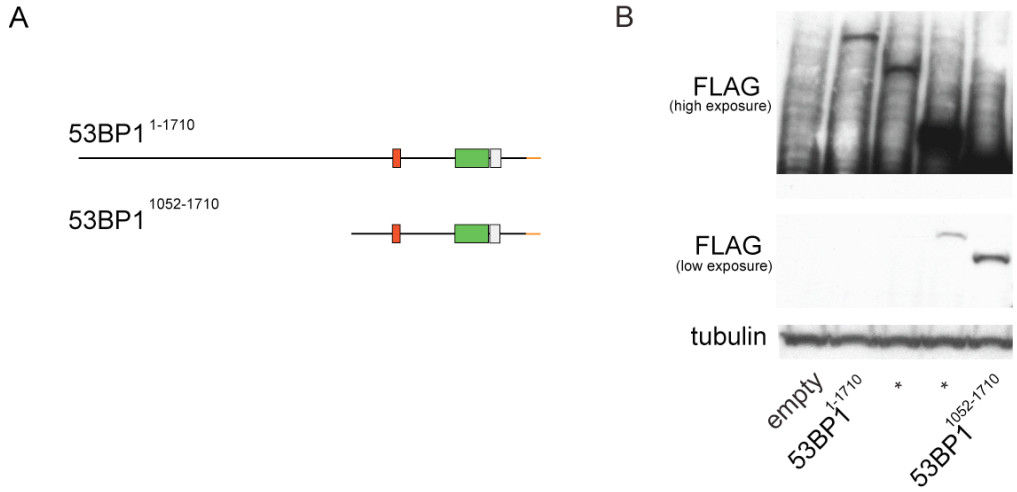

Figure 5.16. The focus forming region of 53BP1 is expressed at elevated levels in infected 53BP1$^{-/-}$ B cells.
(A) Schematic of 53BP1 retroviral construct with the indicated mutations and deletions.
(B) Western blot analysis on whole cell lysates to confirm that a protein of the expected size is produced upon retroviral infection. Asterisks (*) denote lanes with unrelated samples, to be disregarded.

However, despite high levels of expression retrovirally expressed 53BP1$^{1052-1710}$ was unable to rescue CSR (Figure 5.17 A and B).

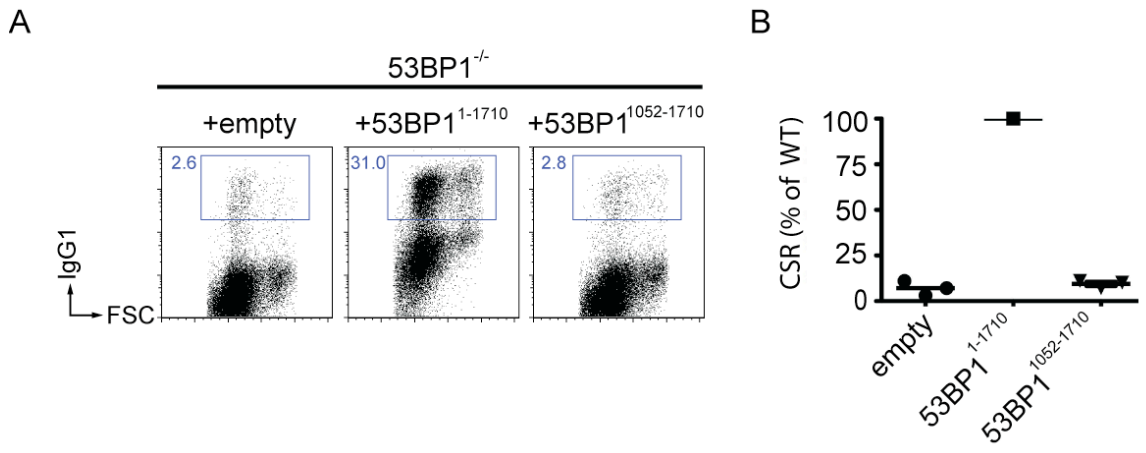

Figure 5.17. The focus forming region of 53BP1 is not sufficient for CSR.

(A) Representative flow cytometry plots measuring CSR after stimulation of 53BP1$^{-/-}$ B cells infected with the indicated retroviruses. Numbers indicate the percentage of IgG1 switched cells. CFSE dye tracks cell division.

(B) Summary dot plot indicating CSR as a percentage of WT value within the same experiment. The bar indicates the mean. Each dot represents an independent experiment.

We next determined the chromatin binding status and assayed whether the minimal focus forming fragment was able to protect DNA ends from resection. We found that despite retaining its ability to bind chromatin, DNA ends were processed such that radial structures were prevented similar to 53BP1 deficiency (Figure 5.18 A and B)

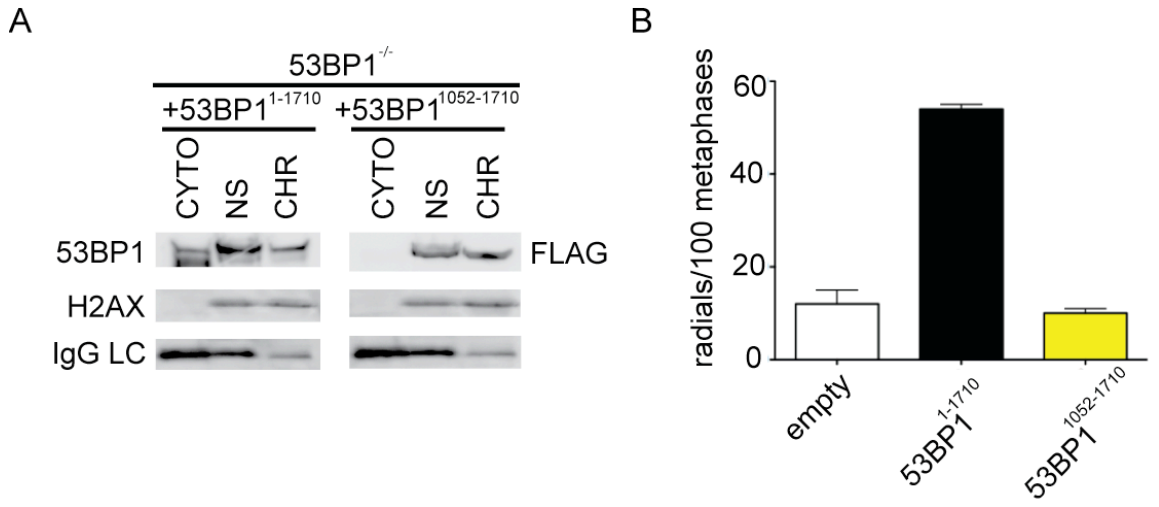

Figure 5.18. The focus forming region of 53BP1 binds to chromatin but does not prevent end resection.

(A) Western blots of fractionated 53BP1$^{-/-}$ B cells stimulated and infected with 53BP1$^{1\text{-}1710}$ or 53BP1$^{1052\text{-}1710}$. CYTO, cytoplasmic fraction; NS, nuclear soluble fraction; CHR, chromatin fraction.

(B) Brca1$^{\Delta 11/\Delta 11}$ 53BP1$^{-/-}$ B cells reconstituted with 53BP1 mutant retroviruses. Histogram quantitating the number of radial structures upon infection with the indicated retroviruses. Error bars indicate standard error of the mean. Two independent experiments.

We conclude that chromatin binding, oligomerization, and focus formation are insufficient to promote CSR, suggesting that the N-terminus of 53BP1 may play an important role in this reaction.

Phosphorylation sites at the N-terminus of 53BP1

To examine the role of the N-terminus of 53BP1 in CSR, we produced and tested additional mutants, including: (1) smaller N-terminal deletions (53BP1$^{901\text{-}1710}$ and 53BP1$^{459\text{-}1710}$), (2) internal deletions corresponding to the amino acids encoded by

exons 3-12 (53BP1$^{D61-901}$), 7-12 (53BP1$^{D216-901}$) and 12 alone (53BP1$^{D459-901}$ (75, 78)). We found that all of the deletion mutants were unable to rescue CSR (Figure 5.19).

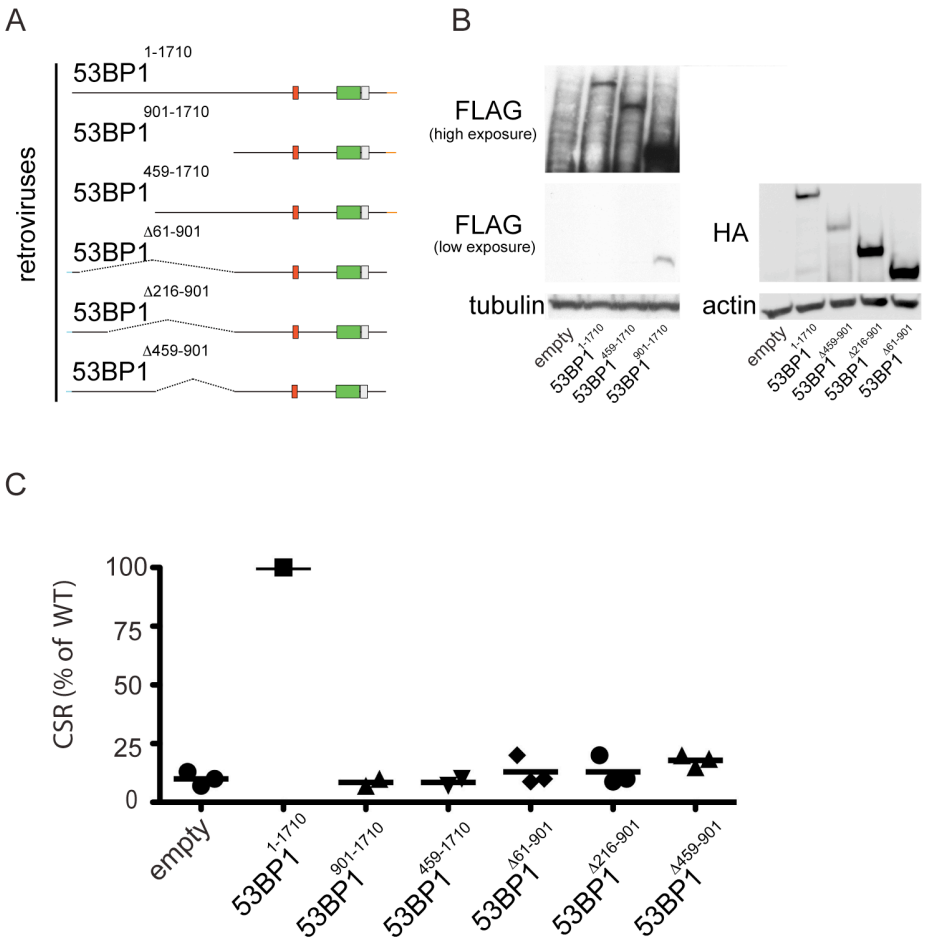

Figure 5.19. 53BP1 N-terminus is required for efficient CSR.

(A) Cartoon diagram of 53BP1 N-terminal deletion mutants.

(B) Control western blot analysis on whole cell lysates from a representative experiment to confirm that a protein of the expected size is produced upon retroviral infection.

(C) Percentage of 53BP1$^{1-1710}$ class switching for each mutant (right). 53BP1$^{D61-901}$, 53BP1$^{D216-901}$, and 53BP1$^{D459-901}$ are N-terminally HA-tagged (blue). Each dot represents an independent experiment; the bar indicates the mean value.

We next generated alanine substitution mutants of S/T-Q consensus sites for ATM phosphorylation (53BP1^{8A}, 53BP1^{7A}, 53BP1^{15A}, 53BP1^{28A}; Figure 15.20).

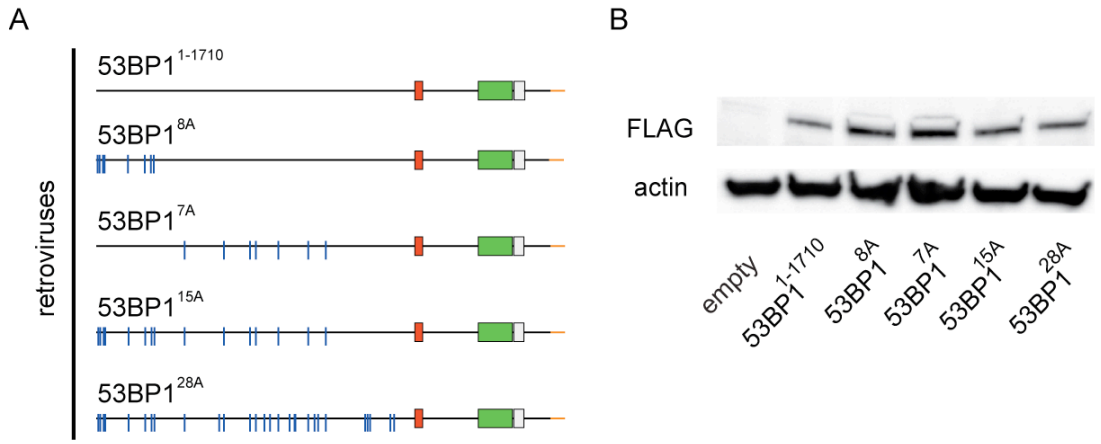

Figure 5.20. Retroviruses containing 53BP1 N-terminal alanine substitution mutations of S/T-Q phosphorylation sites are expressed at normal levels.

(A) Schematic of 53BP1 retroviral construct with the indicated mutations.

(B) Western blot analysis on whole cell lysates to confirm that a protein of the expected size is produced upon retroviral infection.

The alanine substitution mutants 53BP1^{8A}, 53BP1^{7A}, 53BP1^{15A} and 53BP1^{28A} displayed a CSR defect that correlated in severity with the number of substitutions. 53BP1^{8A} showed 90% of WT CSR whereas 53BP1^{28A} was similar to the null mutant (Figure 15.21).

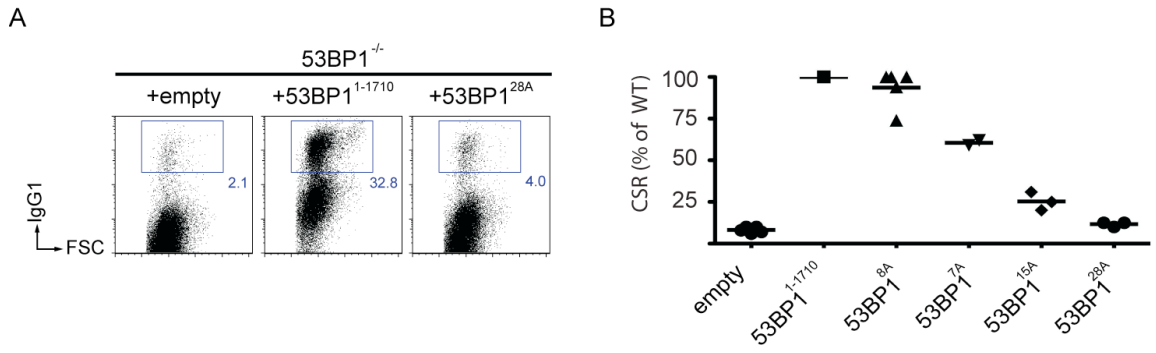

Figure 5.21. N-terminal phosphorylation of 53BP1 is required for CSR.

(A) Representative flow cytometry plots measuring CSR after stimulation of 53BP1$^{-/-}$ B cells infected with the indicated retroviruses. Numbers indicate the percentage of IgG1 switched cells. CFSE dye tracks cell division.

(B) Summary dot plot indicating CSR as a percentage of WT value within the same experiment. The bar indicates the mean. Each dot represents an independent experiment.

Despite its inability to rescue CSR, 53BP1^{28A} bound to chromatin and formed IR-foci (Figure 15.22 A and B). We conclude that multiple S/T-Q target sites for ATM phosphorylation at the N-terminus of 53BP1 are required for CSR. Lastly, we determined whether 53BP1^{28A} was able to protect DNA ends from resection. We found that despite retaining its ability to bind chromatin, DNA ends were processed such that radial structures were prevented similar to 53BP1 deficiency (Figure 5.22 C).

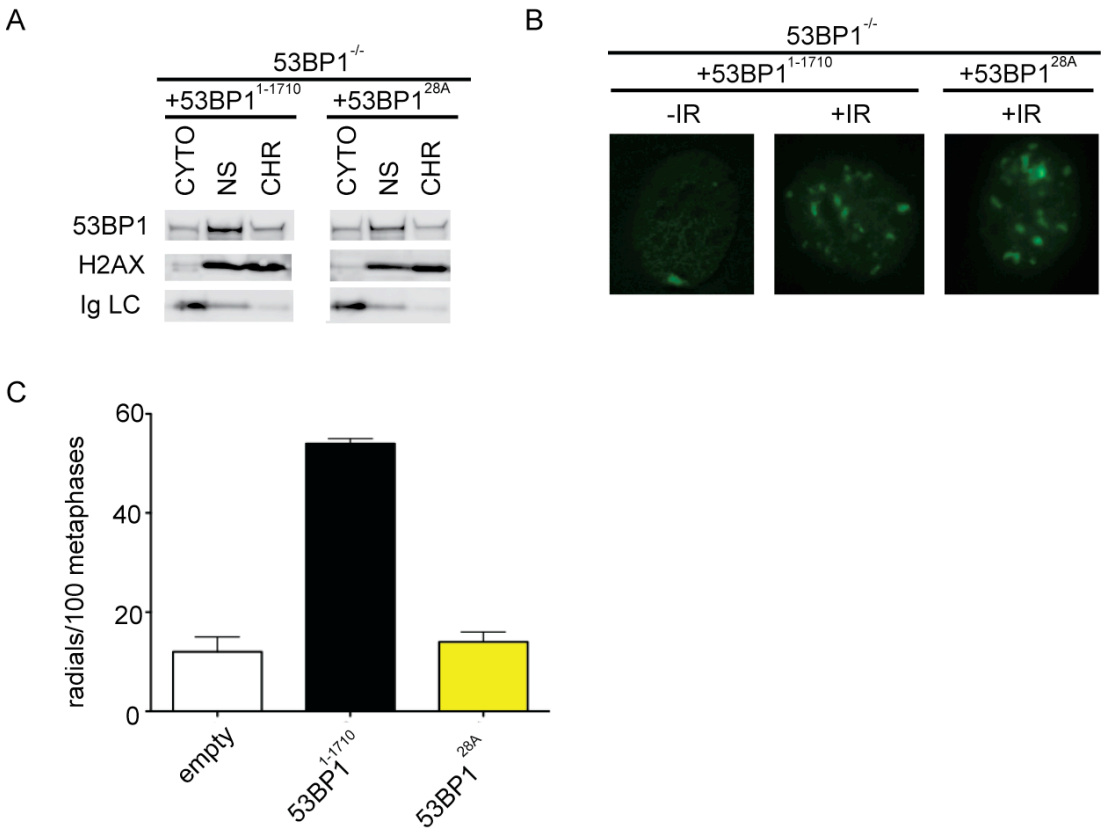

Figure 5.22. N-terminal phosphorylation of 53BP1 is required for preventing end resection but is dispensable for chromatin binding and IR induced focus formation.

(A) Western blots of fractionated 53BP1$^{-/-}$ B cells stimulated and infected with 53BP1$^{1\text{-}1710}$ or 53BP1^{28A}.

(B) Focus formation after treatment of 10 Gy of IR after retroviral infection of 53BP1$^{-/-}$ MEFs with the indicated retroviruses

(C) Brca1$^{\Delta 11/\Delta 11}$53BP1$^{-/-}$ B cells reconstituted with the indicated 53BP1 mutant retroviruses. Histogram quantitating the number of radial structures upon infection with the indicated retroviruses. Error bars indicate standard errors of the mean.Two independent experiments.

CHAPTER 6:

Discussion

AID is responsible for the DSB at c-myc that is required for c-myc/IgH translocation

Hematologic malignancies such as leukemias and lymphomas frequently harbor clonal chromosome translocations. Chromosome translocations require the joining of two spatially proximal DSBs on heterologous chromosomes. DSBs rarely accumulate in somatic cells, but they are obligate intermediates in CSR, a reaction that involves introduction of multiple targeted DSBs in the *IgH* locus in mature B lymphocytes. Normally, the ATM-, p53- and $p19^{Arf}$-dependent pathways that detect and signal DNA damage protect the B cell genome from chromosome translocations (208). Nevertheless, these protective mechanisms sometimes fail, as evidenced by the involvement of the *IgH* locus in nearly all cancer-associated chromosomal translocations in mature B cell lymphomas and multiple myeloma (243).

AID creates the lesions in the *IgH* locus that lead to translocations (153, 163, 208, 223). Although necessary, DSBs in *IgH* alone are not sufficient for translocation - a second DSB on a heterologous chromosome is required. However, the source of DNA damage at genes that are translocated in mature B cell malignancies has not been determined (243).

In Burkitt's lymphoma and in murine plasmacytoma *IgH* is translocated to *c-myc*, leading to deregulated expression of *c-myc* and malignant transformation (211-222).

Although AID was found to be required for *c-myc*/*IgH* translocation and to increase the translocation rate, this effect could have been due to higher levels of DNA breaks on *c-myc* or *IgH* or both (208, 244, 245). Previous work suggested that DSBs in *c-myc* are AID independent and might be due to increased susceptibility of fragile non-B-DNA to environmental agents like reactive oxygen intermediates, transcriptional or replication-linked DNA damage (246-249). This idea was supported by the finding of AID independent DSBs in *c-myc* in B cell lymphomas (250), the relative rarity of somatic mutations in *c-myc* (251), and the lack of deletions or duplications in *c-myc* that would mark DSB formation (177-181, 251, 252).

Here we present experiments that clearly show a requirement for AID in the formation of mutations and lesions at *c-myc*. We demonstrate that AID is essential for DSB formation in *c-myc* that result in *c-myc*/*IgH* translocation in primary nouse B cells. Based on the finding that artificial DSBs at *c-myc* induced with the I-SceI endonuclease increase *c-myc*/*IgH* translocation frequency, we conclude that the DSB at *c-myc* is limiting for the reaction. Consistent with this finding is the paucity of easily detectable DNA damage under physiologic AID expression levels and the absence of mutations at the *c-myc* locus (178). However, AID over-expression leads to the AID mutation footprint at *c-myc* as well as focus formation of DNA damage factors. We conclude that AID-induced DSB formation at *c-myc* is much less efficient than at *IgH* under physiologic conditions, but that these rare off-targeting events are responsible for the lesion at *c-myc* that leads to the formation of the *c-myc*/*IgH* translocation

Differential DNA repair at different loci

We observed that the extent of DNA processing and the structure of the intermolecular joints differed depending on whether the lesion was induced by AID or I-SceI. The most extensive resection of DNA ends was found at *c-myc* with I-SceI mediated translocations in the absence of AID. The same extent of end resection was not detected at IgH under the same conditions. Moreover, whereas I-SceI induced breaks were resolved by a mechanism biased toward junctional microhomology reminiscent of alternative NHEJ (253), AID breaks produced a combination of blunt and short microhomology joints similar to those found in CSR. The difference in trans-chromosomal joints between I-SceI and AID may be explained by recruitment of a distinct set of repair enzymes to the two types of DNA damage. In the case of I-SceI a DSB is introduced directly by the yeast endonuclease and must be recognized by the DNA damage recognition and repair system before being processed and joined. In contrast, AID induced U:G mismatches are recognized by mismatch and base excision repair enzymes before recruitment of additional repair factors that then process the lesions to produce DSBs. Thus, the difference in the joints produced by I-SceI breaks and AID lesions may in part be due to the distinct mechanisms that recognize the initial lesion and produce the DSB.

Although the precise mechanism by which AID introduces lesions in DNA is still debated, AID is thought to produce U:G mismatches in DNA by cytidine deamination (200, 254, 255). In B cells undergoing SHM or CSR, uracil is detected and removed from antibody genes by error prone mechanisms leading to mutations or DSBs. Other genes, including oncogenes, appear to repair such

lesions in a relatively error free manner, which may explain the nearly undetectable level of AID mediated mutation in genes like *c-myc* (178, 181, 251).

The role of distance in DSB joining

While joining of paired DNA breaks on disparate chromosomes leads to translocations resulting in loss of genetic material in some cases, joining of paired intra-chromosomal breaks always results in loss of genetic information. HO, I-SceI, and zinc finger nucleases that produce unique DSBs in yeast and mammalian genomes have primarily been used to explore the biology of chromosome translocations. However, much less is known about the role of DNA repair factors in protecting cells against intrachromosomal deletions.

Deletions are commonly observed in cancer, where they are often recurrent and contribute to malignant transformation (256). In fact, recent high-throughput paired-end sequencing of breast cancer genomes indicated that intra-chromosomal rearrangements are ~6-fold more common than trans-chromosomal rearrangements (257). The distribution of intra-chromosomal rearrangements appeared to be non-random: the great majority of deletions occurred between sites separated by less than 2 Mbs of genomic distance. This indicates that certain architectural features of the chromosome lead to a higher likelihood of DSB joining within 2 Mbs than more distal DSB joining. However, cancer genomes are highly selected populations and larger deletions may have been selected against. Unbiased approaches to map chromosome topology and genome architecture revealed that the nucleus is highly compartmentalized and that chromosomes are organized in a non-random fashion. Specifically, using "Hi-C", a technique that samples the interaction probabilities between different

loci genome-wide, showed with a resolution of 1 Mb that chromosomes display "polymer-like" behavior, where the contact probability between two loci depends on the 3 D distance between them (258).

Although chromosome deletions are often pathogenic and contribute to malignant transformation, deletions are required intermediates in immune cell diversification reactions. For instance, CSR in B cells involves the programmed deletion of DNA segments separated by 60-200 kb at the IgH locus of mouse chromosome 12 (255). While the distance between two loci inversely correlates with their contact probability on a global scale, local chromosome organization induced by cis- and trans-acting factors, regulatory DNA elements and chromatin status, may impact substantially on rearrangement efficiencies. For example, enhancer elements at the IgH locus in B cells induce looping, resulting in the close physical proximity of distant sites (229). Hence, genomic distance does not necessarily represent the actual physical 3D distance in an interphase nucleus especially at a local scale.

To study the role of distance in the joining of tandem intra-chromosomal DSBs in mammalian cells with an emphasis on CSR, we compared joining between I-SceI induced breaks on chromosome 12 spaced by 1.2 kb, 96 kb, and 27 Mb. Our analysis reveals that DSBs separated by 1.2 kb or 96 kb are more likely to join than those separated by 27 Mb on mouse chromosome 12. In fact, when DSBs are separated by 27 Mb, the rate of joining in cis is similar to trans-chromosomal joining between *IgH* and *c-myc*. One potential caveat of our comparative analysis is that I-SceI cutting efficiency may vary depending on the genomic location. In our set of experiments we do not control for cutting efficiency and the

conclusions from the comparative analysis are drawn assuming that cutting efficiency is the same for I-SceI sites located in *Iμ*, *Cγ* and *c-fos* and *c-myc*.

The fact that very distal intra-chromosomal DSBs are joined less frequently than more proximal DSBs is in agreement with genome wide conformation-capture data and also with findings from cancer genome sequencing that show a striking enrichment for intra-chromosomal rearrangements in a 2 Mb window (257). Moreover, the Hi-C dataset showed that contact probabilities between distal sites (>20 Mb) within one chromosome are of the same order of magnitude as contact probabilities between two heterologous chromosomes, which is entirely consistent with our observation that joining of DSBs separated by 27 Mb occurs at similar efficiencies to DSB joining between different chromosomes.

Although our data concerning the joining of DSBs at discrete distances matches the observations of genome-wide chromosome organization experiments (257, 258), genome-wide architectural studies such as Hi-C sample the steady state, while cancer genome sequencing presents a highly selected end-product. Both methods may not entirely reflect what happens during DSB joining, as DSB formation leads to local changes in chromatin structure that may alter interaction probabilities between different loci, leading to an altered likelihood of local DSB joining than steady-state contact probability would predict.

The contribution of 53BP1 to joining efficiency

53BP1 is a large nuclear protein that forms foci in response to DNA damage. This protein plays an interesting role in the joining of DNA breaks, as it promotes the

joining of DSBs between two distal S-regions during CSR, but is dispensable for the joining of proximal DSBs within one S-region (194-196). Similarly, distal V-DJ recombination at the TCRα locus is impaired in the absence of 53BP1 as well as the joining of TRF2 depleted telomeres (124, 152). Those findings suggest that 53BP1 does not affect DSB joining per se, but only affects joining across certain distances.

Here we systematically analyze which distances are affected by the absence of 53BP1 by measuring the joining frequency of DSBs separated by 1.2 kb, 96 kb, 27 Mb and on different chromosomes in the presence and absence of 53BP1. We found that 53BP1 selectively facilitates joining of DSBs separated by 96 kb, and does not affect more proximal, very distal or trans-chromosomal joining events.

Several non-mutually exclusive hypotheses have been proposed to account for the effect of 53BP1 on DSB joining. One model proposes that 53BP1 enhances chromatin mobility after DSB formation and is based on observations made at dysfunctional telomeres, where 53BP1 was shown to promote telomere mobility, thereby facilitating trans-chromosomal telomere fusion events (124). In a protected, undamaged state, telomere movement constrained to a maximum displacement of ~ 0.5 μm. Upon de-protection and activation of the DNA damage response, telomere mobility in 53BP1 proficient cells increases ~ two-fold, while 53BP1 deficient cells display significantly reduced mobility. However, it is not clear whether telomeres, which represent one DSB at the end of a chromosome, behave similar to DSBs that occur within one chromosome. In fact, the movement of chromosome internal DSBs has been shown to be highly restricted, due to the rapid accumulation of bridging factors such as the KU70/80

complex at the site of the break, which is thought to hold the broken ends in close proximity to facilitate DNA repair (259). By extension, it is unclear what role 53BP1 dependent chromosome mobility plays in the repair of random or programmed chromosome internal DSBs.

An alternative explanation for the selective effects on DSB joining displayed by 53BP1 derives from the finding that 53BP1 allows for a higher probability of interactions between DNA elements 28-172 kb apart during rearrangements of the TCRα locus (152). 53BP1 was proposed to facilitate joining by coating regions adjacent to broken DNA to mediate the "synapsing" of RAG induced DSBs by homo-oligomerization.

Recently, the preferential joining of S-region breaks by C-NHEJ and the exclusion of A-NHEJ has been proposed to facilitate DSB joining during CSR (198). B cells deficient for the C-NHEJ factors XRCC4 and Ku70 display reduced CSR levels to ~ 50% of wild type levels. However, 53BP1 deletion leads to a more drastic defect in CSR, hence the repair pathway choice may be a contributing factor to CSR defects.

Our data do not provide direct evidence for either the synapsis model or the chromatin mobility model that have been proposed to account for 53BP1 dependent DSB joining. However, we reasoned that the selectivity on the joining of paired breaks separated by 96 kb coincides with the proposed spread of DNA damage factors along the chromosome in response to DSBs (49, 228). Indeed, the extent of γH2AX spreading from an I-SceI induced DSB at the IgH locus is confined to ~ 1 Mb surrounding the break. Since DSBs produced during CSR are separated by 60-200 kb, our findings support a model in which 53BP1 and

possibly other focus forming factors promote the synapsis of DSBs if they fall within the range of spread of the H2AX/RNF8 dependent DNA damage response . This model correctly predicts that trans-chromosomal DSB joining, or joining of DSBs that occur at distances beyond the spread of the DNA damage response are not affected by the loss of 53BP1.

Interestingly, loss of 53BP1 does not affect recombination efficiency mediated by Cre/loxP, a recombination reaction that is independent of the DNA damage response. This finding substantiates that 53BP1 acts downstream of a DSB, mediating synapsis of broken ends as part of the DNA damage response.

The role of 53BP1 in DNA repair

DSBs can be repaired with a high degree of fidelity during the S and G2 phases of the cell cycle by HR, which uses the undamaged sister chromatid as a template for repair. HR requires 5'-3' resection of DNA ends to produce ssDNA, which recruits RPA, leading to deposition of RAD51, a factor that is essential in homology search (260). End resection is believed to occur during two stages: in the first phase, relatively shorstretches of ssDNA are produced by the combined action of MRE11/RAD50/NBS1 (MRN) and CTIP; in a second phase, longer stretches of ssDNA are produced by the combined action of Bloom's helicase, EXO1 and WRN (81, 84-86, 111, 261, 262). ATM is implicated as a regulator of the resection process because it phosphorylates all of the enzymes known to be involved in resection (89) and is required for optimal ATR activation and for CTIP recruitment to DNA ends (234, 260, 263, 264). Recent work from a number of laboratories indicates that the critical choice between HR and NHEJ in the

S/G2/M phases of the cell cycle is regulated at the level of DNA end resection (82, 87, 88).

In the absence of a template sister chromatid during CSR in G1, DSBs are repaired by error-prone C-NHEJ or A-NHEJ. However, little is known about the choice between C-NHEJ and A-NHEJ. Under physiological circumstances the majority of switch joins are blunt or show minimal microhomology, suggesting that C-NHEJ is the dominant pathway (255). Nevertheless, A-NHEJ is a robust pathway, which can reconstitute up to 50% of normal levels of CSR in the absence of core C-NHEJ factors such as LIG4, or XRCC4, or KU70/ 80 or even the combination of KU70 and LIG4 (113, 147, 197, 198).

A-NHEJ can also mediate plasmid re-circularization in transfected cells (108), joining of I-SceI breaks (265), oncogenic translocations (116, 206-208), and finally V(D)J recombination when the end protection function of the RAG recombinase is disabled (148). However, other than the preponderance of microhomologies found at the junctions (266, 267) and the suggestion that MRN is required for A-NHEJ (111, 261, 268, 269), this pathway remains poorly defined.

In addition to NHEJ, the DNA damage response is also essential for physiological CSR (270). Among the factors that mediate this response, 53BP1 has the most profound effect on CSR and specifically affects long-range joining between different switch regions (194, 196). In contrast, 53BP1 deficient B cells show increased short-range intra-switch joining, which involves ligation of highly repetitive DNA (196).

Here we provide evidence that the DNA damage response factor 53BP1 influences the choice between C-NHEJ and A-NHEJ by preventing end-resection of DSBs. End processing is essential for the production of the ssDNA required for microhomology based A-NHEJ. Therefore, by interfering with end processing, 53BP1 normally impairs A-NHEJ, which leads to enhanced C-NHEJ. The choice of repair pathway is particularly crucial during CSR. While different (distal) S-regions are highly repetitive internally, they are not homologous with respect to each other. The extensive end-resection observed in the absence of 53BP1 reveals the abundant microhomologies within one S-region, providing substrates for efficient S-region internal ligations, which would normally be prevented. Loss of 53BP1 therefore favors switch region internal deletions by enhancing resection dependent A-NHEJ, and disfavors C-NHEJ dependent recombination between two non-homologous switch regions. Consistent with this idea, inhibition of end resection by interfering with ATM activity enhances CSR in 53BP1 deficient B cells.

Interestingly, the other severe defect in the absence of 53BP1 is the inability to join dysfunctional telomeres. Similarly to S-regions, telomeres consist of highly repetitive sequence. It is possible that analogous to its protective role in CSR, 53BP1 protects dysfunctional telomeres from end degradation. Resected ends are refractory to ligation by C-NHEJ, therefore 53BP1 dependent maintenance of telomere integrity could be a crucial contribution towards joining of chromosome ends.

Similar to our findings, a parallel study showed that 53BP1 mediates the choice between HR and NHEJ by preventing end resection. Specifically, inhibition of

PARP in BRCA1 deficient cells leads to abundant formation of NHEJ dependent radial structures. 53BP1 deficiency abrogates radial structure formation by allowing repair of PARP inhibitor induced DSBs by HR rather than NHEJ (242).

In summary, we have uncovered a novel function for 53BP1 in promoting the choice between classical and alternative NHEJ pathways. Based on these findings we propose a model in which CSR is facilitated by 53BP1 dependent C-NHEJ pathway. However, C-NHEJ deficient B cells can undergo CSR with up to 50% of wild type efficiency, which is far above the observed rates for CSR in 53BP1 deficient B cells (197, 198). Therefore, the severe 53BP1 defect cannot exclusively be explained with the "choice of repair pathway" model. Alternative models such as the 53BP1 chromatin mobility or DSB synapsis models remain to be tested and established in the context of CSR.

Structure/Function Analysis

We have shown that 53BP1 facilitates end joining in cis and that this effect is limited to DSBs separated by 96 kb, as loss of 53BP1 does not reduce the joining frequency of proximal, very distal or transchromosomal DSBs. The selective effect of 53BP1 on joining paired breaks separated by 96 kb suggested a role for DNA damage factors that spread along the chromosome in response to DSBs in an H2AX/RNF8 dependent manner (49, 228). In addition to forming repair foci at DNA ends we have provided evidence that 53BP1 protects DNA ends from resection and thereby favors repair by C-NHEJ while preventing A-NHEJ. However, end protection is not sufficient to explain the effects of 53BP1 on CSR

since H2AX deficiency promotes extensive end resection and yet produces a milder CSR defect (193).

The way in which 53BP1 mediates end protection and facilitates joining was investigated by analyzing the contribution of the structural domains of 53BP1 to DNA end protection and class switching in B lymphocytes. Human 53BP1 binds to the histone mark H4K20me2 via its tudor domain and mutation of amino acid D1521 in the tudor domain abrogates 53BP1's ability to form DNA damage foci in response to IR (64, 65). We find that 53BP1 is chromatin associated even in the absence of DNA damage or H2AX, which is consistent with previous reports showing that H4K20me2 is a constitutive chromatin modification (65, 66) and that 53BP1 chromatin association is RNF8 and 53BP1-foci independent (53). These studies suggest that even in the context of undamaged chromatin this modification is accessible to 53BP1. Furthermore, a knock-in mutant of the tudor domain ($53BP1^{DR}$) that fails to form foci in response to DNA damage also fails to associate with chromatin in non-irradiated cells. Therefore, an intact tudor domain is required for both constitutive binding to chromatin and DNA damage induced focus formation. As predicted from its inability to bind chromatin or form DNA damage foci, $53BP1^{DR}$ was unable to protect DNA ends from resection or to support CSR.

The absence of 53BP1's oligomerization domain and deficiency in H2AX both impair the formation of stable DNA damage foci (70-73). In contrast, we find that neither the oligomerization domain of 53BP1 nor H2AX are required for 53BP1 binding to chromatin. However, DNA end protection and CSR are impaired in the absence of either. Thus the ability to bind constitutively to chromatin appears to be necessary but not sufficient for end protection or CSR.

Consistent with this idea, a fragment of 53BP1, which binds chromatin and forms DNA damage inducible foci ($53BP1^{1052\text{-}1710}$), is unable to support either end protection or CSR. Interestingly and unlike 53BP1, H2AX deficiency does not rescue the formation of radial fusions observed in PARP inhibitor treated Brca1 mutant B cells (Figure 4C). Although H2AX and 53BP1 deficiency both lead to increased end-resection (242, 271-273), H2AX in contrast to 53BP1 likely plays additional roles in HR and NHEJ which may be essential in Brca1 deficient cells. Similar to H2AX, RNF8 and RNF168 are required for stable 53BP1 focus formation upon IR (51, 52, 55, 56, 73, 236). In this context, it will be interesting to test the effect of RNF8/RNF168 deficiency on PARP inhibitor induced chromosome abnormalities in $Brca1^{\Delta 11/\Delta 11}$ cells, as these ubiquitin ligases lie downstream of H2AX and upstream of 53BP1.

Our analysis of tandem BRCT domains mutant B cells ($53BP1^{\Delta BRCT}$) showed that the C-terminus is dispensable for both CSR and the protection of ends from processing, which suggests a role for the N-terminus in these processes. The N-terminus of 53BP1 lacks known structural domains, but contains S/T-Q consensus target sites for ATM phosphorylation that are implicated in promoting the resolution of γH2AX foci upon IR (75, 78, 238). We find that the putative ATM phosphorylation sites are also required to prevent DNA resection and to support CSR, suggesting that N-terminally phosphorylated 53BP1 may recruit additional factors to regulate DNA repair. In summary, out of all the 53BP1 functional domains tested, the ability to protect DNA ends from resection is the only parameter that correlates with CSR. Chromatin association, focus formation, oligomerization, and intact N-terminal

ATM phosphorylation sites are all essential but by themselves not sufficient to prevent DNA end processing or to support CSR. Therefore, end protection and CSR may not simply be mediated by direct physical association of 53BP1 with DNA ends but appears to require the assembly of a complex composed of H2AX, 53BP1 and possibly additional yet-to-be defined proteins.

CHAPTER 7:

Methods

Mice

$IgH^{I\text{-}1k/+}$, $IgH^{I\text{-}96k/+}$, $IgH^{I\text{-}27M/+}$ were generated by homologous recombination in C57BL/6 albino embryonic stem (ES) cells. Details of the targeting vectors, screening by Southern blot, and genotyping PCR are provided in the following sections. $IgH^{I/+}$, $Myc^{I/+}$, $53BP1^{\Delta BRCT/+}$, $53BP1^{DR/+}$, and $53BP1^{\Delta 1210\text{-}1447/+}$ mice were generated by Dr. Davide Robbiani, The Rockefeller University, New York. $AID^{-/-}$ (155), $53BP1^{-/-}$ (195), $H2AX^{-/-}$ (37), $Brca1^{lox/lox}$ (274), $Brca1^{\Delta 11/\Delta 11}$ (275), FLPer mice (Rodriguez et al., 2000) and $CD19^{cre}$ mice (276) were previously described. All experiments were performed in accordance with protocols approved by The Rockefeller University and National Institutes of Health (NIH) Institutional Animal Care and Use Committee.

Targeting strategy for $IgH^{I\text{-}196/+}$ mice

$IgH^{I\text{-}1k}$ mice were generated by homologous recombination in C57BL/6 albino embryonic stem (ES) cells. The following primers were used to generate the construct: Long arm of homology: 5′- GCGGCCGC GCATGC CAGATACCCATACTGGAAAGCAGG-3′ and 5′- GCGGCCGC TTAATTAA CCTGGAATAAGTGTCTTCTCTGTGC-3′; Short arm of homology: 5′- GTTTAAAC GGCGCGCC AAGCCTCAGCAGAATGGGAAGTGG-3′ and 5′- GTTTAAAC GGCCGGCC ATTACCCTGTTATCCCTA GCTGTCTGATGTGGGCATCTGTG-3′. I-SceI site is underlined. LoxP site was

present in hygromycin targeting backbone. The frt-flanked hygromycin cassette was removed *in vivo* by crossing to FLPer mice. Genotying primers used on hygro excised germine $IgH^{I\text{-}96k}$ allele: 5′- TCAGGGAACCTAAGAACAGGGACC-3′ and 5′-TAGGAAAATGCCCCACCTGC′-3, 38 cycles of PCR amplification (95 C, 45 s; 57 C, 45 s; and 72 C, 30 s). Primers used for amplification of probe: 5′-GGTGCTGAGGTTCAAAGGCAG -3′ and 5′-TTTTAGGTGCTTGCTTAGGAGGTC-3′).

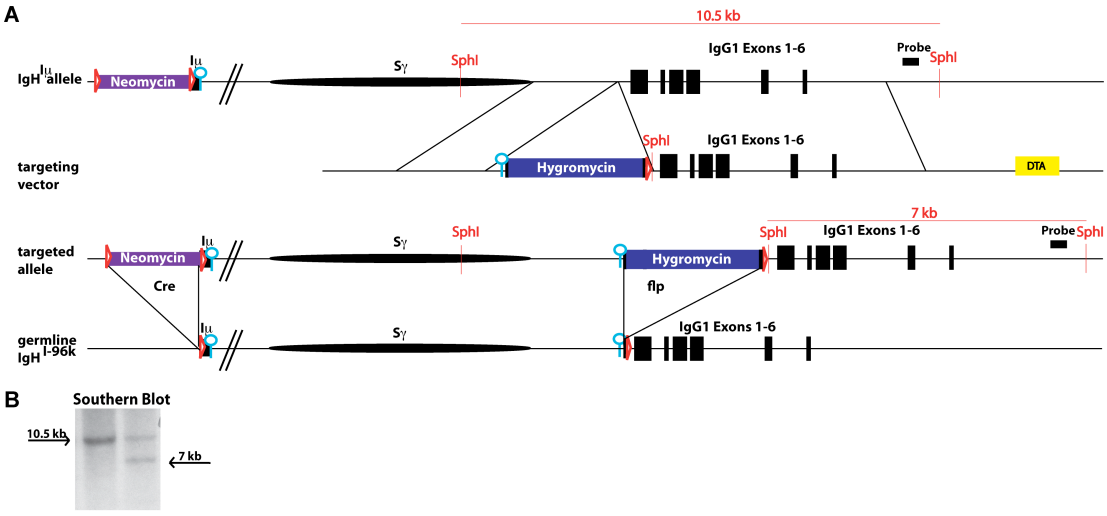

Figure 7.1. Gene targeting strategy to generate $IgH^{I\text{-}96k/+}$ mice.
(A) Schematic representation of the gene targeting strategy, using $IgH^{I\mu}$ ES cells (Robbiani et al, 2008). The targeting vector, targeted allele and targeted allele upon flp induced hygromycin excision (germline $IgH^{I\text{-}96k}$) are shown. LoxP sites are indicated as red triangles, I-SceI sites are blue circles and frt sites are black bars. DTA was used for negative selection.
(B) Southern Blot analysis of ES cell DNA digested with SphI showed correct integration upon hybridization with a radiolabeled probe.

Targeting strategy for $IgH^{I\text{-}1/+}$ mice

$IgH^{I\text{-}1k}$ were generated by homologous recombination in C57BL/6 albino

embryonic stem (ES) cells. The spacer sequence (human IgHG1 intron 4) was amplified using the following primers: 5′ - CACACAAAGACTCTGGACCTCTCCTGCGAGACTGTGATGGTTCTTTC-3′ and 5′- GGCCGGCCAATATTATTACCCTGTTATCCCTATGTGGCAGGACCCAGGAT GTAG – 3′. The probe for Southern blotting was amplified using the following primers: 5′- TTCCTACCTTCTCCCCTGAGTCTC -3′ and 5′- TTCCCAGAGTCACAGCCTTTGTCC-3′. The frt-flanked hygromycin cassette was removed *in vivo* by crossing to FLPer mice. For genotyping, 38 cycles of PCR amplification (95° C, 45 s; 59° C, 45 s; and 72° C, 30 s) were performed with primers 5′- GCGGGTCCTGCTGAGGGCCAG-3′ and 5′- TAGGAAAATGCCCCACCTGC′-3. The size of the $IgH^{I\text{-}1k}$ allele is 390 bp.

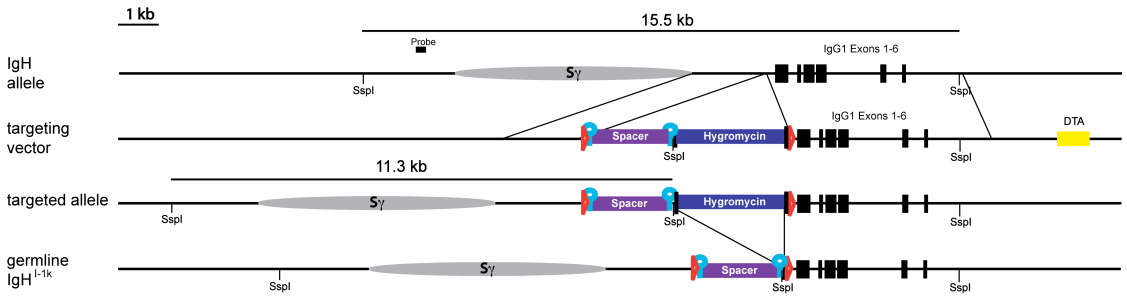

Figure 7.2. Gene targeting strategy to generate $IgH^{I\text{-}1k/+}$ mice.
Schematic representation of the gene targeting strategy to generate $IgH^{I\text{-}1k}$ mice. The targeting vector, targeted allele and targeted allele upon flp induced hygromycin excision (germline $IgH^{I\text{-}1k}$) are shown. LoxP sites are indicated as red triangles, I-SceI sites are blue circles and frt sites are black bars. DTA was used for negative selection.

Targeting strategy for $IgH^{I\text{-}27M}$ mice

The following primers were used to generate the construct: Long arm of homology: 5′- GGCCGGCCAAGCTT ATTACCCTGTTATCCCTA ACCAGTTTGTCAAGATGGGTGG-3′ and 5′- GGCGCGCCAGATGTGCCAGATGTAGGTAGATGC-3′; Short arm of homology: 5′- TTAATTAACTGGATTTGACTGGAGGTCTGC-3′ and 5′- CGATCGGCGGCCGC TCCTCAGAGGCCTTCCTGAAAC -3′. I-SceI site is underlined. LoxP site was present in hygromycin targeting backbone. Probe for Southern blotting was amplified using the following primers: 5′- GCGAGCAACTGAGAAGACTGGATAG -3′ and 5′- AATGGTAGTAGGAAAGGCTGTCCC-3′. The frt-flanked hygromycin cassette was removed *in vivo* by crossing to FLPer mice. For genotyping, 38 cycles of PCR amplification (95° C, 45 s; 55° C, 45 s; and 72° C, 30 s) were performed with primers 5′- ACCCATCTTGACAAACTGGTTAGG-3′ and 5′- TAGGAAAATGCCCCACCTGC′-3. The size of the $IgH^{I\text{-}27M}$ allele is 231 bp.

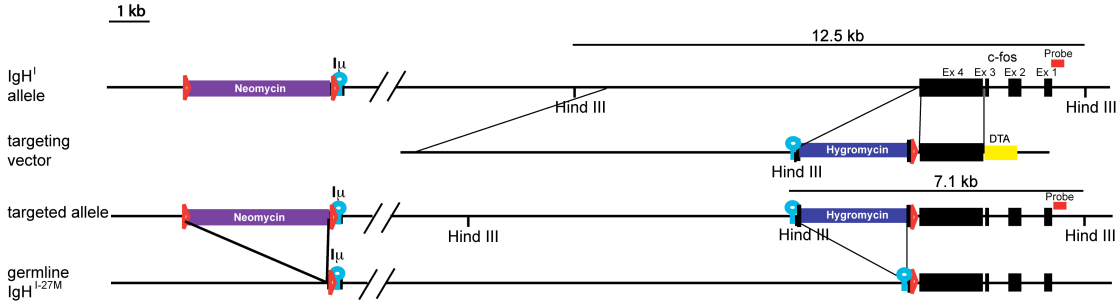

Figure 7.3. Gene targeting strategy to generate IgH$^{I\text{-}27M/+}$ mice.
Schematic representation of the gene targeting strategy to generate IgH$^{I\text{-}27M}$ mice starting from previously targeted IgH^{I} ES cells (Robbiani et al, 2008). The targeting vector, targeted allele and targeted allele upon flp induced hygromycin excision (germline IgH$^{I\text{-}27M}$) are shown. LoxP sites are indicated as red triangles, I-SceI sites are blue circles and frt sites are black bars. DTA was used for negative selection.

B cell cultures

B lymphocytes were isolated from mouse spleens using anti-CD43 MicroBeads (Miltenyi Biotech) and cultured at 0.5x10^6 cells/ml in complete R10 medium (RPMI supplemented with L-Glutamine, Sodium Pyruvate, Hepes, 50μM 2-Mercaptoethanol, antibiotic/antimytotic and 10% fetal calf serum (Hyclone)). For B cell stimulation 25μg/ml lipopolysaccharide (LPS, Sigma) and 5 ng/ml mouse recombinant IL-4 (Sigma) were added to the culture. Where indicated, RP105 (0.5 μg/ml, Pharmingen) or ATMi Ku55933 (2.5 μM) was added to the culture.

Retroviruses

Cre, I-SceI, I-SceI*, and AID were PCR-amplified and cloned into the pMX-IRES-GFP plasmid. In I-SceI*, D44A and D145A substitutions to inactivate the catalytic sites were introduced by PCR. Coding sequences of the human 53BP1 mutants were cloned into a modified pMX (Moloney leukemia virus-based retroviral expression virus (277)) retroviral plasmid with deleted IRES-GFP (courtesy of Dr. Silvia Boscardin), to allow for proper packaging of this large protein. Therefore, in each experiment infection efficiency was monitored by Western Blot. $53BP1^{8A}$ encoded for the following alanine substitutions: S6A; S13A; S25A; S29A; S105A; S166A; S176A; S178A. $53BP1^{7A}$ encoded for: T302A; S452A; S523A; S543A; S625A; S784A; S892A. $53BP1^{15A}$ encoded for the same alanine substitutions as in both $53BP1^{8A}$ and $53BP1^{7A}$. In addition to these, $53BP1^{28A}$ also had S437A; S580A; S674A; T696A; S698A; S831A; T855A; S1068A; S1086A; S1104A; S1148A; T1171A; S1219A. Unless otherwise noted, mutants bore a C-terminal HA-FLAG tag. Plasmids with alanine substitutions were provided by Philip Carpenter and cloned into the pMX retroviral expression system.

Retroviral infections

Retroviral supernatants for B cell infections were produced in BOSC23 (derivative for 293T cell line (278)) by transfection with Fugene 6 with 7μg of pCL-Eco (279) and 7μg plasmids carrying either Cre, Cre*, I-SceI or I-SceI* 72 hrs prior to the first B cell infection (189). Retroviral supernatants were filtered and added to B cell cultures at 20 hrs and 44 hrs after start of stimulation and spun at 1150g for 90 min in the presence of 2.5 μg/ml polybrene. After 6 hrs, retroviral

supernatants were replaced with LPS, IL-4 and RP105 supplemented R10 medium (RPMI supplemented with L-Glutamine, Sodium Pyruvate, Hepes, 50μM 2-Mercaptoethanol, antibiotic/antimytotic and 10% fetal calf serum (Hyclone)). .

FACS analysis

For fluorescence-activated cell sorting (FACS) analysis, spleen cell suspensions were stained with fluorochrome-conjugated anti-CD19, anti-CD3, anti-IgM, anti-IgD, and anti-IgG1 (Pharmingen) in PBS 5% FCS with a final concentration of 1 μg/ml, followed by three washes in PBS 1% FCS.

CFSE labeling

Labeling for cell division was at 37C for 10 min in 5 mM carboxyfluorescein succinimidyl esther (CFSE) in 1 ml of serum free R10, followed by three washes in complete R10 (RPMI supplemented with L-Glutamine, Sodium Pyruvate, Hepes, 50μM 2-Mercaptoethanol, antibiotic/antimytotic and 10% fetal calf serum (Hyclone)).

Translocation PCR assays

PCR reactions were performed on genomic DNA from 10^5 cells, unless otherwise indicated. Using Expand Long Template PCR System nested reactions were performed with the following primers: for derivative chromosome 15 translocations first round, 5-ACTATGCTATGGACTACTGGGGTCAAG-3 and 5-GTGAAAACCGACTGTGGCCCTGGAA-3; for derivative chromosome 15 translocations second round, 5-CCTCAGTCACCGTCTCCTCAGGTA-3 and 5-

GTGGAGGTGTATGGGGTGTAGAC-3. PCR conditions were according to manufacturer instructions with 29 cycles for the first round (10 cycles at 92°C, 10 s; 60°C, 30 s; and 68°C, 7 min; followed by 19 cycles at 92°C, 15 s; 60°C, 30 s; and 68°C, 7 min with 20 s of additional extension time per cycle) and 25 cycles for the second round (10 cycles at 92°C, 10 s; 60°C, 30 s; and 68°C, 4 min; followed by 15 cycles at 92°C, 15 s; 60°C, 30 s; and 68°C, 4 min with 20 s of additional extension time per cycle). PCR products were gel-purified and sequenced.

Intra-chromosomal joining assay

I-SceI infected cells were harvested on day 4 of culture and infection efficiency was determined by FACS analysis using the GFP reporter encoded by the pMX-I-SceI-IRES-GFP or pMX-I-SceI*-IRES-GFP retroviruses. DNA was phenol-chloroform extracted and precipitated with ethanol, before quantification.

The first round of PCR for $IgH^{I\text{-}1k}$ joining was done with the following primers: 5′- CAGACCTGGGAATGTATGGTTGTG-3′ and 5′-AGACAGGACAGGACAGGACCAAAC-3′. The following conditions were used for the first round of amplification: 10 cycles at 92°C, 10 s; 56°C, 30 s; and 68°C, 40 s; followed by 25 cycles at 92°C, 15 s; 56°C, 30 s; and 68°C, 40 s with 2 s of additional extension time per cycle. The second round of PCR for both $IgH^{I\text{-}1k}$ and $IgH^{I\text{-}27M}$ was done with the following primers: 5′ – ATGTATGGTTGTGGCTTCTGGG-3′ and 5′ - CCTGCTTTCCAGTATGGGTATCTG-3′ using the following conditions: 10 cycles at 92°C, 10 s; 55°C, 30 s; and 68°C, 30s; followed by 15 cycles at 92°C, 15 s; 55°C, 30 s; and 68°C, 30 s with 2 s of additional extension time per cycle).

For the I-SceI joining frequencies in the $IgH^{I\text{-}96k}$ system, nested PCR reactions were performed with the Expand Long Template PCR System. The first round of PCR was done with the following primers: 5′-CCAATACCCGAAGCATTTACAGT-3′ and 5′-AGACAGGACAGGACAGGACCAAAC-3′ and the following conditions: ten cycles at 92°C, 10 s; 56°C, 30 s; and 68°C, 40 s; followed by 25 cycles at 92°C, 15 s; 56°C, 30 s; and 68°C, 40 s with 2 s of additional extension time per cycle. The second round of PCR was done with the following primers: 5′ – ATGTATGGTTGTGGCTTCTGGG-3′ and 5′ - CCTGCTTTCCAGTATGGGTATCTG-3′ using the following conditions: ten cycles at 92°C, 10s; 55°C, 30 s; and 68°C, 30 s; followed by 15 cycles at 92°C, 15 s; 55°C, 30 s; and 68°C, 30 s with 2 s of additional extension time per cycle).

The first round of PCR for $IgH^{I\text{-}27M}$ joining was done with the following primers: 5′- CCAATACCCGAAGCATTTACAGT-3′ and 5′-TAGGAAAATGCCCCACCTGC-3′. The following conditions were used for the first round of amplification: 10 cycles at 92°C, 10s; 56°C, 30 s; and 68°C, 40s; followed by 25 cycles at 92°C, 15 s; 56°C, 30 s; and 68°C, 40 s with 2 s of additional extension time per cycle. The second round of PCR for both $IgH^{I\text{-}1k}$ and $IgH^{I\text{-}27M}$ was done with the following primers: 5′ – ATGTATGGTTGTGGCTTCTGGG-3′ and 5′ - CCTGCTTTCCAGTATGGGTATCTG-3′ using the following conditions: 10 cycles at 92°C, 10 s; 55°C, 30 s; and 68°C, 30 s; followed by 15 cycles at 92°C, 15 s; 55°C, 30 s; and 68°C, 30 s with 2 s of additional extension time per cycle).

For each experiment and genotype, serial dilutions were tested, and events were counted at the dilution that showed a maximum of two joining events per lane. PCR products were then isolated from gels and sequenced

Southern Blot

Southern blot analysis was performed as described (208). Oligoprobes were: for der15 c-myc 5- GCCGCCACTTTACTGGACTGCGCAGG-3; for der15 IgH 5-GAGGGAGCCGGCTGAGAGAAGTTGGG-3; for der12 c-myc 5-GCAGCGATTCAGCACTGGGTGCAGG-3; for der12 IgH (3′ of switch m) 5-CCTGGTATACAGGACGAAACTGCAGCAG-3; for der12 IgH (5′ of switch m) 5- TTCAGTCATTGCTTTAGGGGGAG-3.

Cell Fractionation and Western Blot

The cytoplasmic fraction from $5x10^6$ splenic B cells (treated or not with 10 Gy IR and allowed 90 min recovery) was separated from the nuclei using the ProteoJET Cytoplasmic and Nuclear Protein Extraction Kit (Fermentas Cat# K0311) following the manufacturer's instructions. To separate nuclear-soluble and chromatin fractions, the manufacturer's nuclei lysis buffer was supplemented with the provided Nuclei Lysis reagent and with 30 mM EDTA, 2 mM EGTA, and 10 mM dithiothreitol. The nuclear extract was centrifuged at 1700g for 20 min at 4°C; the supernatant was saved at −80°C as the "nuclear-soluble fraction", and the chromatin pellet was washed twice in 250 μl of 3 mM EDTA, 0.2 mM EGTA, 1 mM dithiothreitol, and protease inhibitors (Roche). Chromatin was resuspended in 30 μl of 10 mM Hepes, 10 mM KCl, 1 mM $MgCl_2$, 10% glycerol, 1

mM $CaCl_2$, 1 mM EDTA, 1× protease inhibitors (Roche), and 5 U of micrococcal nuclease (New England Biolabs), and then incubated for 45 min at 37°C. The reaction was stopped by the addition of EGTA to 1 mM, and the digested pellet was stored at −80°C as the "chromatin-bound fraction." For retroviral reconstitution experiments, splenocytes were stimulated and fractionated on day 4. Expression of wild type and mutant 53BP1 proteins was detected with antisera to 53BP1 (Bethyl A300-272A), 53BP1 phosphorylated on Serine 25 (Bethyl A300-652A), FLAG (SIGMA F1804), or HA (Abcam ab 9110), as indicated. Controls for DNA damage, cell fractionation and for loading were with antibodies to γH2AX (Millipore 05-636), H2AX (Bethyl A300-083A), $H4K20^{me1}$ (Abcam ab9051), IgG LC (Jackson Immunoresearch Laboratories 015-030-007), tubulin (Abcam ab4074) or actin (SIGMA A5060).

Immuno-FISH

After stimulation, $1x10^6$ B cells were spun onto 24-well plates containing 12-mm coverslips (Fisher) coated with 150 g ml^{-1} poly-L-lysine (Sigma). Cells were fixed with methanol (-20°C), blocked with 5% goat serum/1% bovine serum albumin (BSA)/1x PBS overnight, incubated with either γH2AX (1:500), or 53BP1 (1:200) polyclonal antibodies, washed and then stained with Alexa-568 conjugated goat anti-rabbit antibody (Molecular Probes). For ICC-FISH, antibodies were cross-linked using 50 mM ethylene glycol bis (succinimidyl succinate) for 30 min at 37°C followed by RNase (100 g/ml) treatment for 60 min at 37 °C. Chromosomal DNA was denatured in 0.07 M NaOH (pH 13.0) for 2 min followed by immersion in cold PBS. The biotin-labelled DNA probe was hybridized at 37 °C overnight,

followed by standard FISH washes. DNA probes were detected with avidin-fluorescein isothiocyanate (FITC), and then amplified with biotinylated goat anti-avidin and avidin-FITC (all antibodies diluted 1:200 in 3% BSA/4 SSC/0.05% Tween 20; Vector Laboratories).

Ionizing radiation induced foci

For IRIF, mouse embryonic fibroblasts (MEFs) were grown overnight on glass coverslips in 30 mm culture dishes, then exposed to 5 Gy (53BP1 mutant MEFs) or 10 Gy ($53BP1^{-/-}$ MEFs reconstituted with mutant retroviruses) ionizing radiation and allowed to recover for 90 min. Cells were then fixed with 4% paraformaldehyde/PBS, followed by 0.5% Triton X-100/PBS permeabilzation and processed for immunofluorescent staining. Images were acquired using an LSM 510 META microscope (Zeiss) or with DeltaVision (Applied Precision). Primary antibodies used for immunofluorescence were rabbit anti-53BP1 (Novus Biologicals NB 100-304), mouse anti γH2AX (Millipore 05-636), and mouse anti-FLAG-M2 (SIGMA F1804). Secondary antibodies were Alexa568- and Alexa488-conjugated (Molecular Probes). DNA was counterstained with 4',6-diamidino-2-phenylindole (DAPI).

Chromatin Immunoprecipitation (ChIP).

Cells were fixed by adding 1% paraformaldehyde at 37°C for 10 min. Cells were then collected, washed once with cold PBS and lysed in RIPA buffer in the presence of Protease Inhibitor Cocktail (Roche), 0.5 mM PMSF and 5 mM NaF followed by sonication (Diagenode BIORUPTOR, 20 min with 30 s on/30 s off)

to produce DNA fragments 200-500 bp in length. Meanwhile, the γH2AX antibody (Millipore 05-636) was bound to Dynabeads Protein A (Invitrogen) following the manufacturer's instructions. The supernatants of sonicated samples were collected after centrifugation at 14000 rpm at 4°C for 5 min and added to the γH2AX binding beads overnight. The next day, beads were washed 2X with RIPA, 2X with RIPA + 0.3 M NaCl, 2X with LiCl buffer (0.25 M LiCl, 0.5% NP-40, 0.5% NaDOC), 1X with TE+0.2% Triton X and 1X with TE. Beads were then resuspended in TE and cross-linking was reversed using 3% SDS and Proteinase K (Sigma) at 65°C for 4 hrs. After removal of beads DNA was extracted with Phenol/Chloroform and precipitated with EtOH and NaOAc in the presence of glycogen. The qPCR was performed using SybrGreen reagent (Agilent/Strategene). Primer sequences used for amplification the indicated distances 3′ of the I-SceI site in μ:

5 kb (5′-TGAGCAACTGAACCTGAGGGAG-3′ and
TGGTCACATACTTCTCTTGGGGC),
25 kb (5′-GCATTTCCCTGATGACTAAGGACTG and 5′-
GACACCAACAAACCAAAGAACCC-3′),
80 kb (5′-GGCTTTTTTTGGCTGGGAGAC-3′ and 5′-
CTGAAGAACCTGGATGAAATGGAC-3′),
100 kb (5′-TACTGCCTACATCCTATGCCCCTC-3′ and 5′-
CACCCACATCTCACCCTTACCTAAC-3′),
120 kb (5′-CACCATCTTCATCAGCCTCTTCC-3′ and 5′-
TGGGGACAGCAAAGTAACATCCTAC-3′),

145 kb (5′-ACAGTGGAGTCCGTAGCAGGAAAG-3′ and 5′-GTTCTGGGTCATCTGAGTTCTATGC-3′),
195 kb (5′-CACCATCCTGTCCTGAAAGCAG-3′ and 5′-CAGCAAACCTGAGCCAGATAAGC-3′),
345 kb (5′-TGGCGAAAGGTAAGGCTGTATTC-3′ and 5′-AAATGCTGAGAAGTAGTCCCCCCG-3′),
595 kb (5′-TTGAGTGACACATACCGAGAGCC-3′ and 5′-TGAACCAAAGAAGAGGGGACCG-3′),
1 Mb (5′-CGCCAATCCTGTGACCATTTC-3′ and 5′-CACTCCAAAACAAGCCAAGAGC-3′) and
27 Mb (5′-GCTTCCTTTTCTGACGAGGCTG-3′ and 5′-CCCTGATAGTTTACTGTGTCCCTGG-3′).

To calculate γH2AX enrichment, the γH2AX signal was normalized to the GAPDH signal at all locations (average of triplicates). Primers used for amplification of GAPDH: (5′-TGAAGCAGGCATCTGAGGG-3′ and 5-CGAAGGTGGAAGAGTGGGAG-3′).

CHAPTER 8:

References

1. Hopfner KP, Karcher A, Craig L, Woo TT, Carney JP, Tainer JA. 2001. Structural biochemistry and interaction architecture of the DNA double-strand break repair Mre11 nuclease and Rad50-ATPase. *Cell* 105: 473-85

2. Moreno-Herrero F, de Jager M, Dekker NH, Kanaar R, Wyman C, Dekker C. 2005. Mesoscale conformational changes in the DNA-repair complex Rad50/Mre11/Nbs1 upon binding DNA. *Nature* 437: 440-3

3. Lee JH, Paull TT. 2005. ATM activation by DNA double-strand breaks through the Mre11-Rad50-Nbs1 complex. *Science* 308: 551-4

4. Williams RS, Moncalian G, Williams JS, Yamada Y, Limbo O, Shin DS, Groocock LM, Cahill D, Hitomi C, Guenther G, Moiani D, Carney JP, Russell P, Tainer JA. 2008. Mre11 dimers coordinate DNA end bridging and nuclease processing in double-strand-break repair. *Cell* 135: 97-109

5. Usui T, Ohta T, Oshiumi H, Tomizawa J, Ogawa H, Ogawa T. 1998. Complex formation and functional versatility of Mre11 of budding yeast in recombination. *Cell* 95: 705-16

6. de Jager M, Dronkert ML, Modesti M, Beerens CE, Kanaar R, van Gent DC. 2001. DNA-binding and strand-annealing activities of human Mre11: implications for its roles in DNA double-strand break repair pathways. *Nucleic Acids Res* 29: 1317-25

7. Paull TT, Gellert M. 1999. Nbs1 potentiates ATP-driven DNA unwinding and endonuclease cleavage by the Mre11/Rad50 complex. *Genes Dev* 13: 1276-88

8. Hopfner KP, Karcher A, Shin DS, Craig L, Arthur LM, Carney JP, Tainer JA. 2000. Structural biology of Rad50 ATPase: ATP-driven conformational control in DNA double-strand break repair and the ABC-ATPase superfamily. *Cell* 101: 789-800

9. de Jager M, van Noort J, van Gent DC, Dekker C, Kanaar R, Wyman C. 2001. Human Rad50/Mre11 is a flexible complex that can tether DNA ends. *Mol Cell* 8: 1129-35

10. Williams RS, Dodson GE, Limbo O, Yamada Y, Williams JS, Guenther G, Classen S, Glover JN, Iwasaki H, Russell P, Tainer JA. 2009. Nbs1 flexibly tethers Ctp1 and Mre11-Rad50 to coordinate DNA double-strand break processing and repair. *Cell* 139: 87-99

11. Falck J, Coates J, Jackson SP. 2005. Conserved modes of recruitment of ATM, ATR and DNA-PKcs to sites of DNA damage. *Nature* 434: 605-11

12. You Z, Chahwan C, Bailis J, Hunter T, Russell P. 2005. ATM activation and its recruitment to damaged DNA require binding to the C terminus of Nbs1. *Mol Cell Biol* 25: 5363-79

13. Lee JH, Xu B, Lee CH, Ahn JY, Song MS, Lee H, Canman CE, Lee JS, Kastan MB, Lim DS. 2003. Distinct functions of Nijmegen breakage syndrome in ataxia telangiectasia mutated-dependent responses to DNA damage. *Mol Cancer Res* 1: 674-81

14. Theunissen JW, Kaplan MI, Hunt PA, Williams BR, Ferguson DO, Alt FW, Petrini JH. 2003. Checkpoint failure and chromosomal instability without lymphomagenesis in Mre11(ATLD1/ATLD1) mice. *Mol Cell* 12: 1511-23

15. Kang J, Bronson RT, Xu Y. 2002. Targeted disruption of NBS1 reveals its roles in mouse development and DNA repair. *Embo J* 21: 1447-55

16. Difilippantonio S, Celeste A, Fernandez-Capetillo O, Chen HT, Reina San Martin B, Van Laethem F, Yang YP, Petukhova GV, Eckhaus M, Feigenbaum L, Manova K, Kruhlak M, Camerini-Otero RD, Sharan S, Nussenzweig M, Nussenzweig A. 2005. Role of Nbs1 in the activation of the Atm kinase revealed in humanized mouse models. *Nat Cell Biol* 7: 675-85

17. Varon R, Vissinga C, Platzer M, Cerosaletti KM, Chrzanowska KH, Saar K, Beckmann G, Seemanova E, Cooper PR, Nowak NJ, Stumm M, Weemaes CM, Gatti RA, Wilson RK, Digweed M, Rosenthal A, Sperling K, Concannon P, Reis A. 1998. Nibrin, a novel DNA double-strand break repair protein, is mutated in Nijmegen breakage syndrome. *Cell* 93: 467-76

18. Stewart GS, Maser RS, Stankovic T, Bressan DA, Kaplan MI, Jaspers NG, Raams A, Byrd PJ, Petrini JH, Taylor AM. 1999. The DNA double-strand break repair gene hMRE11 is mutated in individuals with an ataxia-telangiectasia-like disorder. *Cell* 99: 577-87

19. Savitsky K, Bar-Shira A, Gilad S, Rotman G, Ziv Y, Vanagaite L, Tagle DA, Smith S, Uziel T, Sfez S, Ashkenazi M, Pecker I, Frydman M, Harnik R, Patanjali SR, Simmons A, Clines GA, Sartiel A, Gatti RA, Chessa L, Sanal O, Lavin MF, Jaspers NG, Taylor AM, Arlett CF, Miki T, Weissman SM, Lovett M, Collins FS, Shiloh Y. 1995. A single ataxia telangiectasia gene with a product similar to PI-3 kinase. *Science* 268: 1749-53

20. Kim ST, Lim DS, Canman CE, Kastan MB. 1999. Substrate specificities and identification of putative substrates of ATM kinase family members. *J Biol Chem* 274: 37538-43

21. O'Neill T, Dwyer AJ, Ziv Y, Chan DW, Lees-Miller SP, Abraham RH, Lai JH, Hill D, Shiloh Y, Cantley LC, Rathbun GA. 2000. Utilization of oriented peptide libraries to identify substrate motifs selected by ATM. *J Biol Chem* 275: 22719-27

22. Matsuoka S, Ballif BA, Smogorzewska A, McDonald ER, 3rd, Hurov KE, Luo J, Bakalarski CE, Zhao Z, Solimini N, Lerenthal Y, Shiloh Y, Gygi SP, Elledge SJ. 2007. ATM and ATR substrate analysis reveals extensive protein networks responsive to DNA damage. *Science* 316: 1160-6

23. Linding R, Jensen LJ, Ostheimer GJ, van Vugt MA, Jorgensen C, Miron IM, Diella F, Colwill K, Taylor L, Elder K, Metalnikov P, Nguyen V, Pasculescu A, Jin J, Park JG, Samson LD, Woodgett JR, Russell RB, Bork P, Yaffe MB, Pawson T. 2007. Systematic discovery of in vivo phosphorylation networks. *Cell* 129: 1415-26

24. Banin S, Moyal L, Shieh S, Taya Y, Anderson CW, Chessa L, Smorodinsky NI, Prives C, Reiss Y, Shiloh Y, Ziv Y. 1998. Enhanced phosphorylation of p53 by ATM in response to DNA damage. *Science* 281: 1674-7

25. Canman CE, Lim DS, Cimprich KA, Taya Y, Tamai K, Sakaguchi K, Appella E, Kastan MB, Siliciano JD. 1998. Activation of the ATM kinase by ionizing radiation and phosphorylation of p53. *Science* 281: 1677-9

26. Falck J, Petrini JH, Williams BR, Lukas J, Bartek J. 2002. The DNA damage-dependent intra-S phase checkpoint is regulated by parallel pathways. *Nat Genet* 30: 290-4

27. Lim DS, Kim ST, Xu B, Maser RS, Lin J, Petrini JH, Kastan MB. 2000. ATM phosphorylates p95/nbs1 in an S-phase checkpoint pathway. *Nature* 404: 613-7

28. Matsuoka S, Huang M, Elledge SJ. 1998. Linkage of ATM to cell cycle regulation by the Chk2 protein kinase. *Science* 282: 1893-7

29. Bakkenist CJ, Kastan MB. 2003. DNA damage activates ATM through intermolecular autophosphorylation and dimer dissociation. *Nature* 421: 499-506

30. Pellegrini M, Celeste A, Difilippantonio S, Guo R, Wang W, Feigenbaum L, Nussenzweig A. 2006. Autophosphorylation at serine 1987 is dispensable for murine Atm activation in vivo. *Nature* 443: 222-5

31. Burma S, Chen BP, Murphy M, Kurimasa A, Chen DJ. 2001. ATM phosphorylates histone H2AX in response to DNA double-strand breaks. *J Biol Chem* 276: 42462-7

32. Rogakou EP, Pilch DR, Orr AH, Ivanova VS, Bonner WM. 1998. DNA double-stranded breaks induce histone H2AX phosphorylation on serine 139. *J Biol Chem* 273: 5858-68

33. Rogakou EP, Boon C, Redon C, Bonner WM. 1999. Megabase chromatin domains involved in DNA double-strand breaks in vivo. *J Cell Biol* 146: 905-16

34. Ward IM, Chen J. 2001. Histone H2AX is phosphorylated in an ATR-dependent manner in response to replicational stress. *J Biol Chem* 276: 47759-62

35. Lou Z, Minter-Dykhouse K, Franco S, Gostissa M, Rivera MA, Celeste A, Manis JP, van Deursen J, Nussenzweig A, Paull TT, Alt FW, Chen J. 2006. MDC1 maintains genomic stability by participating in the amplification of ATM-dependent DNA damage signals. *Mol Cell* 21: 187-200

36. Stucki M, Clapperton JA, Mohammad D, Yaffe MB, Smerdon SJ, Jackson SP. 2005. MDC1 directly binds phosphorylated histone H2AX to regulate cellular responses to DNA double-strand breaks. *Cell* 123: 1213-26

37. Celeste A, Petersen S, Romanienko PJ, Fernandez-Capetillo O, Chen HT, Sedelnikova OA, Reina-San-Martin B, Coppola V, Meffre E, Difilippantonio MJ, Redon C, Pilch DR, Olaru A, Eckhaus M, Camerini-Otero RD, Tessarollo L, Livak F, Manova K, Bonner WM, Nussenzweig MC, Nussenzweig A. 2002. Genomic instability in mice lacking histone H2AX. *Science* 296: 922-7

38. Bassing CH, Chua KF, Sekiguchi J, Suh H, Whitlow SR, Fleming JC, Monroe BC, Ciccone DN, Yan C, Vlasakova K, Livingston DM, Ferguson DO, Scully R, Alt FW. 2002. Increased ionizing radiation sensitivity and genomic instability in the absence of histone H2AX. *Proc Natl Acad Sci U S A* 99: 8173-8

39. Bassing CH, Suh H, Ferguson DO, Chua KF, Manis J, Eckersdorff M, Gleason M, Bronson R, Lee C, Alt FW. 2003. Histone H2AX: a dosage-dependent suppressor of oncogenic translocations and tumors. *Cell* 114: 359-70

40. Celeste A, Difilippantonio S, Difilippantonio MJ, Fernandez-Capetillo O, Pilch DR, Sedelnikova OA, Eckhaus M, Ried T, Bonner WM, Nussenzweig A. 2003. H2AX haploinsufficiency modifies genomic stability and tumor susceptibility. *Cell* 114: 371-83

41. Fernandez-Capetillo O, Mahadevaiah SK, Celeste A, Romanienko PJ, Camerini-Otero RD, Bonner WM, Manova K, Burgoyne P, Nussenzweig A. 2003. H2AX is required for chromatin remodeling and inactivation of sex chromosomes in male mouse meiosis. *Dev Cell* 4: 497-508

42. Lukas C, Melander F, Stucki M, Falck J, Bekker-Jensen S, Goldberg M, Lerenthal Y, Jackson SP, Bartek J, Lukas J. 2004. Mdc1 couples DNA double-strand break recognition by Nbs1 with its H2AX-dependent chromatin retention. *Embo J* 23: 2674-83

43. Stewart GS, Wang B, Bignell CR, Taylor AM, Elledge SJ. 2003. MDC1 is a mediator of the mammalian DNA damage checkpoint. *Nature* 421: 961-6

44. Lee MS, Edwards RA, Thede GL, Glover JN. 2005. Structure of the BRCT repeat domain of MDC1 and its specificity for the free COOH-terminal end of the gamma-H2AX histone tail. *J Biol Chem* 280: 32053-6

45. Spycher C, Miller ES, Townsend K, Pavic L, Morrice NA, Janscak P, Stewart GS, Stucki M. 2008. Constitutive phosphorylation of MDC1 physically links the MRE11-RAD50-NBS1 complex to damaged chromatin. *J Cell Biol* 181: 227-40

46. Melander F, Bekker-Jensen S, Falck J, Bartek J, Mailand N, Lukas J. 2008. Phosphorylation of SDT repeats in the MDC1 N terminus triggers retention of NBS1 at the DNA damage-modified chromatin. *J Cell Biol* 181: 213-26

47. Wu L, Luo K, Lou Z, Chen J. 2008. MDC1 regulates intra-S-phase checkpoint by targeting NBS1 to DNA double-strand breaks. *Proc Natl Acad Sci U S A* 105: 11200-5

48. Chapman JR, Jackson SP. 2008. Phospho-dependent interactions between NBS1 and MDC1 mediate chromatin retention of the MRN complex at sites of DNA damage. *EMBO Rep* 9: 795-801

49. Bekker-Jensen S, Lukas C, Kitagawa R, Melander F, Kastan MB, Bartek J, Lukas J. 2006. Spatial organization of the mammalian genome surveillance machinery in response to DNA strand breaks. *J Cell Biol* 173: 195-206

50. Huen MS, Huang J, Leung JW, Sy SM, Leung KM, Ching YP, Tsao SW, Chen J. 2010. Regulation of chromatin architecture by the PWWP domain-containing DNA damage-responsive factor EXPAND1/MUM1. *Mol Cell* 37: 854-64

51. Kolas NK, Chapman JR, Nakada S, Ylanko J, Chahwan R, Sweeney FD, Panier S, Mendez M, Wildenhain J, Thomson TM, Pelletier L, Jackson SP, Durocher D. 2007. Orchestration of the DNA-damage response by the RNF8 ubiquitin ligase. *Science* 318: 1637-40

52. Mailand N, Bekker-Jensen S, Faustrup H, Melander F, Bartek J, Lukas C, Lukas J. 2007. RNF8 ubiquitylates histones at DNA double-strand breaks and promotes assembly of repair proteins. *Cell* 131: 887-900

53. Santos MA, Huen MS, Jankovic M, Chen HT, Lopez-Contreras AJ, Klein IA, Wong N, Barbancho JL, Fernandez-Capetillo O, Nussenzweig MC, Chen J, Nussenzweig A. 2010. Class switching and meiotic defects in mice lacking the E3 ubiquitin ligase RNF8. *J Exp Med* 207: 973-81

54. Li L, Halaby MJ, Hakem A, Cardoso R, El Ghamrasni S, Harding S, Chan N, Bristow R, Sanchez O, Durocher D, Hakem R. 2010. Rnf8 deficiency impairs class switch recombination, spermatogenesis, and genomic integrity and predisposes for cancer. *J Exp Med* 207: 983-97

55. Doil C, Mailand N, Bekker-Jensen S, Menard P, Larsen DH, Pepperkok R, Ellenberg J, Panier S, Durocher D, Bartek J, Lukas J, Lukas C. 2009. RNF168 binds and amplifies ubiquitin conjugates on damaged chromosomes to allow accumulation of repair proteins. *Cell* 136: 435-46

56. Stewart GS, Panier S, Townsend K, Al-Hakim AK, Kolas NK, Miller ES, Nakada S, Ylanko J, Olivarius S, Mendez M, Oldreive C, Wildenhain J, Tagliaferro A, Pelletier L, Taubenheim N, Durandy A, Byrd PJ, Stankovic T, Taylor AM, Durocher D. 2009. The RIDDLE syndrome protein mediates a ubiquitin-dependent signaling cascade at sites of DNA damage. *Cell* 136: 420-34

57. Iwabuchi K, Bartel PL, Li B, Marraccino R, Fields S. 1994. Two cellular proteins that bind to wild-type but not mutant p53. *Proc Natl Acad Sci U S A* 91: 6098-102

58. Iwabuchi K, Li B, Massa HF, Trask BJ, Date T, Fields S. 1998. Stimulation of p53-mediated transcriptional activation by the p53-binding proteins, 53BP1 and 53BP2. *J Biol Chem* 273: 26061-8

59. Koonin EV, Altschul SF, Bork P. 1996. BRCA1 protein products ... Functional motifs. *Nat Genet* 13: 266-8

60. Schultz LB, Chehab NH, Malikzay A, Halazonetis TD. 2000. p53 binding protein 1 (53BP1) is an early participant in the cellular response to DNA double-strand breaks. *J Cell Biol* 151: 1381-90

61. Anderson L, Henderson C, Adachi Y. 2001. Phosphorylation and rapid relocalization of 53BP1 to nuclear foci upon DNA damage. *Mol Cell Biol* 21: 1719-29

62. Rappold I, Iwabuchi K, Date T, Chen J. 2001. Tumor suppressor p53 binding protein 1 (53BP1) is involved in DNA damage-signaling pathways. *J Cell Biol* 153: 613-20

63. Iwabuchi K, Basu BP, Kysela B, Kurihara T, Shibata M, Guan D, Cao Y, Hamada T, Imamura K, Jeggo PA, Date T, Doherty AJ. 2003. Potential role for 53BP1 in DNA end-joining repair through direct interaction with DNA. *J Biol Chem* 278: 36487-95

64. Huyen Y, Zgheib O, Ditullio RA, Jr., Gorgoulis VG, Zacharatos P, Petty TJ, Sheston EA, Mellert HS, Stavridi ES, Halazonetis TD. 2004. Methylated lysine 79 of histone H3 targets 53BP1 to DNA double-strand breaks. *Nature* 432: 406-11

65. Botuyan MV, Lee J, Ward IM, Kim JE, Thompson JR, Chen J, Mer G. 2006. Structural basis for the methylation state-specific recognition of histone H4-K20 by 53BP1 and Crb2 in DNA repair. *Cell* 127: 1361-73

66. Sanders SL, Portoso M, Mata J, Bahler J, Allshire RC, Kouzarides T. 2004. Methylation of histone H4 lysine 20 controls recruitment of Crb2 to sites of DNA damage. *Cell* 119: 603-14

67. Schotta G, Lachner M, Sarma K, Ebert A, Sengupta R, Reuter G, Reinberg D, Jenuwein T. 2004. A silencing pathway to induce H3-K9 and H4-K20 trimethylation at constitutive heterochromatin. *Genes Dev* 18: 1251-62

68. Yang H, Pesavento JJ, Starnes TW, Cryderman DE, Wallrath LL, Kelleher NL, Mizzen CA. 2008. Preferential dimethylation of histone H4 lysine 20 by Suv4-20. *J Biol Chem* 283: 12085-92

69. Schotta G, Sengupta R, Kubicek S, Malin S, Kauer M, Callen E, Celeste A, Pagani M, Opravil S, De La Rosa-Velazquez IA, Espejo A, Bedford MT, Nussenzweig A, Busslinger M, Jenuwein T. 2008. A chromatin-wide transition to H4K20 monomethylation impairs genome integrity and programmed DNA rearrangements in the mouse. *Genes Dev* 22: 2048-61

70. Celeste A, Fernandez-Capetillo O, Kruhlak MJ, Pilch DR, Staudt DW, Lee A, Bonner RF, Bonner WM, Nussenzweig A. 2003. Histone H2AX phosphorylation is dispensable for the initial recognition of DNA breaks. *Nat Cell Biol* 5: 675-9

71. Fernandez-Capetillo O, Chen HT, Celeste A, Ward I, Romanienko PJ, Morales JC, Naka K, Xia Z, Camerini-Otero RD, Motoyama N, Carpenter PB, Bonner WM, Chen J, Nussenzweig A. 2002. DNA damage-induced G2-M checkpoint activation by histone H2AX and 53BP1. *Nat Cell Biol* 4: 993-7

72. Ward IM, Minn K, Jorda KG, Chen J. 2003. Accumulation of checkpoint protein 53BP1 at DNA breaks involves its binding to phosphorylated histone H2AX. *J Biol Chem* 278: 19579-82

73. Yuan J, Chen J. 2010. MRE11-RAD50-NBS1 complex dictates DNA repair independent of H2AX. *J Biol Chem* 285: 1097-104

74. Pei H, Zhang L, Luo K, Qin Y, Chesi M, Fei F, Bergsagel PL, Wang L, You Z, Lou Z. 2011. MMSET regulates histone H4K20 methylation and 53BP1 accumulation at DNA damage sites. *Nature* 470: 124-8

75. Ward I, Kim JE, Minn K, Chini CC, Mer G, Chen J. 2006. The tandem BRCT domain of 53BP1 is not required for its repair function. *J Biol Chem* 281: 38472-7

76. Zgheib O, Pataky K, Brugger J, Halazonetis TD. 2009. An oligomerized 53BP1 tudor domain suffices for recognition of DNA double-strand breaks. *Mol Cell Biol* 29: 1050-8

77. Xie A, Hartlerode A, Stucki M, Odate S, Puget N, Kwok A, Nagaraju G, Yan C, Alt FW, Chen J, Jackson SP, Scully R. 2007. Distinct roles of chromatin-associated proteins MDC1 and 53BP1 in mammalian double-strand break repair. *Mol Cell* 28: 1045-57

78. Morales JC, Xia Z, Lu T, Aldrich MB, Wang B, Rosales C, Kellems RE, Hittelman WN, Elledge SJ, Carpenter PB. 2003. Role for the BRCA1 C-terminal repeats (BRCT) protein 53BP1 in maintaining genomic stability. *J Biol Chem* 278: 14971-7

79. Ward IM, Minn K, van Deursen J, Chen J. 2003. p53 Binding protein 53BP1 is required for DNA damage responses and tumor suppression in mice. *Mol Cell Biol* 23: 2556-63

80. Ward IM, Difilippantonio S, Minn K, Mueller MD, Molina JR, Yu X, Frisk CS, Ried T, Nussenzweig A, Chen J. 2005. 53BP1 cooperates with p53 and functions as a haploinsufficient tumor suppressor in mice. *Mol Cell Biol* 25: 10079-86

81. Sartori AA, Lukas C, Coates J, Mistrik M, Fu S, Bartek J, Baer R, Lukas J, Jackson SP. 2007. Human CtIP promotes DNA end resection. *Nature* 450: 509-14

82. Yun MH, Hiom K. 2009. CtIP-BRCA1 modulates the choice of DNA double-strand-break repair pathway throughout the cell cycle. *Nature* 459: 460-3

83. You Z, Shi LZ, Zhu Q, Wu P, Zhang YW, Basilio A, Tonnu N, Verma IM, Berns MW, Hunter T. 2009. CtIP links DNA double-strand break sensing to resection. *Mol Cell* 36: 954-69

84. Mimitou EP, Symington LS. 2008. Sae2, Exo1 and Sgs1 collaborate in DNA double-strand break processing. *Nature* 455: 770-4

85. Zhu Z, Chung WH, Shim EY, Lee SE, Ira G. 2008. Sgs1 helicase and two nucleases Dna2 and Exo1 resect DNA double-strand break ends. *Cell* 134: 981-94

86. Gravel S, Chapman JR, Magill C, Jackson SP. 2008. DNA helicases Sgs1 and BLM promote DNA double-strand break resection. *Genes Dev* 22: 2767-72

87. Huertas P, Cortes-Ledesma F, Sartori AA, Aguilera A, Jackson SP. 2008. CDK targets Sae2 to control DNA-end resection and homologous recombination. *Nature* 455: 689-92

88. Huertas P, Jackson SP. 2009. Human CtIP mediates cell cycle control of DNA end resection and double strand break repair. *J Biol Chem* 284: 9558-65

89. Cortez D, Guntuku S, Qin J, Elledge SJ. 2001. ATR and ATRIP: partners in checkpoint signaling. *Science* 294: 1713-6

90. Zou L, Elledge SJ. 2003. Sensing DNA damage through ATRIP recognition of RPA-ssDNA complexes. *Science* 300: 1542-8

91. Sung P. 1994. Catalysis of ATP-dependent homologous DNA pairing and strand exchange by yeast RAD51 protein. *Science* 265: 1241-3

92. Baumann P, Benson FE, West SC. 1996. Human Rad51 protein promotes ATP-dependent homologous pairing and strand transfer reactions in vitro. *Cell* 87: 757-66

93. Moynahan ME, Jasin M. 2010. Mitotic homologous recombination maintains genomic stability and suppresses tumorigenesis. *Nat Rev Mol Cell Biol* 11: 196-207

94. Lieber MR. 2010. The mechanism of double-strand DNA break repair by the nonhomologous DNA end-joining pathway. *Annu Rev Biochem* 79: 181-211

95. Blier PR, Griffith AJ, Craft J, Hardin JA. 1993. Binding of Ku protein to DNA. Measurement of affinity for ends and demonstration of binding to nicks. *J Biol Chem* 268: 7594-601

96. Mimori T, Hardin JA. 1986. Mechanism of interaction between Ku protein and DNA. *J Biol Chem* 261: 10375-9

97. Yoo S, Kimzey A, Dynan WS. 1999. Photocross-linking of an oriented DNA repair complex. Ku bound at a single DNA end. *J Biol Chem* 274: 20034-9

98. West RB, Yaneva M, Lieber MR. 1998. Productive and nonproductive complexes of Ku and DNA-dependent protein kinase at DNA termini. *Mol Cell Biol* 18: 5908-20

99. Spagnolo L, Rivera-Calzada A, Pearl LH, Llorca O. 2006. Three-dimensional structure of the human DNA-PKcs/Ku70/Ku80 complex assembled on DNA and its implications for DNA DSB repair. *Mol Cell* 22: 511-9

100. Chen L, Trujillo K, Sung P, Tomkinson AE. 2000. Interactions of the DNA ligase IV-XRCC4 complex with DNA ends and the DNA-dependent protein kinase. *J Biol Chem* 275: 26196-205

101. Ma Y, Pannicke U, Schwarz K, Lieber MR. 2002. Hairpin opening and overhang processing by an Artemis/DNA-dependent protein kinase complex in nonhomologous end joining and V(D)J recombination. *Cell* 108: 781-94

102. Nick McElhinny SA, Snowden CM, McCarville J, Ramsden DA. 2000. Ku recruits the XRCC4-ligase IV complex to DNA ends. *Mol Cell Biol* 20: 2996-3003

103. Rooney S, Alt FW, Lombard D, Whitlow S, Eckersdorff M, Fleming J, Fugmann S, Ferguson DO, Schatz DG, Sekiguchi J. 2003. Defective DNA repair and increased genomic instability in Artemis-deficient murine cells. *J Exp Med* 197: 553-65

104. Rooney S, Sekiguchi J, Zhu C, Cheng HL, Manis J, Whitlow S, DeVido J, Foy D, Chaudhuri J, Lombard D, Alt FW. 2002. Leaky Scid phenotype associated with defective V(D)J coding end processing in Artemis-deficient mice. *Mol Cell* 10: 1379-90

105. Moon AF, Garcia-Diaz M, Batra VK, Beard WA, Bebenek K, Kunkel TA, Wilson SH, Pedersen LC. 2007. The X family portrait: structural insights into biological functions of X family polymerases. *DNA Repair (Amst)* 6: 1709-25

106. Gu J, Lu H, Tsai AG, Schwarz K, Lieber MR. 2007. Single-stranded DNA ligation and XLF-stimulated incompatible DNA end ligation by the XRCC4-DNA ligase IV complex: influence of terminal DNA sequence. *Nucleic Acids Res* 35: 5755-62

107. Tsai CJ, Kim SA, Chu G. 2007. Cernunnos/XLF promotes the ligation of mismatched and noncohesive DNA ends. *Proc Natl Acad Sci U S A* 104: 7851-6

108. Kabotyanski EB, Gomelsky L, Han JO, Stamato TD, Roth DB. 1998. Double-strand break repair in Ku86- and XRCC4-deficient cells. *Nucleic Acids Res* 26: 5333-42

109. Verkaik NS, Esveldt-van Lange RE, van Heemst D, Bruggenwirth HT, Hoeijmakers JH, Zdzienicka MZ, van Gent DC. 2002. Different types of V(D)J recombination and end-joining defects in DNA double-strand break repair mutant mammalian cells. *Eur J Immunol* 32: 701-9

110. Wang H, Zeng ZC, Perrault AR, Cheng X, Qin W, Iliakis G. 2001. Genetic evidence for the involvement of DNA ligase IV in the DNA-PK-dependent pathway of non-homologous end joining in mammalian cells. *Nucleic Acids Res* 29: 1653-60

111. Xie A, Kwok A, Scully R. 2009. Role of mammalian Mre11 in classical and alternative nonhomologous end joining. *Nat Struct Mol Biol* 16: 814-8

112. Han L, Yu K. 2008. Altered kinetics of nonhomologous end joining and class switch recombination in ligase IV--deficient B cells. *J Exp Med* 205: 2745-53

113. Boboila C, Jankovic M, Yan CT, Wang JH, Wesemann DR, Zhang T, Fazeli A, Feldman L, Nussenzweig A, Nussenzweig M, Alt FW. 2010. Alternative end-joining catalyzes robust IgH locus deletions and translocations in the combined absence of ligase 4 and Ku70. *Proc Natl Acad Sci U S A* 107: 3034-9

114. Difilippantonio MJ, Petersen S, Chen HT, Johnson R, Jasin M, Kanaar R, Ried T, Nussenzweig A. 2002. Evidence for replicative repair of DNA double-strand breaks leading to oncogenic translocation and gene amplification. *J Exp Med* 196: 469-80

115. Weinstock DM, Brunet E, Jasin M. 2007. Formation of NHEJ-derived reciprocal chromosomal translocations does not require Ku70. *Nat Cell Biol* 9: 978-81

116. Zhu C, Mills KD, Ferguson DO, Lee C, Manis J, Fleming J, Gao Y, Morton CC, Alt FW. 2002. Unrepaired DNA breaks in p53-deficient cells lead to oncogenic gene amplification subsequent to translocations. *Cell* 109: 811-21

117. Goodarzi AA, Noon AT, Deckbar D, Ziv Y, Shiloh Y, Lobrich M, Jeggo PA. 2008. ATM signaling facilitates repair of DNA double-strand breaks associated with heterochromatin. *Mol Cell* 31: 167-77

118. Stoddard BL. 2005. Homing endonuclease structure and function. *Q Rev Biophys* 38: 49-95

119. Palm W, de Lange T. 2008. How shelterin protects mammalian telomeres. *Annu Rev Genet* 42: 301-34

120. Denchi EL, de Lange T. 2007. Protection of telomeres through independent control of ATM and ATR by TRF2 and POT1. *Nature* 448: 1068-71

121. Gong Y, de Lange T. 2010. A Shld1-controlled POT1a provides support for repression of ATR signaling at telomeres through RPA exclusion. *Mol Cell* 40: 377-87

122. Celli GB, de Lange T. 2005. DNA processing is not required for ATM-mediated telomere damage response after TRF2 deletion. *Nat Cell Biol* 7: 712-8

123. Karlseder J, Broccoli D, Dai Y, Hardy S, de Lange T. 1999. p53- and ATM-dependent apoptosis induced by telomeres lacking TRF2. *Science* 283: 1321-5

124. Dimitrova N, Chen YC, Spector DL, de Lange T. 2008. 53BP1 promotes non-homologous end joining of telomeres by increasing chromatin mobility. *Nature* 456: 524-8

125. Dimitrova N, de Lange T. 2006. MDC1 accelerates nonhomologous end-joining of dysfunctional telomeres. *Genes Dev* 20: 3238-43

126. Takai H, Smogorzewska A, de Lange T. 2003. DNA damage foci at dysfunctional telomeres. *Curr Biol* 13: 1549-56

127. Dimitrova N, de Lange T. 2009. Cell cycle-dependent role of MRN at dysfunctional telomeres: ATM signaling-dependent induction of nonhomologous end joining (NHEJ) in G1 and resection-mediated inhibition of NHEJ in G2. *Mol Cell Biol* 29: 5552-63

128. Celli GB, Denchi EL, de Lange T. 2006. Ku70 stimulates fusion of dysfunctional telomeres yet protects chromosome ends from homologous recombination. *Nat Cell Biol* 8: 885-90

129. Chun JJ, Schatz DG, Oettinger MA, Jaenisch R, Baltimore D. 1991. The recombination activating gene-1 (RAG-1) transcript is present in the murine central nervous system. *Cell* 64: 189-200

130. Mombaerts P, Iacomini J, Johnson RS, Herrup K, Tonegawa S, Papaioannou VE. 1992. RAG-1-deficient mice have no mature B and T lymphocytes. *Cell* 68: 869-77

131. Schatz DG, Oettinger MA, Baltimore D. 1989. The V(D)J recombination activating gene, RAG-1. *Cell* 59: 1035-48

132. Oettinger MA, Schatz DG, Gorka C, Baltimore D. 1990. RAG-1 and RAG-2, adjacent genes that synergistically activate V(D)J recombination. *Science* 248: 1517-23

133. Max EE, Seidman JG, Leder P. 1979. Sequences of five potential recombination sites encoded close to an immunoglobulin kappa constant region gene. *Proc Natl Acad Sci U S A* 76: 3450-4

134. Sakano H, Huppi K, Heinrich G, Tonegawa S. 1979. Sequences at the somatic recombination sites of immunoglobulin light-chain genes. *Nature* 280: 288-94

135. Difilippantonio MJ, McMahan CJ, Eastman QM, Spanopoulou E, Schatz DG. 1996. RAG1 mediates signal sequence recognition and recruitment of RAG2 in V(D)J recombination. *Cell* 87: 253-62

136. Roman CA, Baltimore D. 1996. Genetic evidence that the RAG1 protein directly participates in V(D)J recombination through substrate recognition. *Proc Natl Acad Sci U S A* 93: 2333-8

137. Roth DB, Nakajima PB, Menetski JP, Bosma MJ, Gellert M. 1992. V(D)J recombination in mouse thymocytes: double-strand breaks near T cell receptor delta rearrangement signals. *Cell* 69: 41-53

138. McBlane JF, van Gent DC, Ramsden DA, Romeo C, Cuomo CA, Gellert M, Oettinger MA. 1995. Cleavage at a V(D)J recombination signal requires only RAG1 and RAG2 proteins and occurs in two steps. *Cell* 83: 387-95

139. Agrawal A, Schatz DG. 1997. RAG1 and RAG2 form a stable postcleavage synaptic complex with DNA containing signal ends in V(D)J recombination. *Cell* 89: 43-53

140. Hiom K, Gellert M. 1998. Assembly of a 12/23 paired signal complex: a critical control point in V(D)J recombination. *Mol Cell* 1: 1011-9

141. Komori T, Okada A, Stewart V, Alt FW. 1993. Lack of N regions in antigen receptor variable region genes of TdT-deficient lymphocytes. *Science* 261: 1171-5

142. Taccioli GE, Rathbun G, Oltz E, Stamato T, Jeggo PA, Alt FW. 1993. Impairment of V(D)J recombination in double-strand break repair mutants. *Science* 260: 207-10

143. Nussenzweig A, Chen C, da Costa Soares V, Sanchez M, Sokol K, Nussenzweig MC, Li GC. 1996. Requirement for Ku80 in growth and immunoglobulin V(D)J recombination. *Nature* 382: 551-5

144. Gu Y, Seidl KJ, Rathbun GA, Zhu C, Manis JP, van der Stoep N, Davidson L, Cheng HL, Sekiguchi JM, Frank K, Stanhope-Baker P, Schlissel MS, Roth DB, Alt FW. 1997. Growth retardation and leaky SCID phenotype of Ku70-deficient mice. *Immunity* 7: 653-65

145. Frank KM, Sekiguchi JM, Seidl KJ, Swat W, Rathbun GA, Cheng HL, Davidson L, Kangaloo L, Alt FW. 1998. Late embryonic lethality and impaired V(D)J recombination in mice lacking DNA ligase IV. *Nature* 396: 173-7

146. Taccioli GE, Amatucci AG, Beamish HJ, Gell D, Xiang XH, Torres Arzayus MI, Priestley A, Jackson SP, Marshak Rothstein A, Jeggo PA, Herrera VL. 1998. Targeted disruption of the catalytic subunit of the DNA-PK gene in mice confers severe combined immunodeficiency and radiosensitivity. *Immunity* 9: 355-66

147. Corneo B, Wendland RL, Deriano L, Cui X, Klein IA, Wong SY, Arnal S, Holub AJ, Weller GR, Pancake BA, Shah S, Brandt VL, Meek K, Roth DB. 2007. Rag mutations reveal robust alternative end joining. *Nature* 449: 483-6

148. Lee GS, Neiditch MB, Salus SS, Roth DB. 2004. RAG proteins shepherd double-strand breaks to a specific pathway, suppressing error-prone repair, but RAG nicking initiates homologous recombination. *Cell* 117: 171-84

149. Chen HT, Bhandoola A, Difilippantonio MJ, Zhu J, Brown MJ, Tai X, Rogakou EP, Brotz TM, Bonner WM, Ried T, Nussenzweig A. 2000. Response to RAG-mediated VDJ cleavage by NBS1 and gamma-H2AX. *Science* 290: 1962-5

150. Bredemeyer AL, Sharma GG, Huang CY, Helmink BA, Walker LM, Khor KC, Nuskey B, Sullivan KE, Pandita TK, Bassing CH, Sleckman BP. 2006. ATM stabilizes DNA double-strand-break complexes during V(D)J recombination. *Nature* 442: 466-70

151. Yin B, Savic V, Juntilla MM, Bredemeyer AL, Yang-Iott KS, Helmink BA, Koretzky GA, Sleckman BP, Bassing CH. 2009. Histone H2AX stabilizes broken DNA strands to suppress chromosome breaks and translocations during V(D)J recombination. *J Exp Med* 206: 2625-39

152. Difilippantonio S, Gapud E, Wong N, Huang CY, Mahowald G, Chen HT, Kruhlak MJ, Callen E, Livak F, Nussenzweig MC, Sleckman BP, Nussenzweig A. 2008. 53BP1 facilitates long-range DNA end-joining during V(D)J recombination. *Nature* 456: 529-33

153. Franco S, Gostissa M, Zha S, Lombard DB, Murphy MM, Zarrin AA, Yan C, Tepsuporn S, Morales JC, Adams MM, Lou Z, Bassing CH, Manis JP, Chen J, Carpenter PB, Alt FW. 2006. H2AX prevents DNA breaks from progressing to chromosome breaks and translocations. *Mol Cell* 21: 201-14

154. Muramatsu M, Sankaranand VS, Anant S, Sugai M, Kinoshita K, Davidson NO, Honjo T. 1999. Specific expression of activation-induced cytidine deaminase (AID), a novel member of the RNA-editing deaminase family in germinal center B cells. *J Biol Chem* 274: 18470-6

155. Muramatsu M, Kinoshita K, Fagarasan S, Yamada S, Shinkai Y, Honjo T. 2000. Class switch recombination and hypermutation require activation-induced cytidine deaminase (AID), a potential RNA editing enzyme. *Cell* 102: 553-63

156. Revy P, Muto T, Levy Y, Geissmann F, Plebani A, Sanal O, Catalan N, Forveille M, Dufourcq-Labelouse R, Gennery A, Tezcan I, Ersoy F, Kayserili H, Ugazio AG, Brousse N, Muramatsu M, Notarangelo LD, Kinoshita K, Honjo T, Fischer A, Durandy A. 2000. Activation-induced cytidine deaminase (AID) deficiency causes the autosomal recessive form of the Hyper-IgM syndrome (HIGM2). *Cell* 102: 565-75

157. Bransteitter R, Pham P, Scharff MD, Goodman MF. 2003. Activation-induced cytidine deaminase deaminates deoxycytidine on single-stranded DNA but requires the action of RNase. *Proc Natl Acad Sci U S A* 100: 4102-7

158. Chaudhuri J, Tian M, Khuong C, Chua K, Pinaud E, Alt FW. 2003. Transcription-targeted DNA deamination by the AID antibody diversification enzyme. *Nature* 422: 726-30

159. Dickerson SK, Market E, Besmer E, Papavasiliou FN. 2003. AID mediates hypermutation by deaminating single stranded DNA. *J Exp Med* 197: 1291-6

160. Petersen-Mahrt SK, Harris RS, Neuberger MS. 2002. AID mutates E. coli suggesting a DNA deamination mechanism for antibody diversification. *Nature* 418: 99-103

161. Pham P, Bransteitter R, Petruska J, Goodman MF. 2003. Processive AID-catalysed cytosine deamination on single-stranded DNA simulates somatic hypermutation. *Nature* 424: 103-7

162. Ramiro AR, Stavropoulos P, Jankovic M, Nussenzweig MC. 2003. Transcription enhances AID-mediated cytidine deamination by exposing single-stranded DNA on the nontemplate strand. *Nat Immunol* 4: 452-6

163. Petersen S, Casellas R, Reina-San-Martin B, Chen HT, Difilippantonio MJ, Wilson PC, Hanitsch L, Celeste A, Muramatsu M, Pilch DR, Redon C, Ried T, Bonner WM, Honjo T, Nussenzweig MC, Nussenzweig A. 2001. AID is required to initiate Nbs1/gamma-H2AX focus formation and mutations at sites of class switching. *Nature* 414: 660-5

164. Schrader CE, Linehan EK, Mochegova SN, Woodland RT, Stavnezer J. 2005. Inducible DNA breaks in Ig S regions are dependent on AID and UNG. *J Exp Med* 202: 561-8

165. Rada C, Williams GT, Nilsen H, Barnes DE, Lindahl T, Neuberger MS. 2002. Immunoglobulin isotype switching is inhibited and somatic hypermutation perturbed in UNG-deficient mice. *Curr Biol* 12: 1748-55

166. Di Noia J, Neuberger MS. 2002. Altering the pathway of immunoglobulin hypermutation by inhibiting uracil-DNA glycosylase. *Nature* 419: 43-8

167. Imai K, Slupphaug G, Lee WI, Revy P, Nonoyama S, Catalan N, Yel L, Forveille M, Kavli B, Krokan HE, Ochs HD, Fischer A, Durandy A. 2003. Human uracil-DNA glycosylase deficiency associated with profoundly impaired immunoglobulin class-switch recombination. *Nat Immunol* 4: 1023-8

168. Guikema JE, Linehan EK, Tsuchimoto D, Nakabeppu Y, Strauss PR, Stavnezer J, Schrader CE. 2007. APE1- and APE2-dependent DNA breaks in immunoglobulin class switch recombination. *J Exp Med* 204: 3017-26

169. Ehrenstein MR, Neuberger MS. 1999. Deficiency in Msh2 affects the efficiency and local sequence specificity of immunoglobulin class-switch recombination: parallels with somatic hypermutation. *Embo J* 18: 3484-90

170. Ehrenstein MR, Rada C, Jones AM, Milstein C, Neuberger MS. 2001. Switch junction sequences in PMS2-deficient mice reveal a microhomology-mediated mechanism of Ig class switch recombination. *Proc Natl Acad Sci U S A* 98: 14553-8

171. Schrader CE, Edelmann W, Kucherlapati R, Stavnezer J. 1999. Reduced isotype switching in splenic B cells from mice deficient in mismatch repair enzymes. *J Exp Med* 190: 323-30

172. Martin A, Li Z, Lin DP, Bardwell PD, Iglesias-Ussel MD, Edelmann W, Scharff MD. 2003. Msh2 ATPase activity is essential for somatic hypermutation at a-T basepairs and for efficient class switch recombination. *J Exp Med* 198: 1171-8

173. Martomo SA, Yang WW, Gearhart PJ. 2004. A role for Msh6 but not Msh3 in somatic hypermutation and class switch recombination. *J Exp Med* 200: 61-8

174. Bardwell PD, Woo CJ, Wei K, Li Z, Martin A, Sack SZ, Parris T, Edelmann W, Scharff MD. 2004. Altered somatic hypermutation and reduced class-switch recombination in exonuclease 1-mutant mice. *Nat Immunol* 5: 224-9

175. Wilson TM, Vaisman A, Martomo SA, Sullivan P, Lan L, Hanaoka F, Yasui A, Woodgate R, Gearhart PJ. 2005. MSH2-MSH6 stimulates DNA polymerase eta, suggesting a role for A:T mutations in antibody genes. *J Exp Med* 201: 637-45

176. Li Z, Scherer SJ, Ronai D, Iglesias-Ussel MD, Peled JU, Bardwell PD, Zhuang M, Lee K, Martin A, Edelmann W, Scharff MD. 2004. Examination of Msh6- and Msh3-deficient mice in class switching reveals overlapping and distinct roles of MutS homologues in antibody diversification. *J Exp Med* 200: 47-59

177. Gordon MS, Kanegai CM, Doerr JR, Wall R. 2003. Somatic hypermutation of the B cell receptor genes B29 (Igbeta, CD79b) and mb1 (Igalpha, CD79a). *Proc Natl Acad Sci U S A* 100: 4126-31

178. Liu M, Duke JL, Richter DJ, Vinuesa CG, Goodnow CC, Kleinstein SH, Schatz DG. 2008. Two levels of protection for the B cell genome during somatic hypermutation. *Nature* 451: 841-5

179. Muschen M, Re D, Jungnickel B, Diehl V, Rajewsky K, Kuppers R. 2000. Somatic mutation of the CD95 gene in human B cells as a side-effect of the germinal center reaction. *J Exp Med* 192: 1833-40

180. Pasqualucci L, Migliazza A, Fracchiolla N, William C, Neri A, Baldini L, Chaganti RS, Klein U, Kuppers R, Rajewsky K, Dalla-Favera R. 1998. BCL-6 mutations in normal germinal center B cells: evidence of somatic hypermutation acting outside Ig loci. *Proc Natl Acad Sci U S A* 95: 11816-21

181. Pasqualucci L, Neumeister P, Goossens T, Nanjangud G, Chaganti RS, Kuppers R, Dalla-Favera R. 2001. Hypermutation of multiple proto-oncogenes in B-cell diffuse large-cell lymphomas. *Nature* 412: 341-6

182. Yancopoulos GD, DePinho RA, Zimmerman KA, Lutzker SG, Rosenberg N, Alt FW. 1986. Secondary genomic rearrangement events in pre-B cells: VHDJH replacement by a LINE-1 sequence and directed class switching. *Embo J* 5: 3259-66

183. Lutzker S, Rothman P, Pollock R, Coffman R, Alt FW. 1988. Mitogen- and IL-4-regulated expression of germ-line Ig gamma 2b transcripts: evidence for directed heavy chain class switching. *Cell* 53: 177-84

184. Stavnezer J, Radcliffe G, Lin YC, Nietupski J, Berggren L, Sitia R, Severinson E. 1988. Immunoglobulin heavy-chain switching may be directed by prior induction of transcripts from constant-region genes. *Proc Natl Acad Sci U S A* 85: 7704-8

185. Shen HM, Poirier MG, Allen MJ, North J, Lal R, Widom J, Storb U. 2009. The activation-induced cytidine deaminase (AID) efficiently targets DNA in nucleosomes but only during transcription. *J Exp Med* 206: 1057-71

186. Nambu Y, Sugai M, Gonda H, Lee CG, Katakai T, Agata Y, Yokota Y, Shimizu A. 2003. Transcription-coupled events associating with immunoglobulin switch region chromatin. *Science* 302: 2137-40

187. Pavri R, Gazumyan A, Jankovic M, Di Virgilio M, Klein I, Ansarah-Sobrinho C, Resch W, Yamane A, Reina San-Martin B, Barreto V, Nieland TJ, Root DE, Casellas R, Nussenzweig MC. 2010. Activation-induced cytidine deaminase targets DNA at sites of RNA polymerase II stalling by interaction with Spt5. *Cell* 143: 122-33

188. Basu U, Meng FL, Keim C, Grinstein V, Pefanis E, Eccleston J, Zhang T, Myers D, Wasserman CR, Wesemann DR, Januszyk K, Gregory RI, Deng H, Lima CD, Alt FW. 2011. The RNA exosome targets the AID cytidine deaminase to both strands of transcribed duplex DNA substrates. *Cell* 144: 353-63

189. Robbiani DF, Bothmer A, Callen E, Reina-San-Martin B, Dorsett Y, Difilippantonio S, Bolland DJ, Chen HT, Corcoran AE, Nussenzweig A, Nussenzweig MC. 2008. AID is required for the chromosomal breaks in c-myc that lead to c-myc/IgH translocations. *Cell* 135: 1028-38

190. Reina-San-Martin B, Nussenzweig MC, Nussenzweig A, Difilippantonio S. 2005. Genomic instability, endoreduplication, and diminished Ig class-switch recombination in B cells lacking Nbs1. *Proc Natl Acad Sci U S A* 102: 1590-5

191. Lumsden JM, McCarty T, Petiniot LK, Shen R, Barlow C, Wynn TA, Morse HC, 3rd, Gearhart PJ, Wynshaw-Boris A, Max EE, Hodes RJ. 2004. Immunoglobulin class switch recombination is impaired in Atm-deficient mice. *J Exp Med* 200: 1111-21

192. Reina-San-Martin B, Chen HT, Nussenzweig A, Nussenzweig MC. 2004. ATM is required for efficient recombination between immunoglobulin switch regions. *J Exp Med* 200: 1103-10

193. Reina-San-Martin B, Difilippantonio S, Hanitsch L, Masilamani RF, Nussenzweig A, Nussenzweig MC. 2003. H2AX is required for recombination between immunoglobulin switch regions but not for intra-switch region recombination or somatic hypermutation. *J Exp Med* 197: 1767-78

194. Manis JP, Morales JC, Xia Z, Kutok JL, Alt FW, Carpenter PB. 2004. 53BP1 links DNA damage-response pathways to immunoglobulin heavy chain class-switch recombination. *Nat Immunol* 5: 481-7

195. Ward IM, Reina-San-Martin B, Olaru A, Minn K, Tamada K, Lau JS, Cascalho M, Chen L, Nussenzweig A, Livak F, Nussenzweig MC, Chen J. 2004. 53BP1 is required for class switch recombination. *J Cell Biol* 165: 459-64

196. Reina-San-Martin B, Chen J, Nussenzweig A, Nussenzweig MC. 2007. Enhanced intra-switch region recombination during immunoglobulin class switch recombination in 53BP1-/- B cells. *Eur J Immunol* 37: 235-9

197. Yan CT, Boboila C, Souza EK, Franco S, Hickernell TR, Murphy M, Gumaste S, Geyer M, Zarrin AA, Manis JP, Rajewsky K, Alt FW. 2007. IgH class switching and translocations use a robust non-classical end-joining pathway. *Nature* 449: 478-82

198. Boboila C, Yan C, Wesemann DR, Jankovic M, Wang JH, Manis J, Nussenzweig A, Nussenzweig M, Alt FW. 2010. Alternative end-joining catalyzes class switch recombination in the absence of both Ku70 and DNA ligase 4. *J Exp Med* 207: 417-27

199. Soulas-Sprauel P, Le Guyader G, Rivera-Munoz P, Abramowski V, Olivier-Martin C, Goujet-Zalc C, Charneau P, de Villartay JP. 2007. Role for DNA repair factor XRCC4 in immunoglobulin class switch recombination. *J Exp Med* 204: 1717-27

200. Di Noia JM, Neuberger MS. 2007. Molecular mechanisms of antibody somatic hypermutation. *Annu Rev Biochem* 76: 1-22

201. Kuppers R. 2005. Mechanisms of B-cell lymphoma pathogenesis. *Nat Rev Cancer* 5: 251-62

202. Gostissa M, Yan CT, Bianco JM, Cogne M, Pinaud E, Alt FW. 2009. Long-range oncogenic activation of Igh-c-myc translocations by the Igh 3' regulatory region. *Nature* 462: 803-7

203. Curry JD, Schulz D, Guidos CJ, Danska JS, Nutter L, Nussenzweig A, Schlissel MS. 2007. Chromosomal reinsertion of broken RSS ends during T cell development. *J Exp Med* 204: 2293-303

204. Raghavan SC, Swanson PC, Wu X, Hsieh CL, Lieber MR. 2004. A non-B-DNA structure at the Bcl-2 major breakpoint region is cleaved by the RAG complex. *Nature* 428: 88-93

205. Tsai AG, Lu H, Raghavan SC, Muschen M, Hsieh CL, Lieber MR. 2008. Human chromosomal translocations at CpG sites and a theoretical basis for their lineage and stage specificity. *Cell* 135: 1130-42

206. Wang JH, Alt FW, Gostissa M, Datta A, Murphy M, Alimzhanov MB, Coakley KM, Rajewsky K, Manis JP, Yan CT. 2008. Oncogenic transformation in the absence of Xrcc4 targets peripheral B cells that have undergone editing and switching. *J Exp Med* 205: 3079-90

207. Wang JH, Gostissa M, Yan CT, Goff P, Hickernell T, Hansen E, Difilippantonio S, Wesemann DR, Zarrin AA, Rajewsky K, Nussenzweig A, Alt FW. 2009. Mechanisms promoting translocations in editing and switching peripheral B cells. *Nature* 460: 231-6

208. Ramiro AR, Jankovic M, Callen E, Difilippantonio S, Chen HT, McBride KM, Eisenreich TR, Chen J, Dickins RA, Lowe SW, Nussenzweig A, Nussenzweig MC. 2006. Role of genomic instability and p53 in AID-induced c-myc-Igh translocations. *Nature* 440: 105-9

209. Robbiani DF, Bunting S, Feldhahn N, Bothmer A, Camps J, Deroubaix S, McBride KM, Klein IA, Stone G, Eisenreich TR, Ried T, Nussenzweig A, Nussenzweig MC. 2009. AID produces DNA double-strand breaks in non-Ig genes and mature B cell lymphomas with reciprocal chromosome translocations. *Mol Cell* 36: 631-41

210. Jankovic M, Robbiani DF, Dorsett Y, Eisenreich T, Xu Y, Tarakhovsky A, Nussenzweig A, Nussenzweig MC. 2010. Role of the translocation partner in protection against AID-dependent chromosomal translocations. *Proc Natl Acad Sci U S A* 107: 187-92

211. Adams JM, Gerondakis S, Webb E, Corcoran LM, Cory S. 1983. Cellular myc oncogene is altered by chromosome translocation to an immunoglobulin locus in murine plasmacytomas and is rearranged similarly in human Burkitt lymphomas. *Proc Natl Acad Sci U S A* 80: 1982-6

212. Adams JM, Gerondakis S, Webb E, Mitchell J, Bernard O, Cory S. 1982. Transcriptionally active DNA region that rearranges frequently in murine lymphoid tumors. *Proc Natl Acad Sci U S A* 79: 6966-70

213. Adams JM, Harris AW, Pinkert CA, Corcoran LM, Alexander WS, Cory S, Palmiter RD, Brinster RL. 1985. The c-myc oncogene driven by immunoglobulin enhancers induces lymphoid malignancy in transgenic mice. *Nature* 318: 533-8

214. Cory S, Gerondakis S, Adams JM. 1983. Interchromosomal recombination of the cellular oncogene c-myc with the immunoglobulin heavy chain locus in murine plasmacytomas is a reciprocal exchange. *EMBO J* 2: 697-703

215. Crews S, Barth R, Hood L, Prehn J, Calame K. 1982. Mouse c-myc oncogene is located on chromosome 15 and translocated to chromosome 12 in plasmacytomas. *Science* 218: 1319-21

216. Dalla-Favera R, Martinotti S, Gallo RC, Erikson J, Croce CM. 1983. Translocation and rearrangements of the c-myc oncogene locus in human undifferentiated B-cell lymphomas. *Science* 219: 963-7

217. Erikson J, ar-Rushdi A, Drwinga HL, Nowell PC, Croce CM. 1983. Transcriptional activation of the translocated c-myc oncogene in burkitt lymphoma. *Proc Natl Acad Sci U S A* 80: 820-4

218. Hamlyn PH, Rabbitts TH. 1983. Translocation joins c-myc and immunoglobulin gamma 1 genes in a Burkitt lymphoma revealing a third exon in the c-myc oncogene. *Nature* 304: 135-9

219. Leder P, Battey J, Lenoir G, Moulding C, Murphy W, Potter H, Stewart T, Taub R. 1983. Translocations among antibody genes in human cancer. *Science* 222: 765-71

220. Marcu KB, Harris LJ, Stanton LW, Erikson J, Watt R, Croce CM. 1983. Transcriptionally active c-myc oncogene is contained within NIARD, a DNA sequence associated with chromosome translocations in B-cell neoplasia. *Proc Natl Acad Sci U S A* 80: 519-23

221. Stanton LW, Watt R, Marcu KB. 1983. Translocation, breakage and truncated transcripts of c-myc oncogene in murine plasmacytomas. *Nature* 303: 401-6

222. Taub R, Kirsch I, Morton C, Lenoir G, Swan D, Tronick S, Aaronson S, Leder P. 1982. Translocation of the c-myc gene into the immunoglobulin heavy chain locus in human Burkitt lymphoma and murine plasmacytoma cells. *Proc Natl Acad Sci U S A* 79: 7837-41

223. Ramiro AR, Jankovic M, Eisenreich T, Difilippantonio S, Chen-Kiang S, Muramatsu M, Honjo T, Nussenzweig A, Nussenzweig MC. 2004. AID is required for c-myc/IgH chromosome translocations in vivo. *Cell* 118: 431-8

224. Marcu KB, Bossone SA, Patel AJ. 1992. myc function and regulation. *Annu Rev Biochem* 61: 809-60

225. Spencer CA, Groudine M. 1991. Control of c-myc regulation in normal and neoplastic cells. *Adv Cancer Res* 56: 1-48

226. Wierstra I, Alves J. 2008. The c-myc promoter: still MysterY and challenge. *Adv Cancer Res* 99: 113-333

227. Reddy MC, Vasquez KM. 2005. Repair of genome destabilizing lesions. *Radiat Res* 164: 345-56

228. Savic V, Yin B, Maas NL, Bredemeyer AL, Carpenter AC, Helmink BA, Yang-Iott KS, Sleckman BP, Bassing CH. 2009. Formation of dynamic gamma-H2AX domains along broken DNA strands is distinctly regulated by ATM and MDC1 and dependent upon H2AX densities in chromatin. *Mol Cell* 34: 298-310

229. Wuerffel R, Wang L, Grigera F, Manis J, Selsing E, Perlot T, Alt FW, Cogne M, Pinaud E, Kenter AL. 2007. S-S synapsis during class switch recombination is promoted by distantly located transcriptional elements and activation-induced deaminase. *Immunity* 27: 711-22

230. Gopaul DN, Guo F, Van Duyne GD. 1998. Structure of the Holliday junction intermediate in Cre-loxP site-specific recombination. *Embo J* 17: 4175-87

231. Van Duyne GD. 2001. A structural view of cre-loxp site-specific recombination. *Annu Rev Biophys Biomol Struct* 30: 87-104

232. Egli D, Hafen E, Schaffner W. 2004. An efficient method to generate chromosomal rearrangements by targeted DNA double-strand breaks in Drosophila melanogaster. *Genome Res* 14: 1382-93

233. Yu Y, Bradley A. 2001. Engineering chromosomal rearrangements in mice. *Nat Rev Genet* 2: 780-90

234. Jazayeri A, Falck J, Lukas C, Bartek J, Smith GC, Lukas J, Jackson SP. 2006. ATM- and cell cycle-dependent regulation of ATR in response to DNA double-strand breaks. *Nat Cell Biol* 8: 37-45

235. Callen E, Jankovic M, Difilippantonio S, Daniel JA, Chen HT, Celeste A, Pellegrini M, McBride K, Wangsa D, Bredemeyer AL, Sleckman BP, Ried T, Nussenzweig M, Nussenzweig A. 2007. ATM prevents the persistence and propagation of chromosome breaks in lymphocytes. *Cell* 130: 63-75

236. Huen MS, Grant R, Manke I, Minn K, Yu X, Yaffe MB, Chen J. 2007. RNF8 transduces the DNA-damage signal via histone ubiquitylation and checkpoint protein assembly. *Cell* 131: 901-14

237. Adams MM, Carpenter PB. 2006. Tying the loose ends together in DNA double strand break repair with 53BP1. *Cell Div* 1: 19

238. DiTullio RA, Jr., Mochan TA, Venere M, Bartkova J, Sehested M, Bartek J, Halazonetis TD. 2002. 53BP1 functions in an ATM-dependent checkpoint pathway that is constitutively activated in human cancer. *Nat Cell Biol* 4: 998-1002

239. Lee H, Kwak HJ, Cho IT, Park SH, Lee CH. 2009. S1219 residue of 53BP1 is phosphorylated by ATM kinase upon DNA damage and required for proper execution of DNA damage response. *Biochem Biophys Res Commun* 378: 32-6

240. Watanabe K, Iwabuchi K, Sun J, Tsuji Y, Tani T, Tokunaga K, Date T, Hashimoto M, Yamaizumi M, Tateishi S. 2009. RAD18 promotes DNA double-strand break repair during G1 phase through chromatin retention of 53BP1. *Nucleic Acids Res* 37: 2176-93

241. Boisvert FM, Rhie A, Richard S, Doherty AJ. 2005. The GAR motif of 53BP1 is arginine methylated by PRMT1 and is necessary for 53BP1 DNA binding activity. *Cell Cycle* 4: 1834-41

242. Bunting SF, Callen E, Wong N, Chen HT, Polato F, Gunn A, Bothmer A, Feldhahn N, Fernandez-Capetillo O, Cao L, Xu X, Deng CX, Finkel T, Nussenzweig M, Stark JM, Nussenzweig A. 2010. 53BP1 inhibits homologous recombination in Brca1-deficient cells by blocking resection of DNA breaks. *Cell* 141: 243-54

243. Kuppers R, Dalla-Favera R. 2001. Mechanisms of chromosomal translocations in B cell lymphomas. *Oncogene* 20: 5580-94

244. Dorsett Y, Robbiani DF, Jankovic M, Reina-San-Martin B, Eisenreich TR, Nussenzweig MC. 2007. A role for AID in chromosome translocations between c-myc and the IgH variable region. *J Exp Med* 204: 2225-32

245. Takizawa M, Tolarova H, Li Z, Dubois W, Lim S, Callen E, Franco S, Mosaico M, Feigenbaum L, Alt FW, Nussenzweig A, Potter M, Casellas R. 2008. AID expression levels determine the extent of cMyc oncogenic translocations and the incidence of B cell tumor development. *J Exp Med*

246. Belotserkovskii BP, De Silva E, Tornaletti S, Wang G, Vasquez KM, Hanawalt PC. 2007. A triplex-forming sequence from the human c-MYC promoter interferes with DNA transcription. *J Biol Chem* 282: 32433-41

247. Boles TC, Hogan ME. 1987. DNA structure equilibria in the human c-myc gene. *Biochemistry* 26: 367-76

248. Lieber MR, Ma Y, Pannicke U, Schwarz K. 2003. Mechanism and regulation of human non-homologous DNA end-joining. *Nat Rev Mol Cell Biol* 4: 712-20

249. Wang G, Vasquez KM. 2004. Naturally occurring H-DNA-forming sequences are mutagenic in mammalian cells. *Proc Natl Acad Sci U S A* 101: 13448-53

250. Zan H, Wu X, Komori A, Holloman WK, Casali P. 2003. AID-dependent generation of resected double-strand DNA breaks and recruitment of Rad52/Rad51 in somatic hypermutation. *Immunity* 18: 727-38

251. Shen HM, Peters A, Baron B, Zhu X, Storb U. 1998. Mutation of BCL-6 gene in normal B cells by the process of somatic hypermutation of Ig genes. *Science* 280: 1750-2

252. Mullighan CG, Goorha S, Radtke I, Miller CB, Coustan-Smith E, Dalton JD, Girtman K, Mathew S, Ma J, Pounds SB, Su X, Pui CH, Relling MV, Evans WE, Shurtleff SA, Downing JR. 2007. Genome-wide analysis of genetic alterations in acute lymphoblastic leukaemia. *Nature* 446: 758-64

253. Richardson C, Jasin M. 2000. Frequent chromosomal translocations induced by DNA double-strand breaks. *Nature* 405: 697-700

254. Peled JU, Kuang FL, Iglesias-Ussel MD, Roa S, Kalis SL, Goodman MF, Scharff MD. 2008. The Biochemistry of Somatic Hypermutation. *Annu Rev Immunol* 26: 481-511

255. Stavnezer J, Guikema JE, Schrader CE. 2008. Mechanism and Regulation of Class Switch Recombination. *Annu Rev Immunol* 26: 261-92

256. Futreal PA, Coin L, Marshall M, Down T, Hubbard T, Wooster R, Rahman N, Stratton MR. 2004. A census of human cancer genes. *Nat Rev Cancer* 4: 177-83

257. Stephens PJ, McBride DJ, Lin ML, Varela I, Pleasance ED, Simpson JT, Stebbings LA, Leroy C, Edkins S, Mudie LJ, Greenman CD, Jia M, Latimer C, Teague JW, Lau KW, Burton J, Quail MA, Swerdlow H, Churcher C, Natrajan R, Sieuwerts AM, Martens JW, Silver DP, Langerod A, Russnes HE, Foekens JA, Reis-Filho JS, van 't Veer L, Richardson AL, Borresen-Dale AL, Campbell PJ, Futreal PA, Stratton MR. 2009. Complex landscapes of somatic rearrangement in human breast cancer genomes. *Nature* 462: 1005-10

258. Lieberman-Aiden E, van Berkum NL, Williams L, Imakaev M, Ragoczy T, Telling A, Amit I, Lajoie BR, Sabo PJ, Dorschner MO, Sandstrom R, Bernstein B, Bender MA, Groudine M, Gnirke A, Stamatoyannopoulos J, Mirny LA, Lander ES, Dekker J. 2009. Comprehensive mapping of long-range interactions reveals folding principles of the human genome. *Science* 326: 289-93

259. Soutoglou E, Dorn JF, Sengupta K, Jasin M, Nussenzweig A, Ried T, Danuser G, Misteli T. 2007. Positional stability of single double-strand breaks in mammalian cells. *Nat Cell Biol* 9: 675-82

260. Sung P, Klein H. 2006. Mechanism of homologous recombination: mediators and helicases take on regulatory functions. *Nat Rev Mol Cell Biol* 7: 739-50

261. Rass E, Grabarz A, Plo I, Gautier J, Bertrand P, Lopez BS. 2009. Role of Mre11 in chromosomal nonhomologous end joining in mammalian cells. *Nat Struct Mol Biol* 16: 819-24

262. Nimonkar AV, Ozsoy AZ, Genschel J, Modrich P, Kowalczykowski SC. 2008. Human exonuclease 1 and BLM helicase interact to resect DNA and initiate DNA repair. *Proc Natl Acad Sci U S A* 105: 16906-11

263. Cuadrado M, Martinez-Pastor B, Murga M, Toledo LI, Gutierrez-Martinez P, Lopez E, Fernandez-Capetillo O. 2006. ATM regulates ATR chromatin loading in response to DNA double-strand breaks. *J Exp Med* 203: 297-303

264. Myers JS, Cortez D. 2006. Rapid activation of ATR by ionizing radiation requires ATM and Mre11. *J Biol Chem* 281: 9346-50

265. Guirouilh-Barbat J, Rass E, Plo I, Bertrand P, Lopez BS. 2007. Defects in XRCC4 and KU80 differentially affect the joining of distal nonhomologous ends. *Proc Natl Acad Sci U S A* 104: 20902-7

266. Zha S, Boboila C, Alt FW. 2009. Mre11: roles in DNA repair beyond homologous recombination. *Nat Struct Mol Biol* 16: 798-800

267. Haber JE. 2008. Alternative endings. *Proc Natl Acad Sci U S A* 105: 405-6

268. Dinkelmann M, Spehalski E, Stoneham T, Buis J, Wu Y, Sekiguchi JM, Ferguson DO. 2009. Multiple functions of MRN in end-joining pathways during isotype class switching. *Nat Struct Mol Biol* 16: 808-13

269. Deng Y, Guo X, Ferguson DO, Chang S. 2009. Multiple roles for MRE11 at uncapped telomeres. *Nature* 460: 914-8

270. Jankovic M, Nussenzweig A, Nussenzweig MC. 2007. Antigen receptor diversification and chromosome translocations. *Nat Immunol* 8: 801-8

271. Zha S, Guo C, Boboila C, Oksenych V, Cheng HL, Zhang Y, Wesemann DR, Yuen G, Patel H, Goff PH, Dubois RL, Alt FW. 2011. ATM damage response and XLF repair factor are functionally redundant in joining DNA breaks. *Nature* 469: 250-4

272. Helmink BA, Tubbs AT, Dorsett Y, Bednarski JJ, Walker LM, Feng Z, Sharma GG, McKinnon PJ, Zhang J, Bassing CH, Sleckman BP. 2011. H2AX prevents CtIP-mediated DNA end resection and aberrant repair in G1-phase lymphocytes. *Nature* 469: 245-9

273. Bothmer A, Robbiani DF, Feldhahn N, Gazumyan A, Nussenzweig A, Nussenzweig MC. 2010. 53BP1 regulates DNA resection and the choice between classical and alternative end joining during class switch recombination. *J Exp Med* 207: 855-65

274. Xu X, Wagner KU, Larson D, Weaver Z, Li C, Ried T, Hennighausen L, Wynshaw-Boris A, Deng CX. 1999. Conditional mutation of Brca1 in mammary epithelial cells results in blunted ductal morphogenesis and tumour formation. *Nat Genet* 22: 37-43

275. Xu X, Qiao W, Linke SP, Cao L, Li WM, Furth PA, Harris CC, Deng CX. 2001. Genetic interactions between tumor suppressors Brca1 and p53 in apoptosis, cell cycle and tumorigenesis. *Nat Genet* 28: 266-71

276. Rickert RC, Roes J, Rajewsky K. 1997. B lymphocyte-specific, Cre-mediated mutagenesis in mice. *Nucleic Acids Res* 25: 1317-8

277. Kitamura T. 1998. New experimental approaches in retrovirus-mediated expression screening. *Int J Hematol* 67: 351-9

278. Pear WS, Nolan GP, Scott ML, Baltimore D. 1993. Production of high-titer helper-free retroviruses by transient transfection. *Proc Natl Acad Sci U S A* 90: 8392-6

279. Naviaux RK, Costanzi E, Haas M, Verma IM. 1996. The pCL vector system: rapid production of helper-free, high-titer, recombinant retroviruses. *J Virol* 70: 5701-5